OAK RIDGE
NATIONAL LABORATORY
MANAGED BY UT-BATTELLE
FOR THE DEPARTMENT OF ENERGY

NFE-08-01715

**MSTD**

**CRADA Final Report**
**For**
**CRADA Number NFE-08-1715**

# Ionic Liquids as Novel Lubricants and /or Lubricant Additives

**Jun Qu**
**Oak Ridge National Laboratory**

**Michael B. Viola**
**General Motors Compnay**

**Prepared by**
**Oak Ridge National Laboratory**
**Oak Ridge, TN 37831**
**managed by**
**UT-BATTELLE, LLC**
**for the**
**U.S. Department of Energy**
**under contract DE-AC05-00OR22725**

**Approved for**
**Public Release**

UT-BATTELLE
ORNL-27 (4-00)

**CRADA TITLE: Ionic Liquids as Novel Lubricants and/or Lubricant Additives (NFE-08-01715)**

Project Start Date: May 29, 2009
Project End Date: September 28, 2013

**Contractor**: Oak Ridge National Laboratory (ORNL)
**Participant**: General Motors Company (GM)

**CRADA Team:**

ORNL: Jun Qu, Peter J. Blau, Sheng Dai, Huimin Luo, and Bruce G. Bunting (retired)
GM: Michael B. Viola, Gregory Mordukhovich (left GM), and Donald J. Smolenski (retired)

**Technical Contributors:**

ORNL: Todd J. Toops, Brian H. West, Jane Y. Howe, John M. Storey, Samuel A. Lewis Sr., Miaofang Chi, H.M. Meyer III, D.W. Coffey, Bo Yu, Dinesh G. Bansal, Chao Xie, Hanbing Xu, Huaqing Li, and Cheng Ma

GM: Tasfia Ahmed, Meryn D'Silva, Paul Harvath, and Ngoc-Ha Nguyen

**ACKNOWLEDGEMENT**

Research sponsored by the Vehicle Technologies Office, Office of Energy Efficiency and Renewable Energy, U.S. Department of Energy (DOE). Part of the IL synthesis effort was supported by the DOE Office of Basic Energy Sciences, Division of Chemical Sciences, Geosciences, and Biosciences. The characterization work was supported in part by ORNL's SHaRE User Facility, which is sponsored by the DOE Office of Basic Energy Sciences.

**TABLE OF CONTENTS**

**ABSTRACT**

This ORNL-GM CRADA developed ionic liquids (ILs) as novel lubricants or oil additives for engine lubrication. A new group of oil-miscible ILs have been designed and synthesized with high thermal stability, non-corrosiveness, excellent wettability, and most importantly effective anti-scuffing/anti-wear and friction reduction characteristics. Mechanistic analysis attributes the superior lubricating performance of IL additives to their physical and chemical interactions with metallic surfaces. Working with a leading lubricant formulation company, the team has successfully developed a prototype low-viscosity engine oil using a phosphonium-phosphate IL as an anti-wear additive. Tribological bench tests of the IL-additized formulated oil showed 20-33% lower friction in mixed and elastohydrodynamic lubrication and 38-92% lower wear in boundary lubrication when compared with commercial Mobil 1 and Mobil Clean 5W-30 engine oils. High-temperature, high load (HTHL) full-size engine tests confirmed the excellent anti-wear performance for the IL-additized engine oil. Sequence VID engine dynamometer tests demonstrated an improved fuel economy by >2% for this IL-additized engine oil benchmarked against the Mobil 1 5W-30 oil. In addition, accelerated catalyst aging tests suggest that the IL additive may potentially have less adverse impact on three-way catalysts compared to the conventional ZDDP. Follow-on research is needed for further development and optimization of IL chemistry and oil formulation to fully meet ILSAC GF-5 specifications and further enhance the automotive engine efficiency and durability.

## OBJECTIVES

Investigate the potential of using ionic liquids (ILs) as lubricants and/or lubricant additives specifically for internal combustion engine applications. Potential advantages/disadvantages of this new category of lubricants/additives are being explored with a combination of systematic experiments, materials characterization, and modeling.

## BENEFITS TO THE DOE FUNDING OFFICE'S MISSION

This CRADA was sponsored by the DOE Vehicle Technologies Office (VTO) Fuels and Lubricants Technologies Program. The mission of VTO is to develop more energy efficient and environmentally friendly highway transportation technologies that enable America to use less petroleum. One goal of the Fuels and Lubricants Technologies Program is to demonstrate 2% improved fuel efficiency via lubricant advances by 2015. This CRADA successfully developed a new series of ionic liquids (ILs)-based ashless anti-wear additives for automotive engine oils. A prototype IL-additized engine oil with ultra-low viscosities has been developed and demonstrated >2% higher fuel economy and similar engine wear compared to Mobil 1$^{TM}$ 5W-30 engine oil in industrial standard full-size engine dynamometer tests. This positions ORNL at a leading position to meet the program office's goal. Upon further development and optimization, this ionic lubricant technology may potentially save U.S. millions of barrels of crude oil annually. In addition, the ashless ILs have shown less adverse impact effects on the emission catalysts compared to conventional antiwear additives and therefore may potentially reduce the exhaust emissions.

**List of Invention Disclosures, Publications, and Presentations**

***Invention Disclosure***

- J. Qu, B. Yu, D.G. Bansal, H. Luo, S. Dai, P.J. Blau, B.G. Bunting, "Phosphonium Ionic Liquids as Additives for Hydrocarbon Lubricants," ORNL Invention Disclosure # 201002516, DOE S-124,070, Dec. 14, 2010.

***Journal Papers***

1. J. Qu, H. Luo, M. Chi, C. Ma, P.J. Blau, S. Dai, M.B. Viola, "Comparison of an Oil-Miscible Ionic Liquid and ZDDP as a Lubricant Anti-Wear Additive," *Tribology International* (*in review*).
2. G. Mordukhovich, J. Qu, J.Y. Howe, S.S. Bair, B. Yu, H. Luo, D.J. Smolenski, P.J. Blau, B.G. Bunting, S. Dai, "A Low-ViscosityIonic Liquid Demonstrating Superior Lubricating Performance from Mixed to Boundary Lubrication," *Wear* 301 (2013) 740-746.
3. J. Qu, D.G. Bansal, B. Yu, J. Howe, H. Luo, S. Dai, H. Li, P.J. Blau, B.G. Bunting, G. Mordukhovich, D.J. Smolenski, "Anti-Wear Performance and Mechanism of an Oil-Miscible Ionic Liquid As a Lubricant Additive," ACS Applied Materials & Interfaces 4 (2) (2012) 997–1002. ***– Invited candidature by the Scientific Secretariat for the ENI Award 2013.***
4. B. Yu, D.G. Bansal, J. Qu, X. Sun, H. Luo, S. Dai, P.J. Blau, B.G. Bunting, G. Mordukhovich, D.J. Smolenski, "Oil-Miscible and Non-Corrosive Phosphonium-Based Ionic Liquids as Candidate Lubricant Additives," *Wear* 289 (2012) 58–64.
5. J. Qu, M. Chi, H.M. Meyer III, P.J. Blau, S. Dai, H. Luo, "Nanostructure and Composition of Tribo-Boundary Films Formed in Ionic Liquid Lubrication," *Tribology Letters,* Vol. 43, No. 2, Jul. 2011, pp. 205-211.

***Invited Talk***

- J. Qu, "Ionic Liquids as Novel Lubricants or Lubricant Additives," *SAE 2012 High Efficiency IC Engines Symposium*, Detroit, MI, April 22-23, 2012.

***Conference Proceedings, Presentations, and Posters***

1. M.B. Viola, E.A. Bardasz, B.G. Bunting, J.M. Storey, T.J. Toops, S.A. Lewis Sr., H. Luo, S. Dai, P.J. Blau, J. Qu*, "Development of Ionic Liquid-based Anti-Wear Additives for Automotive Engine Lubrication," *STLE 68th Annual Meeting & Exhibition*, Detroit, MI, May 5-10, 2013.
2. G. Mordukhovich, J. Qu*, J.Y. Howe, S.S. Bair, B. Yu, H. Luo, D.J. Smolenski, P.J. Blau, B.G. Bunting, S. Dai, "A Low-ViscosityIonic Liquid Demonstrating Superior Lubricating Performance from Mixed to Boundary Lubrication," *19th International Conference on Wear of Materials,* Portland, OR, April 14-18, 2013.
3. J. Qu, H. Luo, S. Dai, M. Chi, P.J. Blau, M.B. Viola, "Ionic Liquids as Ashless Multifunctional Lubricant Additives," Poster #P80, *19th International Conference on Wear of Materials,* Portland, OR, April 14-18, 2013.
4. J. Qu, H. Luo, S. Dai, P.J. Blau, B.G. Bunting, G. Mordukhovich, D.J. Smolenski, "Oil-Miscible and Non-Corrosive Ionic Liquids as Multifunctional Ashless Lubricant Additives," *ASME International Mechanical Engineering Congress & Exposition*, Houston, TX, Nov. 9-15, 2012.
5. J. Qu, H. Luo, S. Dai, P.J. Blau, B.G. Bunting, G. Mordukhovich, D.J. Smolenski, "Ionic Liquids as Multifunctional Ashless Additives for Engine Lubrication," *18th Directions in Engine-Efficiency and Emissions Research (DEER) Conference,* Detroit, MI, Oct. 16-19, 2012.
6. J. Qu, B. Yu, D.G. Bansal, J. Howe, H. Luo, S. Dai, P.J. Blau, B.G. Bunting, G. Mordukhovich, D.J. Smolenski, "Oil-Miscible and Non-Corrosive Ionic Liquids as Candidate Lubricant Additives," *STLE 67th Annual Meeting & Exhibition*, St. Louis, MO, May 6-10, 2012.

7. J. Qu, M. Chi, H.M. Meyer III, P.J. Blau, S. Dai, H. Luo, "Nanostructure and Composition of Tribo-Boundary Films Formed in Ionic Liquid Lubrication," *STLE 67th Annual Meeting & Exhibition*, St. Louis, MO, May 6-10, 2012.
8. D.G. Bansal, S. Kuiry, B. Yu, H. Luo, D. Koosau, J. Qu, "Tribo-Corrosion Behavior of Selected Imidazolium-Based Ionic Liquids," *Third International Symposium on Tribo-Corrosion*, Atlanta, GA, April 19-20 2012.
9. D.G. Bansal, J. Qu, B. Yu, H. Luo, S. Dai, B. Bunting, P. Blau, G. Mordukhovich, D.J. Smolenskid, "Characterization and Tribological Evaluation of 1-benzyl-3-methylimidazolium bis(trifluoromethylsulfonyl)imide as Neat Lubricant and Oil Additive," *Proceedings of the ASME/STLE 2011 International Joint Tribology Conference (IJTC2011)*, Los Angeles, CA, Oct. 23-26, 2011.
10. J. Qu, B. Yu, D.G. Bansal, J. Howe, H. Luo, S. Dai, H. Li, P.J. Blau, B.G. Bunting, G. Mordukhovich, D.J. Smolenski, "Ionic Liquids as Novel Engine Lubricants or Lubricant Additives," *17th Directions in Engine-Efficiency and Emissions Research (DEER) Conference*, Detroit, MI, Oct. 3-6, 2011.

## TECHNICAL DISCUSSION OF WORK PERFORMED BY ALL PARTIES

### CHAPTER 1. Introduction

In the U.S. today, there are more than 250 million cars and trucks on the road, traveling a whopping three trillion miles per year, which accounts for 70% of the U.S.'s annual oil consumption of ~7 billion barrels. One goal of the DOE VTO's Fuels and Lubricants Technologies Program is to demonstrate 2% improved fuel efficiency via lubricant advances by 2015, which would potentially save U.S. up to 100 million barrels of oil annually.

Engine and powertrain parts like piston rings and cylinder bores, valve guides, cams and tappets, fuel injector pumps and plungers, transmission gearing, and face seals are all affected to some degree by friction [1]. The magnitude of such friction-induced losses depends on engine design, materials of construction, operating conditions, and most importantly lubrication. Automotive companies and lubricant original equipment manufacturers (OEMs) are developing and implementing advanced lubricants to enhance fuel efficiency and engine durability and at the same time, maintain or extend lubricant drain intervals. Lubrication regimes in mechanical devices such as engines can be divided into three general categories: boundary, mixed, and elastohydrodynamic/hydrodynamic lubrication, among which hydrodynamic lubrication has the lowest friction and wear. Modern engines are designed to minimize the contribution of boundary and mixed friction (although these losses cannot be totally eliminated) and their parasitic friction loss (accounting for 10-15% of the total engine-generated energy [1]) is primarily induced by elastohydrodynamic drag between the piston rings and cylinder liners, which is proportional to the lubricant viscosity.

Developing more effective additive packages in combination with balancing lubricant viscosity has proven to be the most successful and cost effective route to improving engine efficiency and durability. Over last decade, the viscosity grade of standard internal combustion engine oils has been continuously reduced in an attempt to improve fuel economy, from SAE 10W-30 to 5W-30, 5W-20, and now 0W-20. On the other hand, the bearing interfaces under BL, such as the top ring reversal region inside the cylinder, set a floor for engine lubricant viscosity to prevent excessive wear. Commercial lubricants are composed of base stock and several categories of additives including anti-wear (AW), friction modifier, viscosity modifier, antioxidant, detergent, dispersant, etc [2]. Specifically, friction modifiers and anti-wear agents play key roles in reducing boundary and mixed friction and wear in engine locations such as the top-ring-reversal region of the piston ring-cylinder liner interface and sliding surfaces in the valve train. Currently, the most common anti-wear additive is zinc dialkyl-dithiophosphate (ZDDP) [2,3]. ZDDP is very effective at wear protection; however, it is known to cause deposits upon thermal decomposition ('ash') and to poison emission catalysts [2]. Therefore, there is a need to develop alternative, ashless, and more effective anti-wear additives with potentially less impact on catalyst systems. Improved wear protection would allow the use of lower-viscosity engine oils, providing a further improvement in engine mechanical efficiency. Alternatively, developing new low-viscosity base lubricants to reduce hydrodynamic drag and meanwhile minimize the wear penalty is also of interest.

Ionic liquids (ILs) [4] are, as the name indicates, composed solely of cations and anions (see Fig. 1.1) instead of neutral molecules. They are primarily used as "green" solvents in chemical synthesis, electrochemistry, and catalysis, due to their ultra-low vapor pressure, non-flammability, high thermal stability, and ability to be tailored to optimize their physical and chemical characteristics.

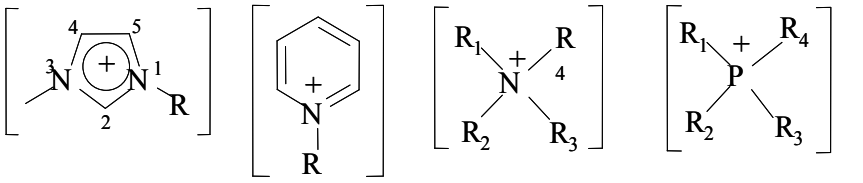

1-alkyl-3-methyl-imidazolium | *N*-alkyl-pyridinium | Tetraalkyl-ammonium | Tetraalkyl-phosphonium ($R_{1,2,3,4}$ = alkyl)

(a) Common cation strictures

$[PF_6]^-$
$[(CF_3SO_2)_2N]^-$ ($Tf_2N$)
$[(C_2F_5SO_2)_2N]^-$ (BETI)
$[BR_1R_2R_3R_4]^-$
**$[P(O)_2(OR)_2]^-$ (phosphate)**
**$[P(O)_2(R)_2]^-$ (phosphinate)**

$[BF_4]^-$
$[CF_3SO_3]^-$

$[CH_3CO_2]^-$
$[CF_3CO_2]^-$, $[NO_3]^-$
$Br^-$, $Cl^-$, $I^-$
$[Al_2Cl_7]^-$, $[AlCl_4]^-$

(b) Common anion strictures

Fig. 1.1. Common cations and anions of ionic liquids.

ILs have been explored as a new category of lubricants over the past dozen years [5-24]. There are currently two approaches in the literature:

- Using ILs as neat lubricants or base stocks [5-18]. This approach would take full advantage of ILs' high thermal stability, low vapor pressure, high viscosity index, strong wear protection in boundary lubrication (BL) by tribo-film formation [5-17], and low friction coefficient in mixed (ML) and elastohydrodynamic (EHL) lubrication resulting from their low pressure-viscosity coefficients [19]. The practical applications of using such fully synthetic ILs-based lubricants however are limited by their relatively high cost compared with hydrocarbon oils.
- Using ILs as ashless lubricant additives. This approach is more cost-effective and would have easier market penetration. The main technical barrier is that most ILs have no or very limited solubility (<<1%) in non-polar hydrocarbon base oils. This is because ions are attracted by polar forces and sometimes hydrogen bonding, whereas non-polar molecules are held together by dispersion forces [25]. Earlier studies in the literature were mostly on unstable oil-IL emulsions or very low IL concentrations [7,8,14,17,19-22] or used polar base oils [23,24]. Therefore, there is a significant opportunity for developing oil-solubility ILs in non-polar lubricating base oils.

In this CRADA, we explored the two approaches stated above and have made great technical progress on both [26-30]. Main efforts were taken on the approach of using ILs as oil additives [28-30] because it has more near-term impact on energy savings, and have made two major breakthroughs: (1) developed a new group of oil-miscible, non-corrosive ILs with superior anti-wear and friction reduction characteristics, (2) produced a prototype fully-formulated low-viscosity engine oil using an IL as ashless AW additive and demonstrated excellent engine wear protection and improved fuel economy.

## CHAPTER 2. Development of Low-viscosity Ionic Liquids as Neat Lubricants

### 2.1. Experimental

Figure 2.1 shows the molecular structure of the ionic liquid 1-butyl-3-methylimidazolium bis(trifluoromethylsulfonyl)imide ([BMIM][$NTf_2$]). It was purchased from Sigma-Aldrich with ≥98% purity and ≤0.5% water.

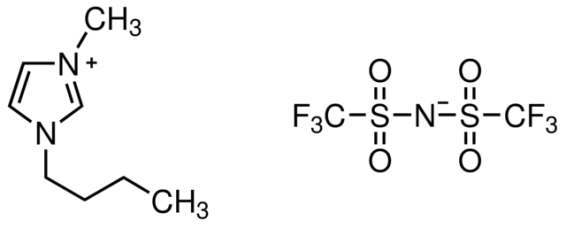

Fig. 2.1. Molecular structure of 1-butyl-3-methylimidazolium bis(trifluoromethylsulfonyl)imide.

Two hydrocarbon lubricating oils, Mobil 1™ poly-alpha-olefin (PAO) 4 cSt base oil (generously provided by ExxonMobil) and Royal Purple™ 0W-10 racing engine oil, were selected to compare with [BMIM][$NTf_2$] because they all have similar kinematic viscosities at 100 °C (see Table 2.1). Viscosities of the IL and reference oils were measured in the temperature range of 0–100 °C using a Petrolab MINIVIS II viscometer base with the falling-ball technique. Each measurement used 0.5 mL of fluid and involved at least four repeated ball drops to ensure a <2% statistical deviation.

The viscosity-pressure coefficient of [BMIM][$NTf_2$] at various temperatures was determined following the procedure described in [31,32] using a high-pressure (up to 400 MPa), high-temperature (up to 150 °C) viscometer at the Center for High-Pressure Rheology, Georgia Institute of Technology, to measure the limiting-low-shear viscosity. The V-P coefficient $\alpha^*$ here is defined by the reciprocal asymptotic isoviscous pressure coefficient as shown in Eq. (2.1) [3], which is the coefficient employed in the Hamrock and Dowson formulas [33] for lubricant film thickness calculations.

$$\alpha^* = \frac{1}{P_{iv,as}} = \left[\eta_0 \int_0^\infty \frac{d\eta}{\eta(p)}\right]^{-1} \tag{2.1}$$

where $p_{iv,as}$ is the asymptotic isoviscous pressure [33], $\eta(p)$ is the lubricant low-shear viscosity under pressure ($p$), and $\eta_0$ is the lubricant atmospheric low-shear viscosity.

Thermogravimetric analysis (TGA) was used to determine the decomposition temperature of the ionic liquid and oil lubricants. Tests were carried out on a TA Instruments TGA-2950 at a 10 °C/min heating rate in a nitrogen atmosphere. The mass density was determined by weighing a known volume, e.g., 1.0 mL, of each fluid. The uncertainty of the density was less than 5%.

The corrosivity of the IL was evaluated using a procedure similar to that described in the ASTM standard D 6594-08, "Standard Test Method for Evaluation of Corrosiveness of Diesel Engine Oil at 135 °C." Gray cast iron and aluminum sticks were dipped into the IL at a constant temperature of 135 °C for 7 days. By the end of the test, the aluminum and iron surfaces were intact without evidence of corrosion.

Tribological evaluations were conducted in lubrication regimes from hydrodynamic to boundary. Stribeck curves were generated using ball-on-disc rolling-sliding tests on a PCS MTM2 tribotester. Both

the ball and disc were made of AISI 52100 steel. The grade-10 bearing ball had a nominal diameter of 19.05 mm, surface hardness of 64 Rc, and maximum arithmetic average roughness ($R_a$) of 0.025 μm. The disc was 46 mm in diameter (wear track diameter: 42 mm) with a measured hardness of 62.5 Rc and $R_a$ of 0.010 μm. The contact area was submerged in a tank of 40 mL of lubricant. Tests were conducted under a constant load of 75 N at 100 $^oC$. The slide-to-roll ratio (SRR), as defined in Eq. (2.2), was maintained at a constant 50%, and the mean velocity ($U_e$) was started at 3.2 m/s in each test and gradually decreased to 0.1 m/s by the end of the test. The dwell time at each speed was six seconds.

$$\text{SRR} = \Delta U / U_e \tag{2.2}$$

where $\Delta U = U_1 - U_2$ is the sliding velocity and $U_e = (U_1 + U_2)/2$ is the mean velocity.

The boundary lubrication behavior was evaluated using a pin-on-disc unidirectional sliding test under starved BL at 150 $^oC$ on a CSM Instrument High-Temperature Tribometer. The material pair again was self-mated AISI 52100 steel. The pin was a grade-25 bearing ball with a 10 mm nominal diameter with maximum $R_a$ of 0.051 μm. The disc was 30 mm in diameter with $R_a$ of 0.020 μm. Only two drops of lubricant were applied prior to each test and no lubricant was added during the test. Tests were conducted under a constant load of 4 N and a sliding speed of 0.5 m/s for 10803 meters of sliding if no scuffing failure; otherwise they were stopped at the onset of scuffing (captured by a sudden rise of the friction coefficient to >0.5). For both the tribological tests, at least two repeat tests were conducted under each test condition. The friction force was acquired in situ during the test and normalized by the normal load to calculate the friction coefficient.

Worn surface morphology was examined using scanning electron microscopy (SEM). Transmission electron microscopy (TEM) and energy-dispersive x-ray spectroscopy (EDS) were to study the nanostructure and chemical composition of the tribo-film and near-surface zone from the cross section. TEM samples were prepared using a Hitachi NB-5000 dual-beam focused ion beam (FIB) system with a gallium source to extract thin cross-sections of the disc wear tracks generated by the scuffing tests. A thin layer of carbon and then a second layer of tungsten were deposited onto the surface prior to the FIB process to protect the surface structure. The FIB lift-out and sample thinning processes are illustrated in Fig. 2.2. The SEM system was a Hitachi S-4800 field-emission SEM and the TEM system was a Hitachi HF-3300 TEM/STEM at 300 kV (1.3 Å resolution) equipped with a Bruker solid-state EDS detector with a 30 $mm^2$ active area. All surfaces were carefully cleaned using acetone followed by isopropanol and dried prior to microscopic examinations.

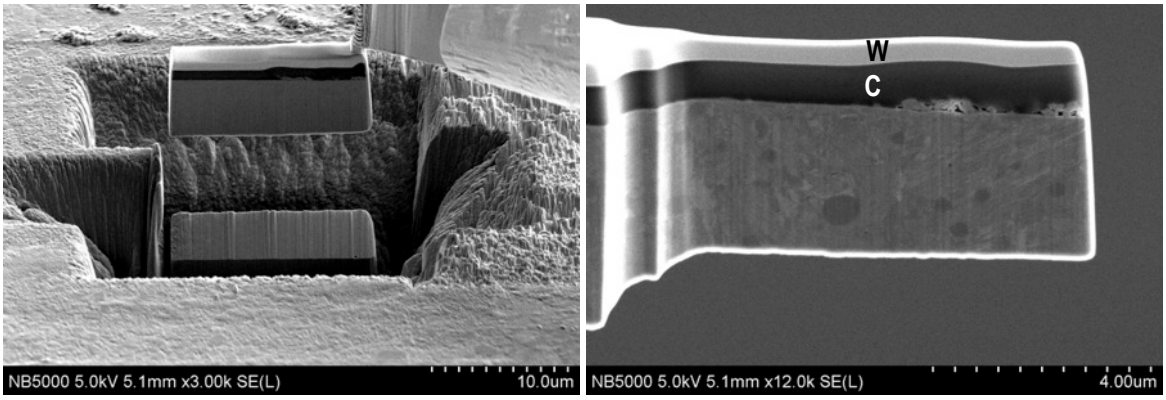


Fig. 2.2. TEM sample preparation using FIB: (a) A thin cross-section lifted out from the worn surface lubricated by 0W-10 engine oil and (b) sample thinning.

## 2.2. Results and Discussion

### *2.2.1. Physical properties*

Table 2.1 compares the density, viscosity, viscosity index, and decomposition temperature of the IL and the two hydrocarbon oils. The density of [BMIM][$NTf_2$] is higher (1.44 g/ml) than that of the oils. The IL has excellent thermal stability and does not decompose until above 472 $^oC$. This onset-of-decomposition temperature is much higher than that of the two baseline oils, PAO 4 cSt base oil and 0W-10 racing engine oil (250 and 236 $^oC$, respectively). The dynamic viscosity of the IL at 100 $^oC$ is higher than that of the oils but the kinematic viscosity falls in between the two oils. The viscosity index (VI=159) of the IL is substantially higher than that of the PAO base oil (VI=111) or the formulated 0W-10 racing engine oil (VI=128).

Table 2.1. Physical properties of [BMIM][$NTf_2$] and baseline oils.

| Lubricant | Density (g/ml, @23$^oC$) | Dynamic viscosity (cP) | | | | Kinematic viscosity (cSt) | Viscos-ity index | Decomp. temp. ($^oC$) |
|---|---|---|---|---|---|---|---|---|
| | | 0 $^oC$ | 23 $^oC$ | 40 $^oC$ | 100 $^oC$ | 100 $^oC$ | | |
| [BMIM][$NTf_2$] | 1.44 | 207.6 | 56.8 | 28.4 | 6.5 | 4.6 | 159 | 472 |
| PAO 4 base oil | 0.80 | 95.2 | 27.6 | 14.0 | 3.0 | 3.9 | 111 | 250 |
| 0W-10 engine oil | 0.87 | 158.7 | 44.0 | 21.4 | 4.2 | 5.0 | 128 | 236 |

The measured viscosity-pressure curves of [BMIM][$NTf_2$] at three temperatures are shown in Fig. 3. Based on the measurements, the V-P coefficient $\alpha^*$ was calculated (using Eq. 2.1) as 11.1, 6.5, and 5.5 $GPa^{-1}$ at 22, 100, and 150 $^oC$, respectively. These values are substantially lower than the V-P coefficients of common hydrocarbon lubricating oils (including mineral oils and PAOs), which are reported in the range of 15-25 $GPa^{-1}$ at room temperature and 10-15 $GPa^{-1}$ at 100 $^oC$ [32,34,35]. Specifically, the V-P coefficient $\alpha^*$ of the PAO 4 cSt base oil was reported to be 15.0 and 10.9 $GPa^{-1}$ at 40 and 100 $^oC$ in [34] and 12.4, 10.6, 9.4, and 8.4 $GPa^{-1}$ at 70, 100, 140, and 180 $^oC$ in [32], respectively. The V-P coefficients of the ionic liquid and PAO 4 cSt oil are compared in Table 2.2 for readers' convenience. A low V-P coefficient is usually considered as a two-edged sword. The less-increased viscosity under the contact pressure may lead to a lower friction coefficient under EHL and ML, if the trend persists to the contact pressure (1.3 GPa for the rolling-sliding tests in this study). On the other hand, a low V-P coefficient is also expected to decrease the lubricant film thickness, challenging the wear protection.

Table 2.2. Viscosity-pressure coefficients of [BMIM][$NTf_2$] and PAO 4 cSt oil.

| Lubricant | 22 $^oC$ | 40 $^oC$ | 70 $^oC$ | 100 $^oC$ | 140 $^oC$ | 150 $^oC$ | 180 $^oC$ |
|---|---|---|---|---|---|---|---|
| [BMIM][$NTf_2$] | 11.1 | | | 6.5 | | 5.5 | |
| PAO 4 base oil | | 15.0[34] | 12.4[32] | 10.9[34], 10.6[32] | 9.4[32] | | 8.4[32] |

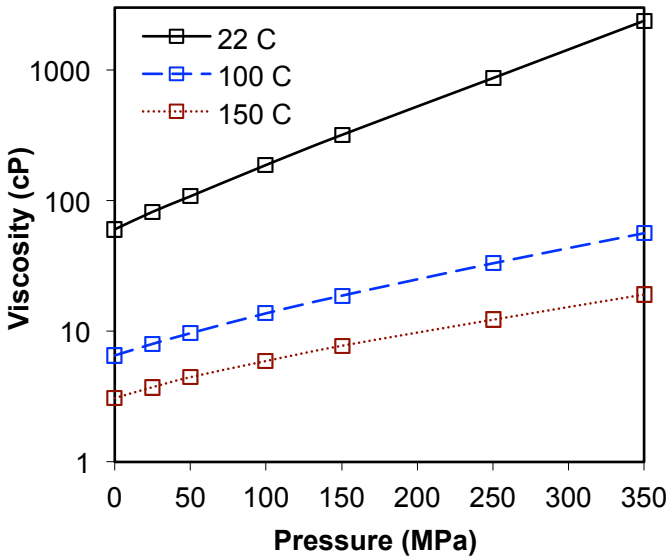


Fig. 2.3. Viscosity-pressure curves of [BMIM][$NTf_2$] at various temperatures.

### *2.2.2. Lubricating behavior – ML*

In theoretical modeling, the minimum lubricant film thickness is designated for lambda ratio calculations to determine the lubrication regime. In practical situations, the central film thickness is more often used because the lubricant film between the surfaces in relative motion has an almost constant thickness and the central value can well represent much of the Hertzian contact zone [33]. For the rolling-sliding tests in this study, the central lubricant film thickness ($h$) was estimated using the Hamrock and Dowson formulas [33] for the IL and the PAO oil at the mean speeds of 0.1, 0.5, 1.0, and 3.2 m/s, as shown in Table 2.3. (Note that the 0W-10 engine oil is multigrade in viscosity and so the classical film thickness formulas do not apply.) Since the bearing balls in grades 10 and 5 have $R_a$ tolerances of 0.025 and 0.013 μm, respectively, we assume the $R_a$ of the grade 10 test ball at the median point, 0.019 μm. In general, $R_q$ is 20-40% higher than $R_a$ and here we assume $R_q \approx 1.3R_a$. Thus, the composite roughness $\sigma$ of the contact surfaces, as defined in Eq. (2.3), was estimated to be 0.028 μm. The lambda ratio ($\lambda = h/\sigma$) was computed accordingly and is shown in Table 2.3. The lambda ratios suggest that the rolling-sliding tests started at ML with relatively high lambda ratios (near EHL) at 3.2 m/s and transited to BL between 1.0 and 0.5 m/s.

$$\sigma = \sqrt{R_{q,1}^2 + R_{q,2}^2} \tag{2.3}$$

where the $R_{q,1}$ and $R_{q,2}$ are the *root-mean-square* average roughness of the contact surfaces.

Table 2.3. Central lubricant film thickness ($h$) and lambda ratio ($\lambda$) in rolling-sliding tests at 100 °C.

| $U_e$ (m/s) | 0.1 | | 0.5 | | 1.0 | | 3.2 | |
|---|---|---|---|---|---|---|---|---|
| Lubricant | $h$ (μm) | λ | $h$ (μm) | λ | $h$ (μm) | λ | $h$ (μm) | λ |
| [BMIM][$NTf_2$] | 0.008 | 0.3 | 0.024 | 0.9 | 0.039 | 1.4 | 0.085 | 3.0 |
| PAO 4 base oil | 0.007 | 0.2 | 0.020 | 0.7 | 0.031 | 1.1 | 0.068 | 2.4 |

The measured Stribeck curves of [BMIM][$NTf_2$] and baseline oils from the rolling-sliding tests are compared in Fig. 2.4a, where each curve represents an average of 2–4 repeat tests. High repeatability was observed as demonstrated by the four curves for [BMIM][$NTf_2$] in Fig. 2.4b. For all lubricants at the mean speed of 1.0 m/s or above, the friction coefficient was relatively stable and below 0.03, a typical level for ML with a relatively high lambda ratio (near EHL). The rapid change of friction coefficient from 0.02-0.03 to ~0.05 suggests a transition from ML to BL. The experimental observations in Fig. 2.4 are in line with the predicted lubrication regimes in Table 2.3.

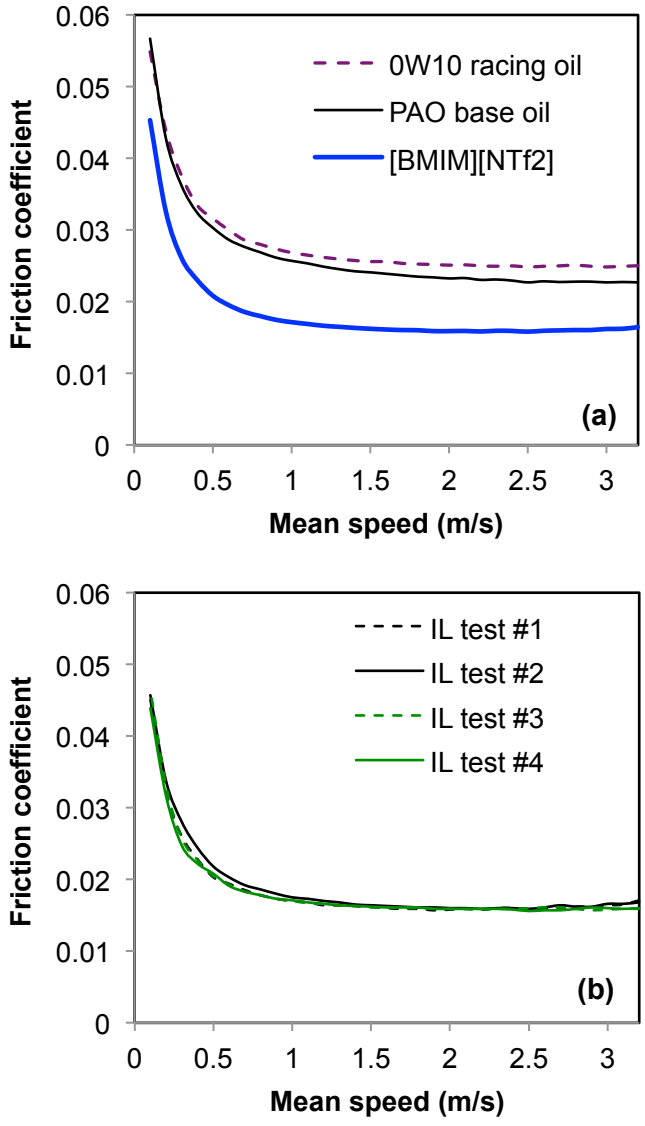


Fig. 2.4. Stribeck curves at 100 $^{o}$C showing (a) lower ML friction for [BMIM][$NTf_2$] than for the of baseline oils and (b) high repeatability from test to test for [BMIM][$NTf_2$].

Although [BMIM][$NTf_2$] has a higher dynamic viscosity (6.5 cP) than PAO 4 (3.0 cP) or 0W-10 (4.2 cP), it exhibited significant lower friction coefficient by ~30% in ML, as shown in Fig. 2.4a. ML can be

considered as regions of EHL separated by mild asperity contacts. The much lower V-P coefficient of the IL compared to that of the PAO oil may help reduce the shear resistance at the EHL regions, as a result of a less-increased viscosity than the oils at the rolling-sliding contact. The viscosity response to shear is unknown for the IL but could play a role as well.

### *2.2.3. Lubricating behavior – BL*

The IL has demonstrated a lower friction coefficient in the ML regime, however, its low V-P coefficient increases the wear challenge in BL. To investigate the lubricating behavior in BL, scuffing tests were conducted at 150 $^{o}$C using a pin-on-disc unidirectional sliding configuration under starved lubrication. The composite roughness was estimated to be 0.066 μm. The viscosity and V-P coefficient of [BMIM][$NTf_2$] at 150 $^{o}$C were measured at 3.1 cP and 5.5 $GPa^{-1}$, respectively. The PAO's viscosity and V-P coefficient at 150 $^{o}$C were not readily available and so were interpolated from their data at 100, 140, and 180 $^{o}$C [32]. For both the IL and the PAO oil, the lubricant film thickness was calculated at below 0.01 μm and the lambda ratios were about 0.1 (<1) – confirming the BL regime.

In the scuffing tests, the friction coefficient for all lubricants started at around 0.1, the typical value in BL, and showed a rapid transition to above 0.5 when scuffing occurred, as shown in Fig. 2.5. In both repeat tests, [BMIM][$NTf_2$] resisted the scuffing much longer than did the oils. (It was unexpected that the 0W-10 racing engine oil had the worst performance, with scuffing occurring in a very early stage of testing.) It is known that anti-scuffing/anti-wear performance largely depends on the lubricant's ability to form a protective tribo-film on the contact surfaces. For steady-state BL, direct evidence of tribo-film formation has been revealed in the literature for oil lubricants containing zinc dithiophosphate (ZDDP) [3,36] and ILs as either neat lubricants [26] or oil additives [29].

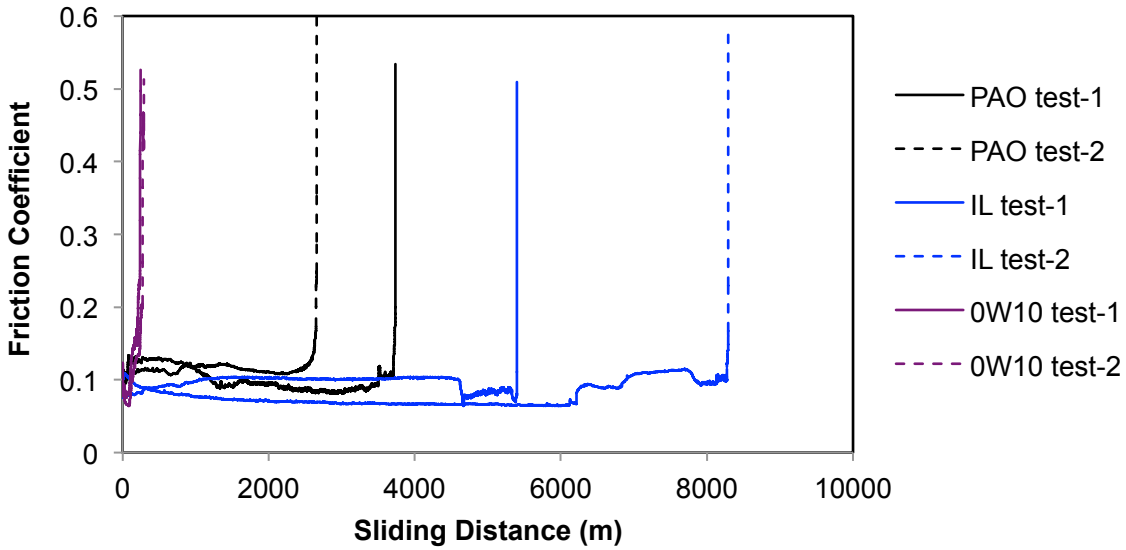


Fig. 2.5. BL scuffing tests showing higher scuffing resistance of [BMIM][$NTf_2$] than that of baseline oils.

To study the wear mode and tribo-film, the worn surface morphology was first examined. Figure 2.6 compares the SEM top views (300× and 1000×) of the wear tracks on the discs tested in the IL and the oils. The arrow on each image indicates the sliding direction. The scuffing damage on all three wear tracks appears to be dominated by discrete material spallation upon lubricant failure, suggesting adhesive wear in a "stick-slip" mode. The scuffed zone produced in the IL lubricant (Fig. 2.6a) is narrower and the

surface damage seems less severe compared with the scuffed areas produced in the two hydrocarbon oils (Figs. 2.6b and 2.6c).

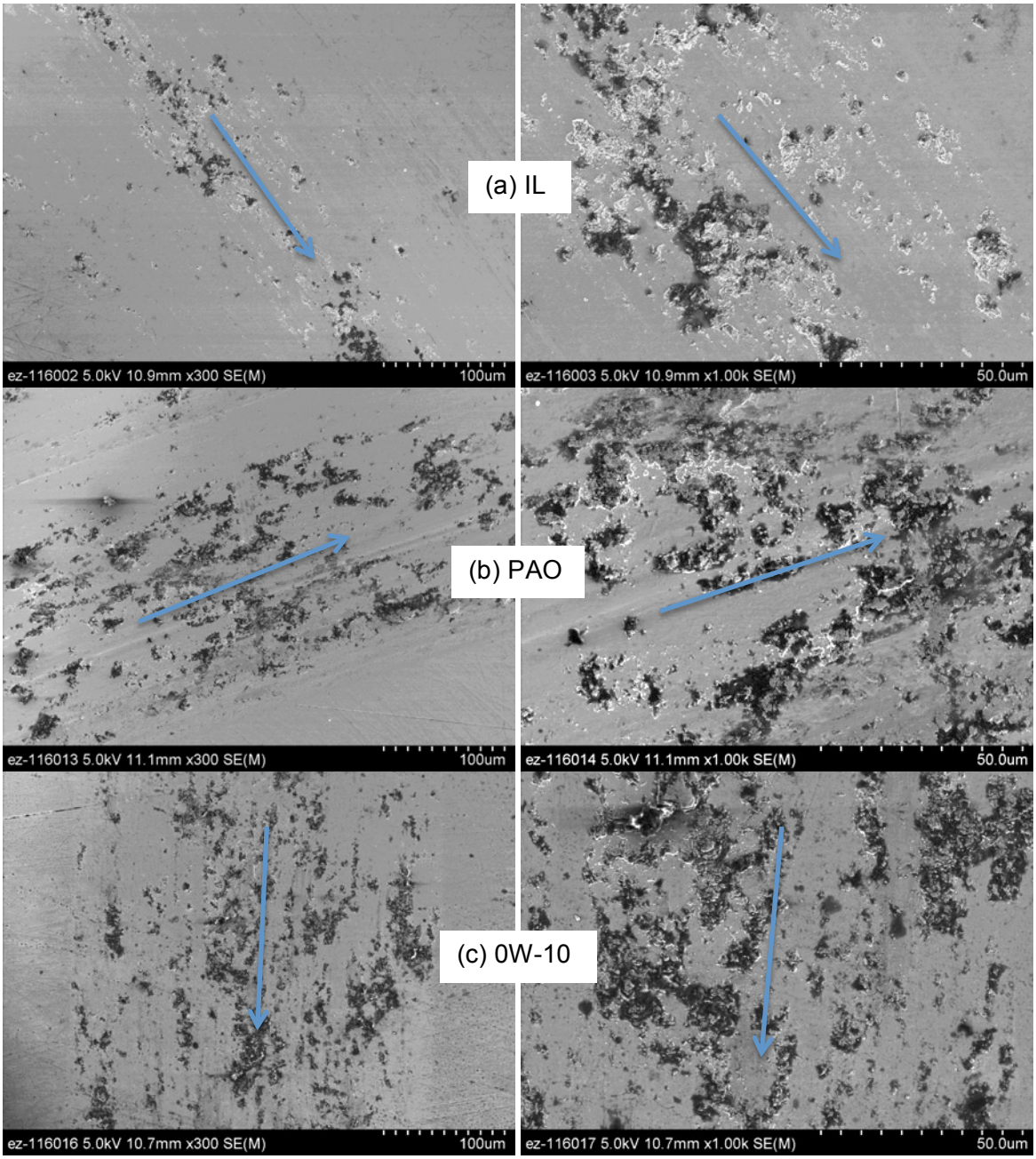


Fig. 2.6. SEM top views (300× and 1000×) of the disc wear tracks tested in (a) [BMIM][$NTf_2$], (b) PAO 4 cSt base oil, and (c) 0W-10 racing engine oil. The arrow on each image indicates the sliding direction.

TEM and EDS were used for further examination from the cross section, as shown in Fig. 2.7. Aided by FIB, thin sections were lifted from the wear tracks along the sliding direction, as illustrated in Fig. 2.2. All samples were extracted from relatively smooth, less-scuffed regions. Figure 2.7a shows a TEM image and an EDS element map from the cross section for the disc worn surface tested in [BMIM][$NTf_2$]. A thin

tribo-film was observed on the surface under TEM and the sulfur concentration as detected by EDS suggests that it is a result of the tribochemical reactions between the steel surface and the IL. The tribo-films formed in bis(trifluoromethylsulfonyl)imide ILs usually contain fluorine compounds [26], but fluorine was not resolved in the EDS elemental mapping because the x-ray energy peaks of fluorine and iron largely overlap. The ~20 nm tribo-film presented here is, however, significantly thinner than the 60–100 nm tribo-film reported [26] for a steel surface (non-scuffed) under steady-state lubrication by an IL with a longer alkyl on the cation but otherwise identical in molecular structure to [BMIM][$NTf_2$]. Although we cannot entirely rule out the effect of the IL molecular structure on the tribo-film thickness, we attribute the thinner tribo-film primarily to the scuffing damage. The tribo-film formation and removal (due to wear) are two competing processes and will reach equilibrium in steady-state BL. When scuffing occurs, the wear rate increases by orders of magnitude, breaking the equilibrium and quickly destroying the tribo-film. As a result, no tribo-film was found on the wear tracks tested in the two oils, as shown in Figs. 2.7b and 2.7c. EDS results suggest that the loose material on the oil-lubricated surface is composed of oxides and no active lubricant agent such as phosphorous or sulfur was detected. The sustained tribo-film in IL lubrication (though relatively thin) suggests stronger tribo-film forming activity, which may be responsible for the IL's higher resistance to scuffing and surface damage propagation compared with the hydrocarbon oils.

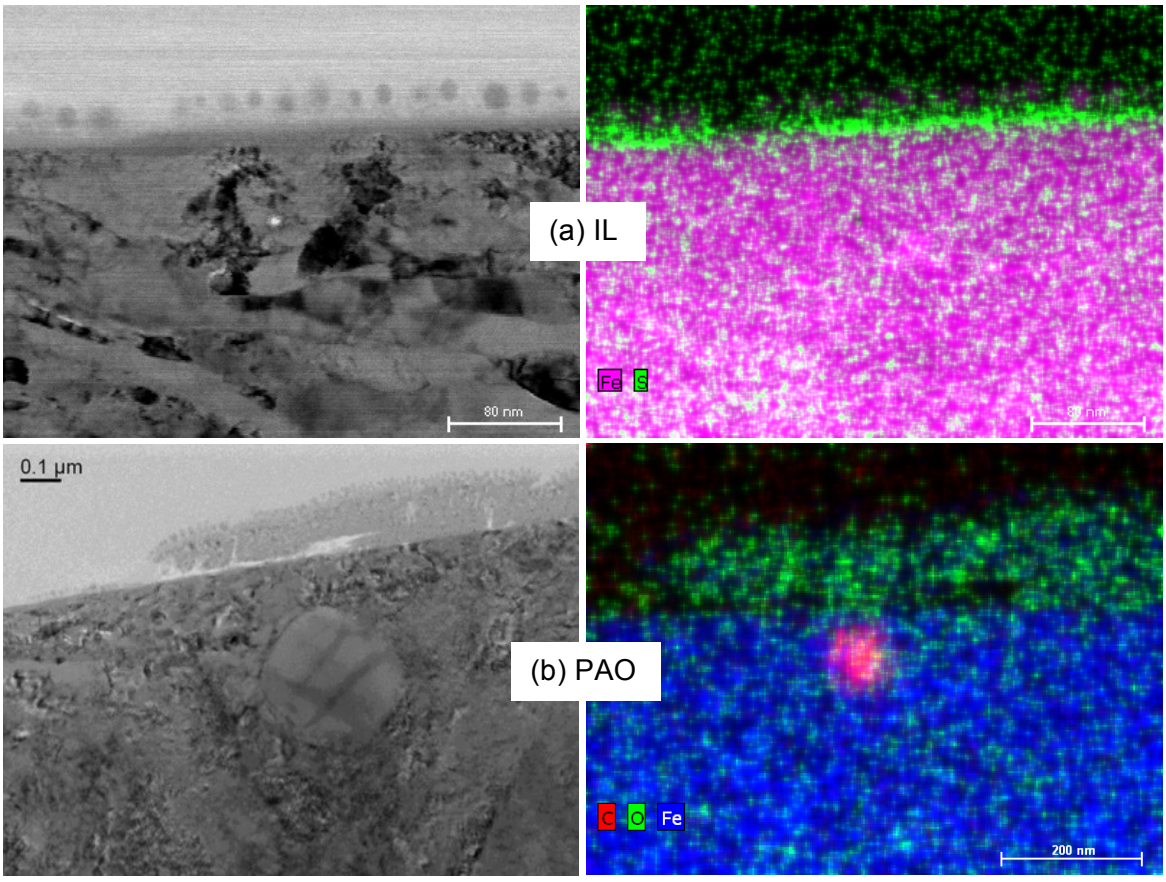

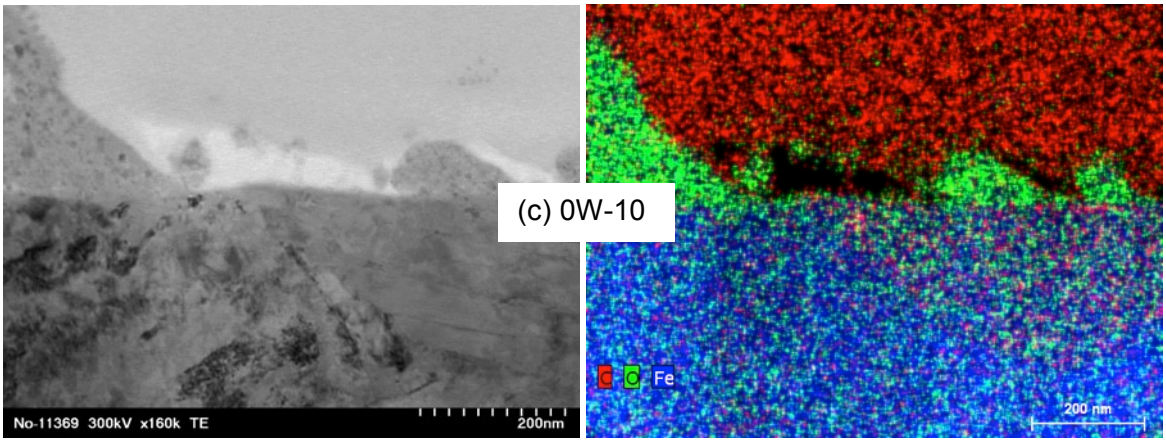


Fig. 2.7. TEM images and EDS element maps of the cross sections of the disc wear tracks tested in (a) [BMIM][$NTf_2$], (b) PAO 4 cSt base oil, and (c) 0W-10 racing engine oil.

### 2.3. Conclusion for the development of low-viscosity ionic liquids as neat lubricants

A low-viscosity ionic liquid [BMIM][$NTf_2$] was evaluated as a candidate lubricant. Its viscosity at 100 $^{o}$C is 4.7 cSt, similar to that of PAO 4 cSt base oil and 0W-10 racing engine oil, but it has a higher viscosity index than the oils. This IL is more thermally stable than hydrocarbon oils: it can sustain up to 472 $^{o}$C whereas most oils decompose at around 250 $^{o}$C. The lubricating performance of [BMIM][$NTf_2$] was benchmarked against that of the PAO and 0W-10 oils under both ML and BL. The ML friction coefficient of the IL was consistently lower than that of the oils by ~30%. This is possibly due to the IL's lower V-P coefficient and a hypothetical layered-structure boundary film. Although a low V-P coefficient usually is a challenge to BL, the IL exhibited higher scuffing resistance and less surface damage than did oils in the scuffing tests. This is attributed to the formation of a protective tribo-film in IL lubrication, which was revealed by FIB-aided cross-sectional TEM microstructural examination and EDS analysis.

## CHAPTER 3. Development of Oil-Miscible Ionic Liquids as Ashless Lubricant Additives

### 3.1. Design and synthesis of oil-miscible ILs and initial anti-wear performance

#### *3.1.1. Experimental*

Figure 3.1.1. shows the molecular structures of selected phosphonium-based ILs. Both cations and anions are in quaternary structures. The four PP-ILs have identical cations with varying anion structures.

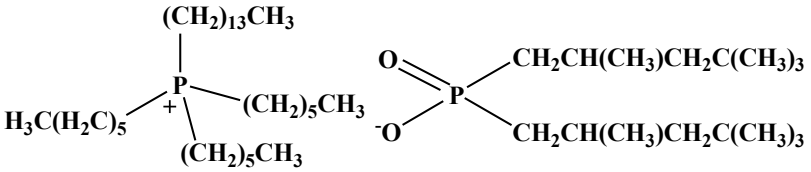


PP-IL1: Trihexyltetradecylphosphonium bis(2,4,4-trimethylpentyl) phosphinate ([$P_{66614}$][BTMPP])

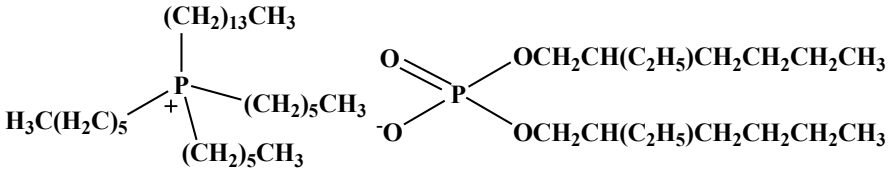


PP-IL2: Trihexyltetradecylphosphonium bis(2-ethylhexyl) phosphate ([$P_{66614}$][DEHP])

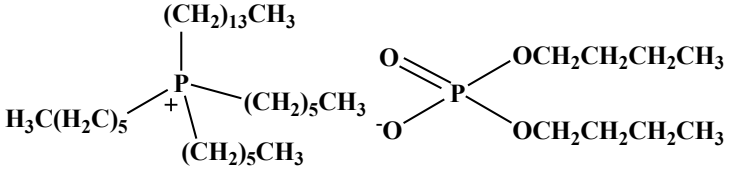


PP-IL3: Trihexyltetradecylphosphonium dibutyl phosphate

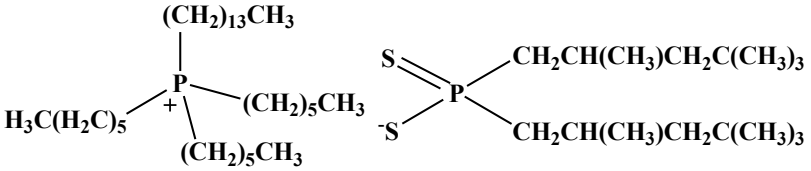


PP-IL4: Trihexyltetradecylphosphonium bis(2,4,4-trimethylpentyl) dithiophosphinate

Fig. 3.1.1. Molecular structures of selected phosphonium ILs.

All four PP-ILs were synthesized in our organic chemistry laboratory. Most feed stocks, including tetradecyl trihexyl phosphonium bromide, bis(2-ethylhexyl) hydrogen phosphate, and sodium hydroxide, were purchased from Aldrich. Bis(2,4,4-trimethylpentyl) phosphinic acid was kindly provided by Cytec Industries Inc., Canada. All solvents used in this study were analytical grade reagents. PP-IL1 was synthesized following the procedure described in Ref. 35. In summary, 4.760 g (0.1635 mol) bis(2,4,4-trimethylpentyl) phosphinic acid was first mixed with 9.216 g (0.1635 mol) tetradecyl trihexyl phosphonium bromide in 15 g hexane. A solution of 0.654 g (0.1635 mol) NaOH and 18g deionized water (18.2MΩcm) was then added dropwise into the reaction system and the mixture was stirred at room temperature over 4 hours. The organic phase of the mixture was separated and washed by distilled water three times. The solvent was removed by distillation and the product was dried under vacuum. The yield was ~95%. PP-ILs 2-4 were prepared using similar procedures as that for PP-IL1 and all four products are clear liquids and appear light yellow.

Thermogravimetric analysis (TGA) was carried out on a TA Instruments TGA-2950 at a 10 $^{o}$C/min heating rate in a nitrogen atmosphere. The mass density was determined by weighing a known volume, e.g., 1.0 mL, of each PP-IL. The uncertainty of the density was less than 5%. Kinematic viscosities of neat PP-ILs and oil-IL blends were measured in the temperature range of 0-100 $^{o}$C using a Petrolab MINIVIS II viscometer base on the falling-ball technique. A 0.5 mL of fluid was used in each test, and each measurement involved at least four-repeated ball dropping to ensure a <2% statistical deviation.

Three hydrocarbon lubricating oils were used in this work: Mobil 1$^{TM}$ synthetic poly-alpha-olefin (PAO) 4 cSt provided by Exxon Mobil Corp. and SAE 10W base oil and 10W-30 engine oil supplied by Chevron Corp. The 10W and 10W-30 oils are mineral oil based and are mixtures of alkanes.

The effectiveness of PP-IL1 as a lubricant additive was evaluated using a reciprocating sliding test on a Plint TE77 high-frequency tribometer. A segment (5–6 mm long) of a SAE 9254 steel engine piston ring was slid against a square specimen of 25.4 mm × 25.4 mm cut from a cast iron cylinder liner (provided by General Motors Corp.). Tests were conducted at room temperature (~23 ºC) under a normal load of 160 N and an oscillation frequency of 10 Hz with a 10 mm stroke for a sliding distance of 1000 m. Five drops of lubricant were introduced at the interface prior to testing and no additional lubricant was supplied during the test. The calculated thickness of the boundary lubricant film using the Hamrock-Dowson formula [33] was less than the composite roughness, indicating boundary lubrication. Each lubricant was tested twice: one with load ramping from 0 to 160 N during running-in and another under the maximum load from the beginning. The friction force was measured by a piezoelectric load cell and normalized by the normal load to calculate the friction coefficient. The wear volume was measured using a Wyko NT9100 3D optical profiler and normalized by the load and sliding distance to obtain the wear rate in units of mm$^3$/N-m.

A Hitachi$^{TM}$ S3400 scanning electron microscope (SEM) equipped with an energy-dispersive X-ray analyzer attachment was used to examine the morphology and chemical composition of the worn cast iron surfaces.

### *3.1.2. Results and Discussion*

The TGA curves of the phosphonium-based ILs and oils are shown in Fig. 3.1.2. The onset decomposition temperatures are 366, 349, 323, and 316 $^{o}$C, for PP-ILs 1-4, respectively. They are substantially higher than those (~250 $^{o}$C) for the three hydrocarbon lubricants. Interestingly, PP-ILs 2 and 3, which contain oxygen donors in their anion alkyl chains, had a two-step decomposition process. PP-IL4, which has similar structure to PP-IL1 but replaces the oxygen donors with sulfur donors, exhibited a slightly lower thermal stability than PP-IL1.

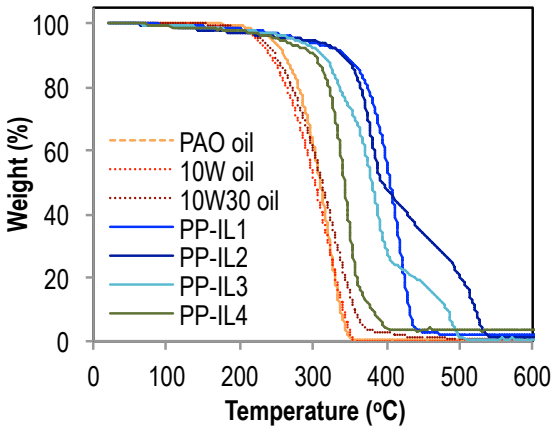


Fig. 3.1.2. TGA curves for PP-ILs and hydrocarbon oils.

Unlike many other ILs for which corrosion is a concern, PP-ILs 1 and 2 showed no corrosive attack to non-protected metals, such as grey cast iron and aluminum, in our tests at either room or elevated temperature. Fig. 3.1.3a shows a cast iron surface after exposure to PP-IL1 in an ambient environment for two months. The droplet spread over almost the entire surface indicating good wettability and remained on the surface due to its low vapor pressure. In contrast, common imidazolium ILs are found to corrode the cast iron in our tests. For example, Fig. 3.1.3b shows that a droplet of 1-benzyl-3-methylimidazolium bis(trifluoromethylsulfonyl)imide ([Bzmim][$NTf_2$]) caused pitting on a cast iron surface under ambient conditions (pitting observed after 2 days of exposure and photo taken on day 7). In addition, PP-IL1 has demonstrated its non-corrosiveness at elevated temperature. The surfaces of cast aluminum 319 and grey cast iron after being held in PP-IL1 at 135 $^{o}$C for seven days showed no signs of corrosion (Fig. 3.13c).


Fig. 3.1.3. PP-IL1 showed no corrosive attack to metals at either room or elevated temperatures. (a) Cast iron exposed to PP-IL1 under ambient conditions for 2 months, (b) Cast iron exposed to [Bzmim][$NTf_2$] at ambient for 7 days, and (c) Cast aluminum and cast iron dipped in PP-IL1 at 135 $^{o}$C for 7 days.

PP-ILs 1 and 2 were discovered to be fully miscible with many hydrocarbon oils. Specifically, these two PP-ILs can easily dissolve into base oils of both mineral based SAE 10W and synthetic PAO at any blend ratio. All blends (1-95 wt.% PP-IL 1 or 2 in oil) appear clear without clouds or phase separation by visual inspection at temperatures as low as -18 $^{o}$C and as high as 175 $^{o}$C and even after months of storage. In contrast, although having similar molecular structures, PP-ILs 3 and 4 showed relatively low solubility (<2 wt%) in oils.

In general, ions and non-polar neutral organic molecules are immiscible, because ions are attracted by polar forces and sometimes hydrogen bonding while non-polar molecules are held together by dispersion forces [37]. Most ILs reported in the literature have poor solubility in hydrocarbon lubricants. The exceptional oil-miscibility of the two phosphonium-based ILs 1 and 2 opens the door for using ILs as oil additives. It is hypothesized that the three-dimensional quaternary structures with high steric hindrance (long hydrocarbon chains) dilute the charge of the ions and therefore improve the compatibility with neutral oil molecules. In contrast, most ILs previously studied for lubrication contains two-dimensional imidazolium cations and/or small anions such as $BF_4$, and $PF_6$, and thus cannot dissolve in oils. As another example, the short alkyl chains on the anion of PP-IL3 are hypothesized to be responsible for its poor oil-solubility (<2 wt.%).

Although PP-IL4 has the identical cation and very similar anion to PP-IL1 with only two sulfur atoms substituting the oxygen donors on the anion, its solubility in oils appears much lower (<2 wt.%). This suggests the oxygen donors play a critical role. Since ions are good hydrogen-bond donors/acceptors because they are charged [38], one possibility is that the oxygen donors on the anion may form H···O bonds with the hydrocarbon alkyls on the cation and form a quasi-neutral molecule (loosely bonded

cation-anion), which becomes compatible with oil molecules. For PP-IL4, however, the possible H···S bonds are too weak to hold the cation and anion together. Similar observations for H···O and H···S bonds have been discussed for extractants containing dialkyloxothio- and dithiophosphinic acids [39]: oxygen donors enable dimerization through H···O bonds in organic solvents while the extractant with sulfur donors tends to be monomeric due to the weak H···S bonds. Determining the exact mechanism for the miscibility between ionic liquids and oils requires further investigation.

Table 3.1.1 presents the measured kinematic viscosities of selected hydrocarbon lubricating oils, neat PP-ILs, and oil-IL blends of different ratios at various temperatures between 0 and 100 °C. The neat PP-ILs are much more viscous than the oils and the blends' viscosities fall in between as expected.

Table 3.1.1. Density and kinematic viscosity of oils, ILs, and blends.

| Lubricant | Density (g/ml, 23 °C) | Kinematic viscosity (cSt) | | | | |
|---|---|---|---|---|---|---|
| | | 0 °C | 10 °C | 23 °C | 40 °C | 100 °C |
| PAO base oil | 0.80 | 119.0 | 67.8 | 34.5 | 17.6 | 3.7 |
| 10W base oil | 0.82 | 432.7 | 203.3 | 89.0 | 36.9 | 5.6 |
| 10W30 engine oil | 0.82 | 916.9 | 422.0 | 178.6 | 74.0 | 10.1 |
| PP-IL1 | 0.90 | *N/A* | *N/A* | 1149.7 | 388.8 | 35.4 |
| PP-IL2 | 0.91 | *NA* | *NA* | 1045.1 | 429.0 | 49.5 |
| PAO+PP-IL1(5%) | 0.81 | 124.6 | 73.7 | 36.6 | 18.3 | 3.8 |
| 10W+PP-IL1(5%) | 0.83 | 440.7 | 207.6 | 90.0 | 38.0 | 5.7 |
| PAO+PP-IL1(50%) | 0.85 | 662.2 | 335.1 | 158.3 | 72.2 | 10.5 |
| 10W+PP-IL1(50%) | 0.86 | 1149.4 | 514.5 | 218.2 | 85.9 | 10.4 |
| PAO+PP-IL2(5%) | 0.81 | 122.8 | 69.9 | 36.6 | 18.4 | 3.8 |
| 10W+PP-IL2(5%) | 0.83 | 430.2 | 202.5 | 88.9 | 37.1 | 5.7 |

*N/A – viscosity above the upper limit (1500 cP) of the measurable range of the instrument.*

For a blend of multiple-component liquids, the viscosity of the blend is a function of the individual viscosities of each component and the blend ratio, as defined by the Refutas equation (applicable only to single-phase solutions, not emulsions) [40]. A simplified version for oil-IL blends is shown below.

$$\upsilon_{blend} = \exp\left(\exp\left(\chi_{oil} \cdot ln\left(ln(\upsilon_{oil} + 0.8)\right) + \chi_{IL} \cdot ln\left(ln(\upsilon_{IL} + 0.8)\right)\right)\right) - 0.8 \quad (3.1.1)$$

where $\upsilon$ is the kinematic viscosity in centistokes, and $\chi_{oil}$ and $\chi_{IL}$ represent the mass fraction of oil and IL in the blend, respectively.

The measured and calculated viscosities for PP-ILs 1 and 2 mixed into the two base oils at different concentrations are compared in Fig 3.1.4. The good agreement confirms the oil-IL blends as single phase solutions, instead of emulsions whose viscosities do not follow the Refutas equation.

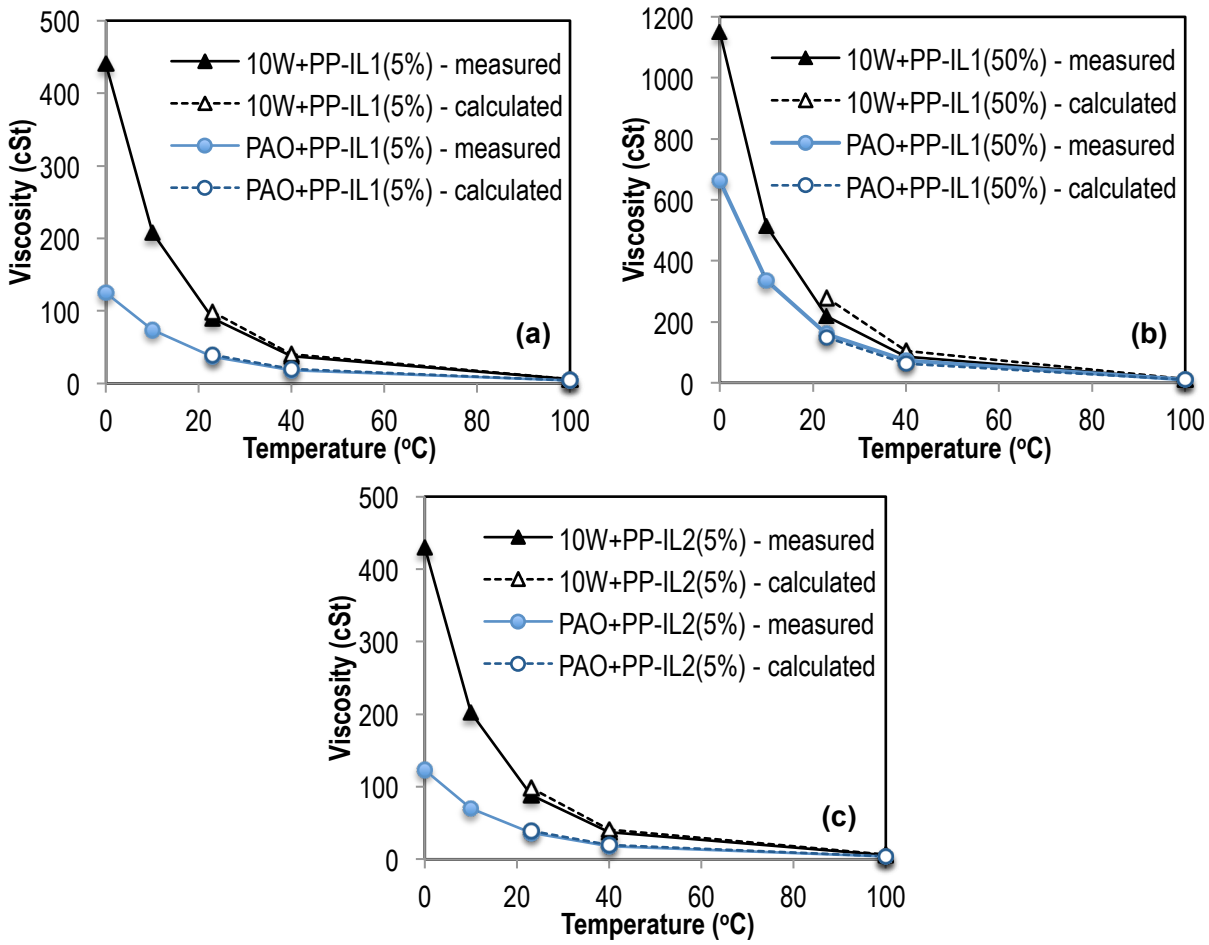


Fig. 3.1.4. Comparison of measured and calculated viscosities of oil-IL blends containing (a) 5 wt.% of PP-IL1, (b) 50 wt.% of PP-IL1, and (c) 5 wt.% of PP-IL2.

The lubricating performance of two oil-IL blends, 10W base oil+5 wt.% PP-IL1 and SAE 10W-30 engine oil+5 wt.% PP-IL1, was evaluated using the cross ring-on-liner reciprocating sliding test described above. Figure 3.1.5 compares the variation in coefficient of friction (COF) during the course of sliding with and without load ramping. For the tests conducted with 10W base oil, the friction coefficient quickly increased above 0.2 in both cases, indicating scuffing – a catastrophic lubrication failure. Both tests were terminated when scuffing occurred. Wear measurements of the liner surfaces in Table 3.1.2 showed a high wear rate of $4.9 \times 10^{-5}$ $mm^3/N\text{-}m$ with load ramping and a 3x higher wear rate without load ramping. In contrast, the addition of 5 wt% PP-IL1 prevented the scuffing failure and the friction coefficient was very stable ~0.1, a typical value for boundary lubrication. Besides friction reduction, the IL additive when added into the 10W base oil reduced the wear rate significantly by 2-3 orders of magnitude, as seen in Table 3.1.2.

It was also observed that the 10W+5% PP-IL1 blend had similar friction behavior and even less material loss compared to the fully formulated 10W-30 engine oil (see Fig. 3.1.5 and Table 3.1.2). Considering the oil-IL blend has a much lower viscosity than the 10W-30 engine oil, such lubricating performance is very encouraging. In addition, the blend of 10W-30 oil+PP-IL1 provided the best wear protection as shown in Table, which suggests a synergistic effect between PP-IL1 and the existing anti-wear additives in the engine oil.

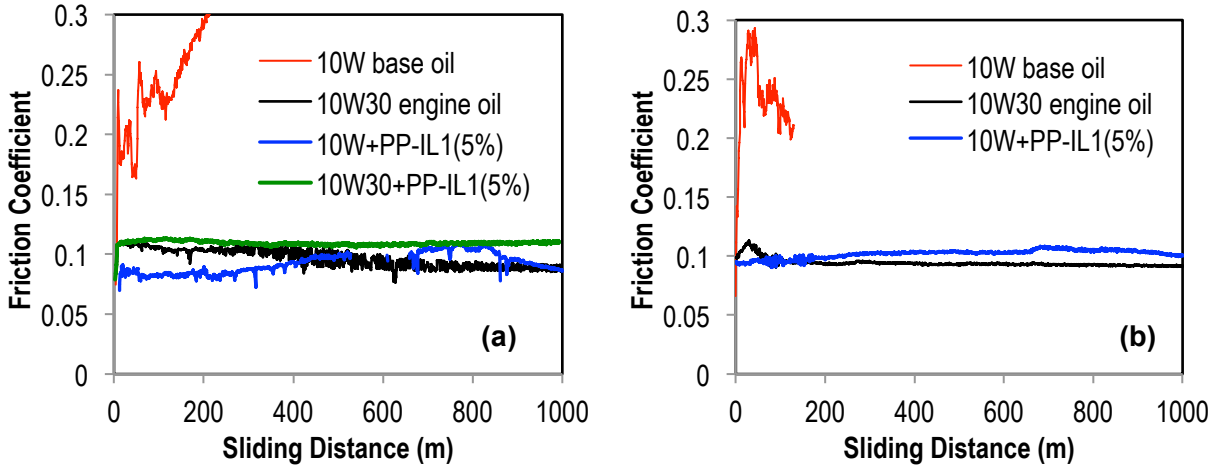


Fig. 3.1.5. Comparison of friction behavior showing significant improvement when adding 5 wt.% PP-IL1 into the SAE 10W base oil. (a) with load ramping and (b) without load ramping.

Table 3.1.2. Comparison of wear rates.

| Lubricant | Viscosity (cSt, 23 °C) | Liner wear rate ($10^{-7}$ mm$^3$/N-m) | |
|---|---|---|---|
| | | w/ load ramping | w/o load ramping |
| 10W base oil | 89.0 | 490 | 1660 |
| 10W+PP-IL1(5%) | 90.0 | 4.7 | 7.5 |
| 10W30 engine oil | 178.6 | 9.0 | 9.9 |
| 10W30+PP-IL1(5%) | 193.5 | 2.5 | *Not tested* |

Figure 3.1.6 shows the SEM morphologies of worn scar on cast iron surface lubricated by the 10W base oil, 10W30 engine oil, and 10W+5% PP-IL1, respectively. The worn surface lubricated by the 10W base oil in Fig. 3.1.5a presents severe grooving and plastic deformation associated with scuffing damage corresponding to the fast friction transition in Fig. 3.1.5. When PP-IL1 was added into the 10W base oil, the scuffing damaged was eliminated and the worn surface was relatively smooth and dominated by mild abrasive wear (Fig. 3.1.6b). The phosphor compounds in EDS spectrum (Fig. 3.1.6e) implies a boundary film on the worn scar probably due to tribo-chemical reactions between the PP-IL1 and the metal surface. On the surface lubricated by the 10W-30 engine oil (Fig. 3.1.6c), no scuffing damage was observed (note: the porosity is inherent for the cast iron, not caused by the tribo-testing) and the worn surface is covered by a dark color boundary film. The EDS detected phosphor contents indicates the involvement of the zinc-dialkyl-dithiophosphate (ZDDP) anti-wear additive of the engine oil in the boundary film formation (Fig. 3.1.6e). It is interesting to observe a high molybdenum signal, which suggests substantial material transfer (adhesive wear) from the ring surface that was thermal-sprayed with a Mo layer. In contrast, the addition of the PP-IL1 into the 5W-30 engine oil minimized the molybdenum content (Fig. 3.1.6e) and the worn surface appeared smoother, implying reduced adhesion. The initial bench tribo-test results suggested great potential for using PP-IL1 as an oil additive for scuffing prevention and wear reduction.

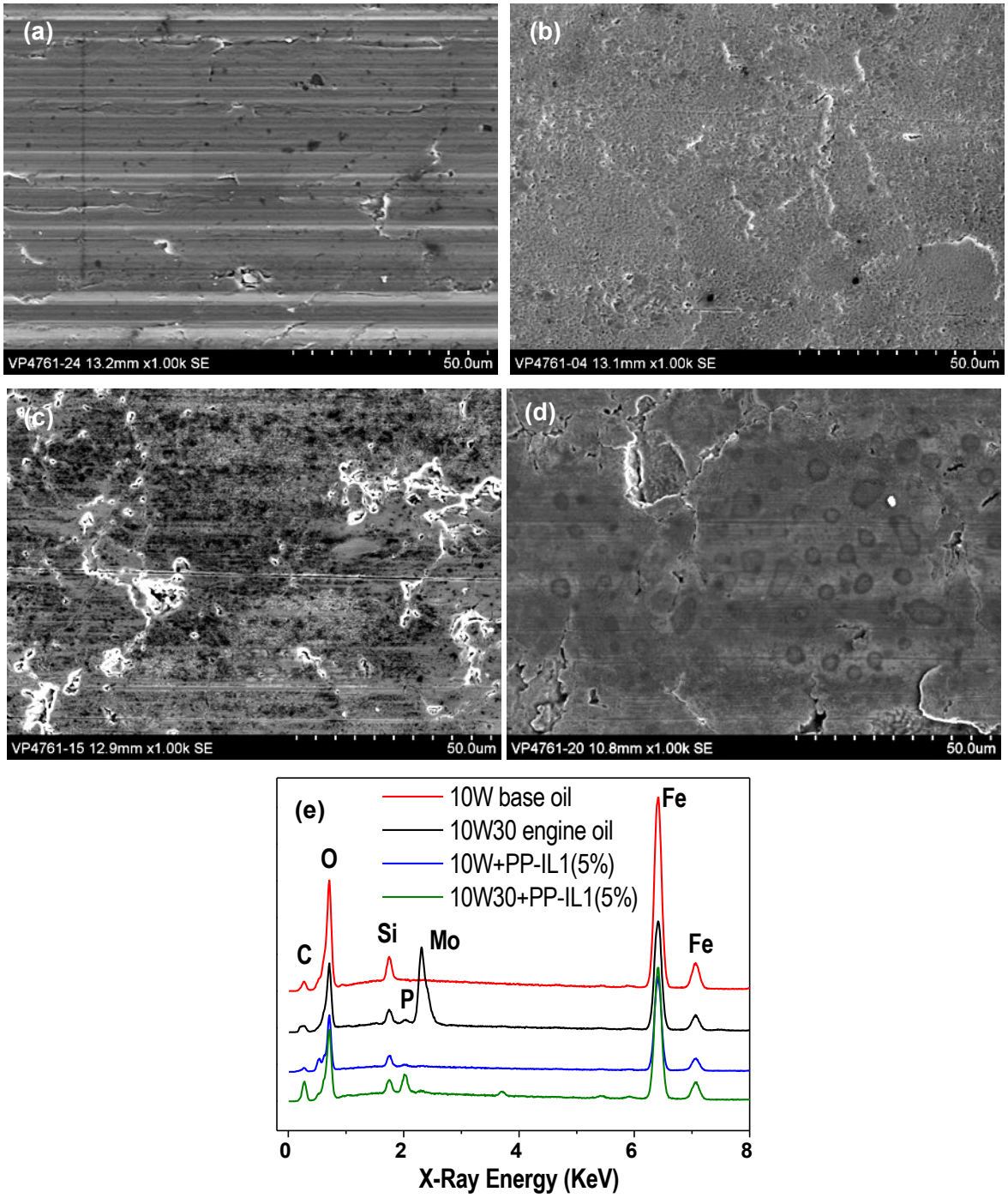


Fig. 3.1.6. SEM images of the cast iron worn surfaces lubricated by (a) 10W base oil, (b) 10W+PP-IL1(5%), (c) 10W-30 engine oil, and (d) 10W30+PP-IL1(5%), and (e) EDS spectra of the worn surfaces.

### 3.2. Anti-Wear Performance and Mechanism of [$P_{66614}$][DEHP]

#### *3.2.1. Experimental*

Two hydrocarbon lubricating oils were used as base stock as well as baseline lubricants: (1) Mobil 1™ synthetic poly-alpha-olefin (PAO) 4 cSt and (2) fully-formulated Mobil 1™ SAE 5W-30 engine oil, which were kindly provided by Exxon Mobil Corp. Two oil-IL blends were prepared by adding 5 wt.% [$P_{66614}$][DEHP] into the PAO base oil and the SAE 5W-30 engine oil, respectively.

The corrosivity of [$P_{66614}$][DEHP] was investigated in both exposure tests and electrochemical evaluation. In the exposure test, a droplet of this IL was placed on a cast iron liner sample surface under ambient conditions for two months. The electrochemical measurement was conducted on a Gamry Instruments™ Reference 600 Potentiostat/Galvanostat/ZRA to generate a potentiodynamic polarization curve. The cast iron working electrode had an exposed surface area of 0.61 $cm^2$ against a Pt counter electrode. Due to the small volume of fluid (~10 ml), Pt was used as a quasi-reference. The potential from -0.5 to 0.5 was scanned with a rate of 1 mV/s.

An optical tensiometer (KVS Instruments™ Theta T200) was used to measure the contact angles of the IL and oils on grey cast iron and AISI 52100 steel surfaces to compare their wetting performance, which is an important criterion for lubricant evaluation. Since the contact angle is sensitive to surface condition, such as flatness, roughness, and cleanliness, all surfaces were prepared using the same metallographic polishing procedure to control the roughness in a narrow range of $R_a$ = 20–30 nm.

The tribological performance of the IL additive in oil was evaluated using a reciprocating sliding test on a Plint TE77 (Phoenix Tribology Ltd) high-frequency tribometer. The upper and lower specimens were cut from an engine piston steel ring and cast iron cylinder liner, respectively, provided by General Motors Corp. Tests were conducted at room temperature (~23 ºC) under a normal load of 160 N and an oscillation frequency of 10 Hz with a 10 mm stroke for a sliding distance of 1000 m. This set of testing conditions were chosen to simulate the contact pressure and sliding speed at the top-ring-reversal region of the piston ring-cylinder liner interface. Based on the lubricant film thickness calculation [33], all tests were under boundary lubrication. At least two replicates were run for each lubricant. The friction coefficient was monitored in-situ by capturing the tangential force (using a piezoelectric load cell) that was then divided by the normal load, and the wear rate, expressed in units of $mm^3$/N-m, was quantified by measuring the wear volume (using a 3D optical interferometer Wyko™ NT9100) and normalized by the load and sliding distance.

The worn surface morphology was examined using a Hitachi™ S-4800 field emission scanning electron microscope (SEM). Transmission electron microscopy (TEM), electron diffraction, and energy dispersive X-ray spectroscopy (EDS) were used in cross section examination to study the nanostructure and composition of the surface boundary film as well as the plastic deformation zone below it. The TEM samples were prepared using a FEI Nova 200 Dual-beam Focused Ion Beam (FIB) System with a Ga source to extract a thin cross-section of the near-surface zone from the wear scar of each specimen. The TEM system was a Hitachi™ HF-3300 TEM/STEM at 300 kV (1.3 Å resolution) equipped with a Bruker solid state EDS detector with a 30 $mm^2$ window.

#### *3.2.2. Results and Discussion*

##### *3.2.2.1. Density, viscosity, and thermal stability*

The densities at room temperature, viscosities from zero to 100 $^oC$, and TGA-determined decomposition temperatures for [$P_{66614}$][DEHP], PAO and 5W-30 oils, and their blends are summarized in Table 3.2.1. The IL has a slightly higher density (0.91 g/cc) but is much more viscous compared with the oils. [$P_{66614}$][DEHP] is hydrophobic and stable in presence of water. No noticeable degradation, e.g., discoloration, was observed when exposed to air at room temperature based on a 2-month exposure test. When heated, [$P_{66614}$][DEHP] is more stable than hydrocarbon oils. TGA tests in a $N_2$ environment

revealed an onset decomposition temperature of 347 °C for [$P_{66614}$][DEHP] versus 250 and 263 °C for the PAO base and SAE 5W-30 engine oils, respectively.

Table 3.2.1. Comparison of decomposition temperature, density, and kinematic viscosity.

| Lubricant | Decomp. temp. (°C) | Density (g/ml 23 °C) | Kinematic viscosity (cSt) | | | | |
|---|---|---|---|---|---|---|---|
| | | | 0 °C | 10 °C | 23 °C | 40 °C | 100 °C |
| PAO 4 cSt base oil | 250 | 0.80 | 119.0 | 67.8 | 34.5 | 17.6 | 3.7 |
| 5W-30 engine oil | 263 | 0.80 | 593.0 | 299.8 | 140.9 | 63.3 | 10.5 |
| [$P_{66614}$][DEHP] | 347 | 0.91 | *NA* | *NA* | 1045.1 | 429.0 | 49.5 |
| PAO+IL(5 wt.%) | *NM* | 0.81 | 122.8 | 69.9 | 36.6 | 18.4 | 3.8 |
| PAO+IL(50 wt.%) | *NM* | 0.86 | 752.8 | 391.9 | 187.1 | 88.3 | 13.0 |
| 5W-30+IL(5 wt.%) | *NM* | 0.81 | 653.7 | 325.3 | 149.9 | 65.8 | 10.5 |

*NA – viscosity above the upper limit (>1500 cP) of the measurable range of the instrument.*
*NM – not measured.*

*3.2.2.2. Corrosivity and wettability*

Unlike many other ILs for which corrosion is a concern due to their ionic nature, [$P_{66614}$][DEHP] showed no corrosive attack to non-protected metals. An active-passive behavior was observed in the electrochemical corrosion test. The potentiodynamic polarization curve in Fig. 3.2.1 shows an active dissolution behavior from $E_{corr}$ at -0.43 V to -0.38 V followed by a region of weak passivation and a transpassive region, beyond which a second passive-transpassive cycle appears. In a simple exposure test, no pitting was observed on a cast iron surface that had a droplet of [$P_{66614}$][DEHP] on it for two months (the end of test). [$P_{66614}$][DEHP] is not only non-corrosive itself, but also help prevent rusting by its strong hydrophobicity.

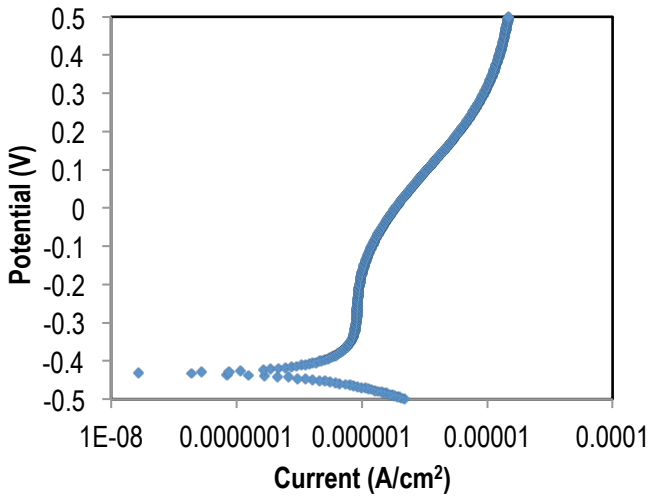


Fig. 3.2.1. Potentiodynamic polarization curve of cast iron in [$P_{66614}$][DEHP].

[$P_{66614}$][DEHP] showed excellent wetting behavior on grey cast iron and AISI 52100 bearing steel surfaces with contact angles of 7.6° and 20.7°, respectively. Its wettability is significantly better than

common imidazolium- and ammonium-based ILs [7] and slightly outperforms the lubricating oils, as seen in Table 3.2.2.

Table 3.2.2. Comparison of contact angles.

| Lubricant | Grey cast iron | AISI 52100 steel |
|---|---|---|
| PAO 4 cSt base oil | 13.0 | 22.4 |
| 5W-30 engine oil | 9.0 | 23.9 |
| $[P_{66614}][DEHP]$ | 7.6 | 20.7 |
| $[C_{10}mim][Tf_2N]$ (Ref. 7) | 33.9 | 29.0 |
| $[C_8H_{17}]_3NH][Tf_2N]$ (Ref. 7) | 22.2 | 16.2 |

*3.2.2.3. Oil-miscibility*

$[P_{66614}][DEHP]$ was found to be fully miscible with a variety of hydrocarbon lubricating oils, both petroleum-derived, such as SAE 10W base oil and SAE 10W30 engine oil, and synthetic, such as Mobil 1™ PAO base oil and SAE 5W-30 engine oil, and Royal Purple™ SAE 0W-10 racing engine oil. All oil-IL blends appear clear without clouds or phase separation by visual inspection over a large temperature range (from -18 to 175 °C). Most oils had no apparent color change after being blended with $[P_{66614}][DEHP]$, except for Mobil 1™ 5W-30 oil which changed from light brown to red (oil remaining clear) implying some reaction between $[P_{66614}][DEHP]$ and existing oil additives. Fig. 3.2.2 compares the measured viscosities for PAO-IL blends in 95:5 and 50:50 ratios with the computed values using the Refutas equation [40] that was derived for single-phase multiple-component liquids. The relatively good agreement confirms the oil-miscibility of $[P_{66614}][DEHP]$.

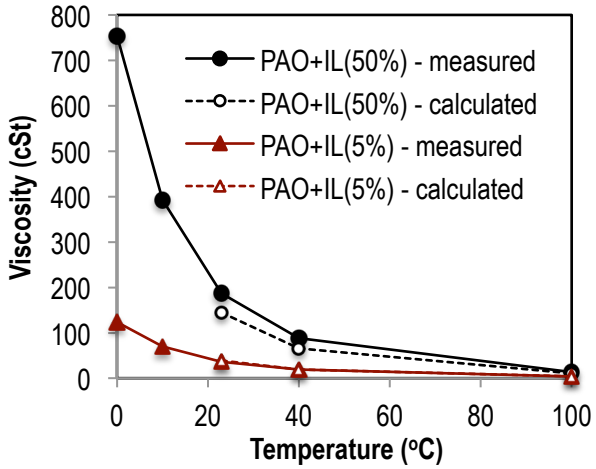


Fig. 3.2.2. Measured viscosities of oil-IL blends compared with calculated values using Refutas equation.

In general, ions and non-polar neutral organic molecules are immiscible, because ions are attracted by polar forces while non-polar molecules are held together by dispersion forces. The exceptional oil-miscibility of $[P_{66614}][DEHP]$ is hypothesized to attribute to its three-dimensional quaternary structures with high steric hindrance (long hydrocarbon chains) that dilute the charge of the ions and therefore improve the compatibility with neutral oil molecules. In contrast, most ILs studied in the literature contain

either two-dimensional cations, e.g., imidazolium-based, or small anions, e.g., bis(tifluoromethylsulfonyl)imide ($Tf_2N$), and thus cannot dissolve in oils. Our experiments also found that, in addition to the quaternary structures, an oil-miscible IL needs to contain at least one alkyl with four carbons or more for both the cation and the anion. The phosphate IL reported by Mori's group in [41] has a similar structure to $[P_{66614}][DEHP]$ but its alkyls on the anion are so short (one carbon each) that we suspect a limited solubility in oils.

*3.2.2.4. Anti-scuffing and anti-wear functionality*

The lubricating performance of the oil-IL blends was benchmarked against that of the PAO and 5W-30 synthetic oils. The friction curves and wear rates are presented in Fig. 3.2.3 and Table 3.2.3, respectively. Each curve or data point represents the average value from two tests.

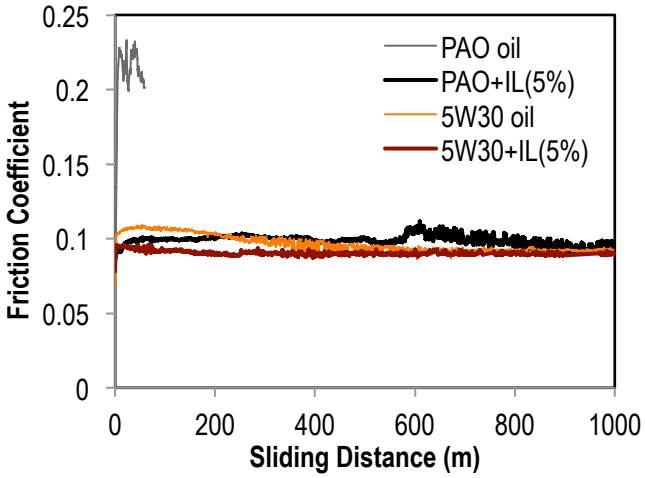


Fig. 3.2.3. Friction behavior of oils with and without addition of $[P_{66614}][DEHP]$.

Table 3.2.3. Comparison of wear rates.

| Lubricant | Viscosity (cSt, 23 °C) | Wear rate ($mm^3$/N-m) | |
|---|---|---|---|
| | | Liner | Ring |
| PAO 4 cSt base oil | 34.5 | $5.9\pm4.7\times10^{-4}$ | $>1.0\times10^{-6}$ |
| PAO+IL(5%) | 36.6 | $5.6\pm3.5\times10^{-7}$ | $1.4\pm0.5\times10^{-8}$ |
| 5W-30 engine oil | 140.9 | $4.7\pm0.3\times10^{-7}$ | $6.6\pm4.9\times10^{-9}$ |
| 5W-30+IL(5%) | 149.9 | $1.3\pm0.2\times10^{-7}$ | $2.0\pm1.6\times10^{-9}$ |

The friction coefficient for the PAO oil started around 0.1, but quickly transitioned to above 0.2 and then fluctuated between 0.2 and 0.25. This sharp friction transition is a classic indication of lubrication failure leading to contact surface scuffing and the following high fluctuation at a high friction level implies the propagation of scuffing damage. The dominating flake-like features on the worn liner surface (Fig. 3.2.4a) confirmed the scuffing-associated adhesive wear and plastic deformation. In contrast, the PAO-IL blend produced a relatively stable friction coefficient around 0.1 throughout the entire test (Fig. 3.2.3) and the wear scar showed mild abrasive wear with no scuffing damage (Fig. 3.2.4b). As compared in Table 3.2.3, the wear rates of the rubbing metallic surfaces were three orders of magnitude in difference for the PAO oil with and without the IL additive.

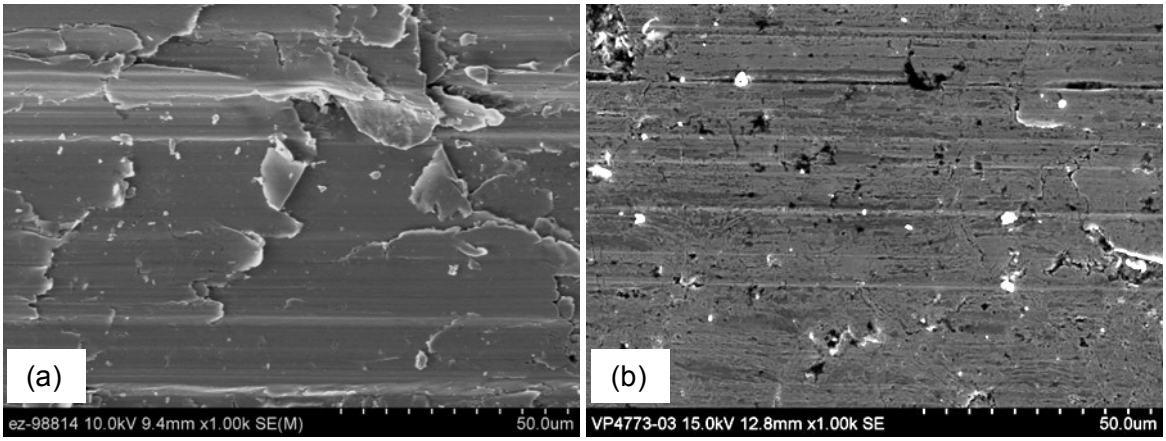


Fig. 3.2.4. SEM images of the worn cast iron surfaces lubricated by (a) PAO oil and (b) PAO+IL(5%).

In spite of being only a single additive blend, PAO+IL(5%) performed nearly as well as the fully formulated 5W-30 engine oil in both friction and wear perspectives (Fig. 3.2.3 and Table 3.2.3). It is worth noting that the PAO-IL blend has a much lower viscosity (36.6 cSt) compared to the 5W-30 engine oil (140.9 cSt). This suggests that the IL additive may potentially allow the usage of lower viscosity engine oil, which in turn improves the engine efficiency by reducing churning losses.

$[P_{66614}][DEHP]$ was also added into the 5W-30 engine oil to investigate its compatibility with a commercial oil additive package. While little change was observed in friction behavior, the wear rates were decreased by ~70% for both sliding surfaces (Table 3.2.3). This implies a possible synergistic effect between the IL and the existing anti-wear additives, especially zinc-dialkyl-dithiophosphate (ZDDP) [3].

The anti-wear mechanism of ZDDP is to form a protective boundary film on a metallic bearing surface in a thickness from tens to a couple of hundred nanometers [3,36]. IL-produced tribo-boundary films were also detected on both ferrous and aluminum surfaces, and their thicknesses, nanostructures, and compositions have recently been reported to be material dependent [26].

In this study, screening EDS chemical analysis from the top surface (under SEM) was first conducted and the spectra indicated P content on the wear scar lubricated by PAO+IL, and P, S, and Zn on the wear scar lubricated either by the 5W-30 engine oil or by the 5W-30+IL blend. No phosphor was detected outside the wear scar. This is in line with the literature observation that tribo-film formation requires thermo-mechanical excitations [3,26,36]. Cross-sectional TEM examination and EDS chemical analysis were then conducted on the cast iron worn surfaces to provide in-depth characterization of the tribo-boundary films.

The TEM image in Fig. 3.2.5a shows a cross section of the near surface region underneath the wear scar lubricated by PAO+IL(5%). It clearly shows a two-layer structure including a top tribo-boundary film (120-180 nm) and a subsurface plastic deformation zone (0.5-0.8 μm) with a refined grain structure. This protective boundary film is believed to be responsible for the anti-scuffing/anti-wear functionality provided by the IL additive. The higher-magnification image of the boundary film in Fig. 3.2.5b (corresponding to the red dashed box in Fig. 3.2.5a) reveals an amorphous matrix embedded with fine nanoparticles (1-10 nm in diameter), and the electron diffraction pattern (insert in Fig. 3.2.5b) confirms the nanocomposite phase structure. The EDS element mapping in Fig. 3.2.5c (corresponding to the blue dashed box in Fig. 3.2.5a) shows high concentrations of P, O, and Fe in the boundary film as a result of interactions between the IL and the metal surface.

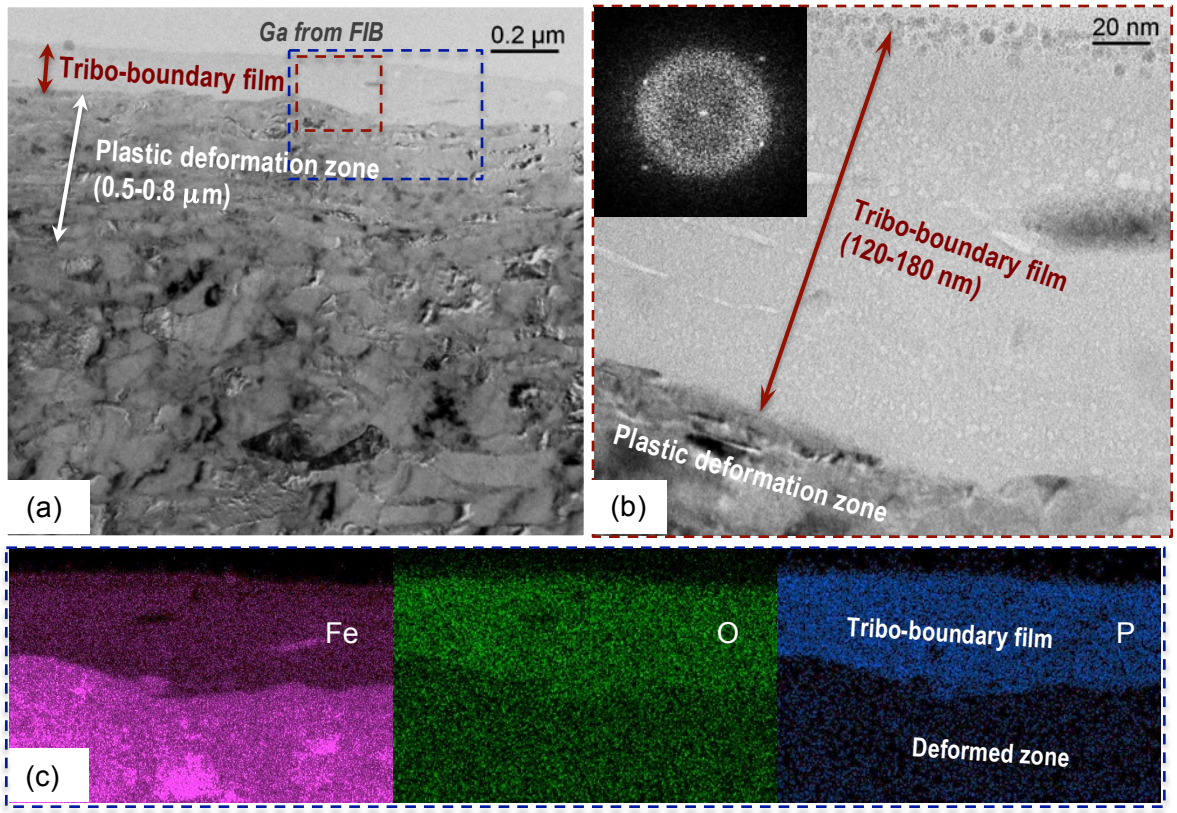


Fig. 3.2.5. (a-b) TEM imaging and (c) EDS element mapping on the cross section of the near surface zone of a cast iron worn surface lubricated by PAO+IL(5%). (b) and (c) corresponding to the red dash line box and blue dot line box marked on (a), respectively.

For comparison, the cross-sectional TEM examination and EDS analysis for the worn surface lubricated by the 5W-30 engine oil are shown in Fig. 3.2.6. A similar two-layer structure was observed with a tribo-boundary film in the thickness of 40-60 nm and a subsurface deformation zone in the thickness of 0.9-1.2 μm. The boundary film is dominated by an amorphous phase containing nanocrystals, as revealed by the high magnification TEM image and electron diffraction pattern in Fig. 3.2.6b. High concentrations of Zn and S in the tribo-boundary film (Fig. 3.2.6c) suggest a contribution from the oil additive package, specifically ZDDP, to film formation. However, little P (another active element of ZDDP) was detected.

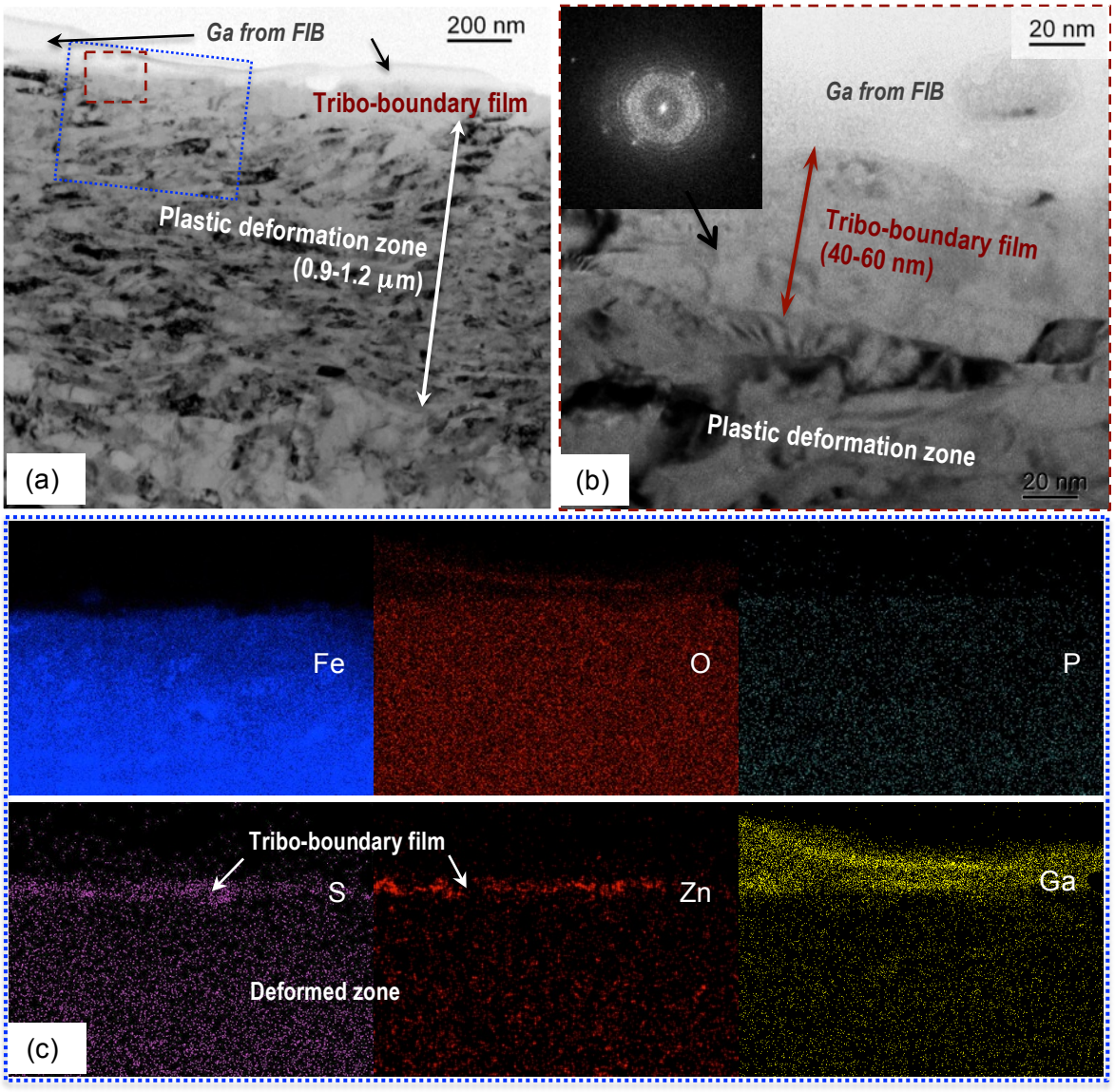


Fig. 3.2.6. (a-b) TEM imaging and (c) EDS element mapping on the cross section of the near surface zone of a cast iron worn surface lubricated by SAE 5W-30 engine oil. (b) and (c) corresponding to the red dash line box and blue dot line box marked on (a), respectively.

Figure 3.2.7 shows the nanostructure and chemical composition of the tribo-boundary film (250-350 nm) and plastic deformation zone (1.8-2.3 μm) when both $[P_{66614}][DEHP]$ and ZDDP were present (5W-30+5%IL). Again the boundary film is nanocomposite in nature (amorphous matrix containing nanocrystals). According to the EDS element mapping in Fig. 3.2.7c, this tribo-boundary film is rich in S and Zn as well as P. This suggests involvement of both $[P_{66614}][DEHP]$ and ZDDP in film formation, which confirms their synergistic effects on wear reduction (Table 3.2.3).

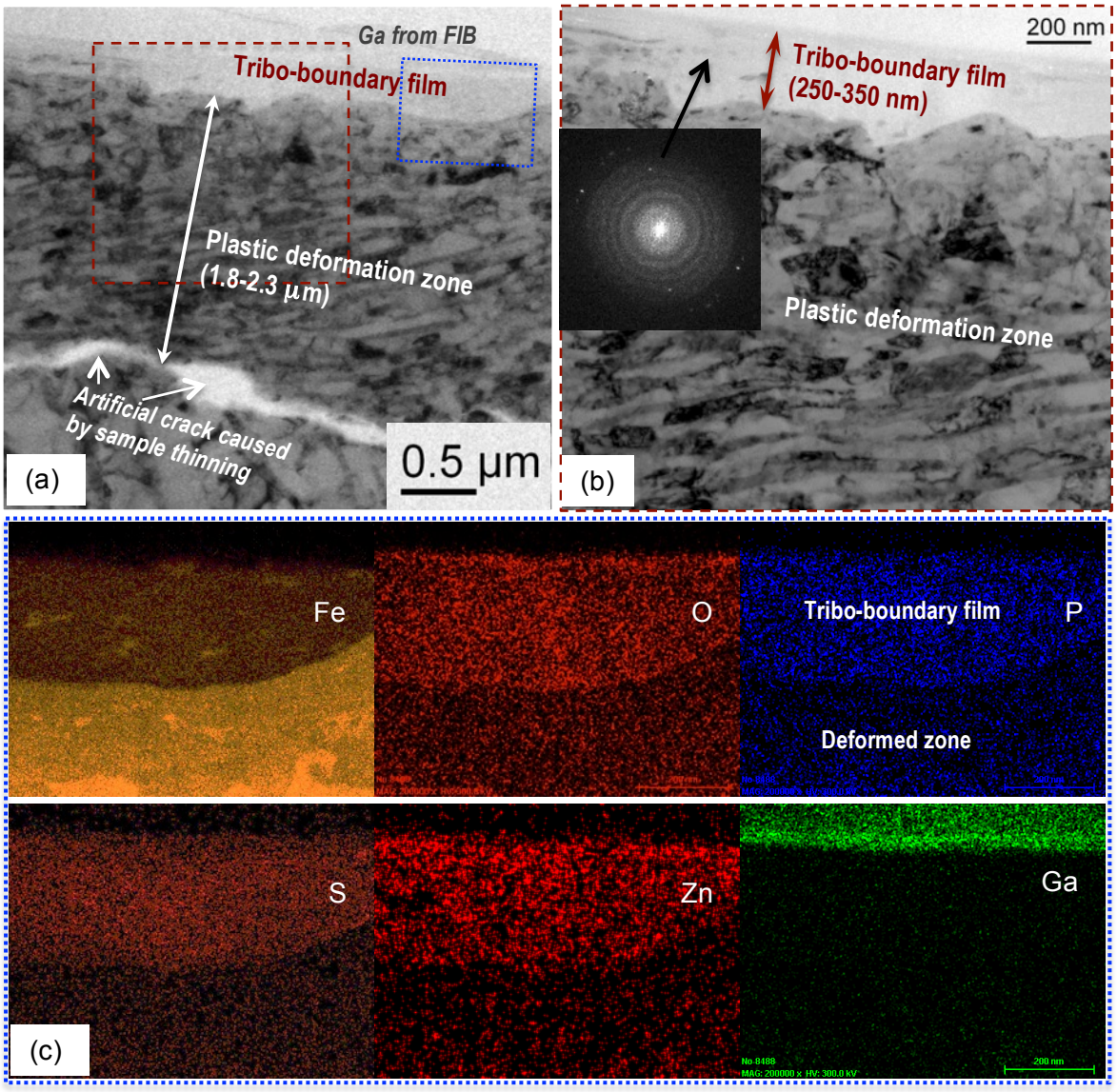


Fig. 3.2.7. (a-b) TEM imaging and (c) EDS element mapping on the cross section of the near surface zone of a cast iron worn surface lubricated by 5W-30+IL(5%). (b) and (c) corresponding to the red dash line box and blue dot line box marked on (a), respectively.

Although the three surfaces described above have similar layered structures, the layer thicknesses are quite different:

- Tribo-boundary film: ZDDP < IL < ZDDP+IL
- Plastic deformation zone: IL < ZDDP < ZDDP+IL

Although localized layer thickness measurement may not be representative (sampling is always an issue for TEM examination), the trend is worth noting. It is known that ZDDP requires high contact pressure and/or elevated temperature to break down into $Zn^{2+}$ and dialkyl-dithiophosphate ($DDP^{-}$) before reacting with the metallic surface to form a boundary film [3,36]. In contrast, the IL additive is naturally in an ionic form, which may allow a more efficient film formation process than ZDDP – leading to a

thicker boundary film. The thickness of the film formed in ZDDP+IL is more than the sum of the two formed separately.

The thickness difference in the plastic deformation zones may be explained by energy dissipation. Wear (localized fracture and delamination) and plastic deformation are the two major energy dissipation sources in steady-state sliding dominated by plowing rather than adhesion [42]. Since non-scuffed lubricated sliding usually involves little adhesion, all frictional energy in the tests could be assumed to dissipate through material removal and plastic deformation. The steady-state friction coefficients of these three lubricants were comparable (Fig. 3.2.3), meaning there was a similar amount of energy input. Thus, one can expect a lower wear rate coupled with a thicker plastic deformation layer, which has been confirmed by measurements: the wear rates for these three tests is ranked as IL > ZDDP > ZDDP+IL (Table 3), which is in the opposite order of deformation zone thicknesses (Figs. 3.2.5, 3.2.6, and 3.2.7).

## 3.3. $[P_{66614}]$[DEHP] benchmarked against ZDDP

### *3.3.2. Experimental*

Mobil 1$^{TM}$ poly-alpha-olefin (PAO) 4 cSt base oil, provided by Exxon Mobil Corp., was used as the base oil in this study. A secondary ZDDP, supplied by the Lubrizol Company, was used as the baseline anti-wear additive to compare with the IL. The treat rate was 1.0 wt% for either additive.

Thermogravimetric analysis (TGA) was carried out on a TA Instruments TGA-2950 at a 10 $^{o}$C/min heating rate in air to represent the oxidation that is inevitable in actual engine applications. Kinematic viscosities of $[P_{66614}]$[DEHP], ZDDP, and oil-additive blends were measured at 23, 40, and 100 $^{o}$C using a Petrolab MINIVIS II viscometer.

The tribological evaluation was conducted using a reciprocating sliding test on a Plint TE77 (Phoenix Tribology Ltd) high-frequency tribometer. The specimens were cut from actual engine piston top rings (with a plasma-sprayed coating) and grey cast iron cylinder liners, provided by General Motors. As shown in Fig. 3.3.1, 5–7 mm long segments were sliced from the piston ring as the top sliders and coupons in 25.4×25.4 mm$^2$ (1×1 in.) were cut from the cylinder liner as the bottom specimens. The ring had an average uncompressed outer diameter of 98 mm and a crown curvature of 8.0 mm in radius. The liner's nominal inner diameter was 94 mm. The test configuration is shown in Fig. 3.3.2, where the ring is oriented 90$^{o}$ with respect to the actual orientation in the engine to enable point contact to eliminate the alignment issue.

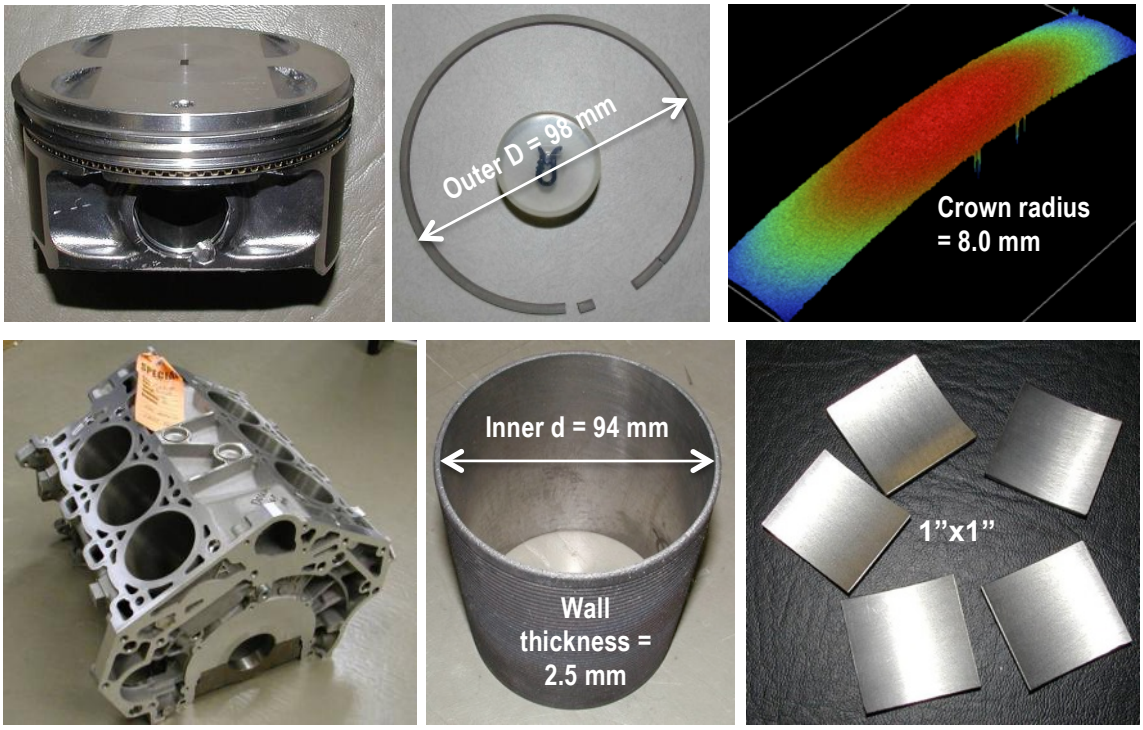


Fig. 3.3.1. Test coupons cut from actual engine piston rings and cylinder liners.

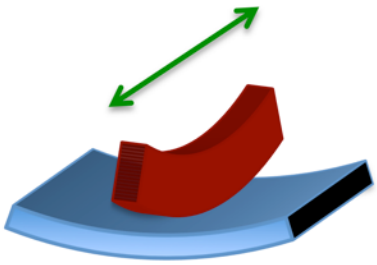

Fig. 3.3.2. Schematic of the ring-on-liner test configuration.

The IL- and ZDDP-additized oils were evaluated and benchmarked at both RT and 100 $^{o}$C (HT) to mimic engine cold start and normal operation temperatures, respectively. The RT tests were conducted under a normal load of 160 N for 1000 m of sliding or terminated when scuffing occurred (friction coefficient >0.2). In the HT tests, a higher load of 240 N and a longer sliding distance of 4320 m (or early termination at the onset of scuffing) were applied. Both RT and HT tests used an oscillation frequency of 10 Hz with a 10 mm stroke. Based on the Hamrock and Dowson formula [33], the maximum (stroke midpoint) central lubricant film thickness ($h_c$) was estimated to be 0.16 μm at RT and 0.03 μm at HT at the beginning of testing. The root-mean-square roughness of the ring ($R_{q,ring}$) and liner ($R_{q,liner}$) surfaces is 1.63 and 0.72 μm, respectively, which result in a composite roughness ($\sigma = \sqrt{R_{q,ring}^2 + R_{q,liner}^2}$) of 1.78 μm at contact. Therefore, the maximum $\lambda$-ratios ($\lambda = h_c/\sigma$) are 0.09 at RT and 0.02 at HT, ensuring boundary lubrication ($\lambda<1$) [33]. At least two replicates were run for each test condition. The tangential force was monitored in situ using a piezoelectric load cell and divided by the normal load to calculate the friction coefficient. The wear rate was quantified by measuring the wear volume (using an optical interferometer Wyko$^{TM}$ NT9100) and normalized by the load and sliding distance (in units of mm$^3$/N-m).

The morphology and chemical compositions of the ring and liner surfaces before and after tribo-testing were examined using a Hitachi™ S-4800 field emission scanning electron microscope (SEM) equipped with energy-dispersive x-ray spectroscopy (EDS). Cross-sectional transmission electron microscopy (TEM), electron diffraction, and EDS element mapping were used to study the IL tribo-films formed in an HT test. TEM samples were prepared using a FEI Nova 200 dual-beam focused ion beam (FIB) system with a gallium source to extract a thin cross-section of the near-surface zone from the wear scar of each specimen. Two TEM systems were used: an aberration-corrected FEI Titan S 80-300 TEM/STEM equipped with a Gatan Image Filter Quantum-865 and a Hitachi™ HF-3300 TEM/STEM equipped with a Bruker solid state EDS detector.

### *3.3.3. Lubricants and Materials Characterization*

#### *3.3.3.1 Viscosity of lubricants*

The viscosities of the PAO base oil, [$P_{66614}$][DEHP], ZDDP, and the two oil-additive blends are shown in Table 3.3.1. The IL and ZDDP, though viscous themselves, only marginally increased the viscosity of the oil due to the low treat rate (1.0 wt%).

Table 3.3.1. Densities and viscosities of the base oil, neat additives, and oil-additive blends

| | 23 °C | | 40 °C | 100 °C |
|---|---|---|---|---|
| | $\rho$ (g/cc) | $\eta$ (cSt) | $\eta$ (cSt) | $\eta$ (cSt) |
| PAO 4 base oil | 0.80 | 34.5 | 17.6 | 3.9 |
| [P66614][DEHP] | 0.91 | 1031 | 418.4 | 49.2 |
| ZDDP | 1.20 | >1250 | 407.6 | 13.5 |
| PAO+IL(1 wt%) | 0.80 | 34.9 | 18.0 | 3.9 |
| PAO+ZDDP(1 wt%) | 0.80 | 35.2 | 17.9 | 3.9 |

#### *3.3.3.2. Thermal stability of [$P_{66614}$][DEHP] and ZDDP*

TGA curves of [$P_{66614}$][DEHP] and ZDDP are compared in Fig. 3.3.3. The IL showed higher thermal stability than ZDDP, with onset of decomposition at a temperature ~100 °C higher (300 vs. 200 °C). ZDDP, when decomposed, left ~20% solid "ash" because of its zinc content. In contrast, all decomposition products of [$P_{66614}$][DEHP] were gaseous, confirming its "ashless" nature.

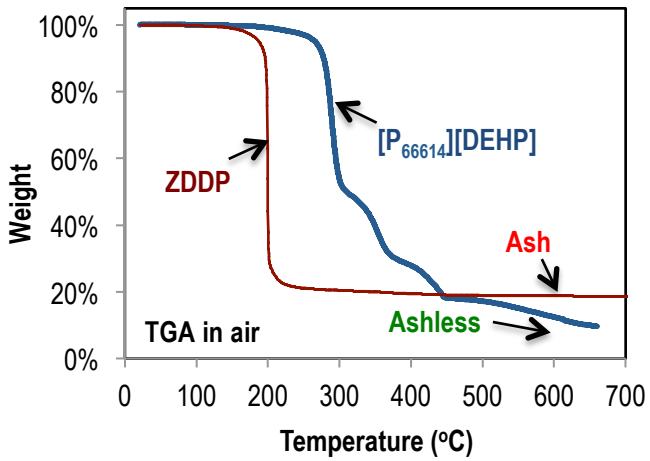


Fig. 3.3.3. [P66614][DEHP] has higher thermal stability and is ashless compared with ZDDP.

*3.3.3.3. Surface morphology and composition of piston ring and cylinder liner*

Figure 3.3.4 shows the surface morphology and composition of the grey cast iron cylinder liner, where honing marks can be clearly seen. The surface morphology and chemical composition of the piston ring are shown in Fig. 3.3.5. The central portion of the outer radial surface of the steel piston ring is covered by a plasma-sprayed coating. The SEM top and side views in Figs. 3.3.5a and 3.3.5c show the coating's width and maximum thickness of ~550 and ~110 μm, respectively. The EDS spectrum in Fig. 3.3.5d and element maps in Fig. 3.3.5e suggest that the coating is a Mo-Ni alloy.

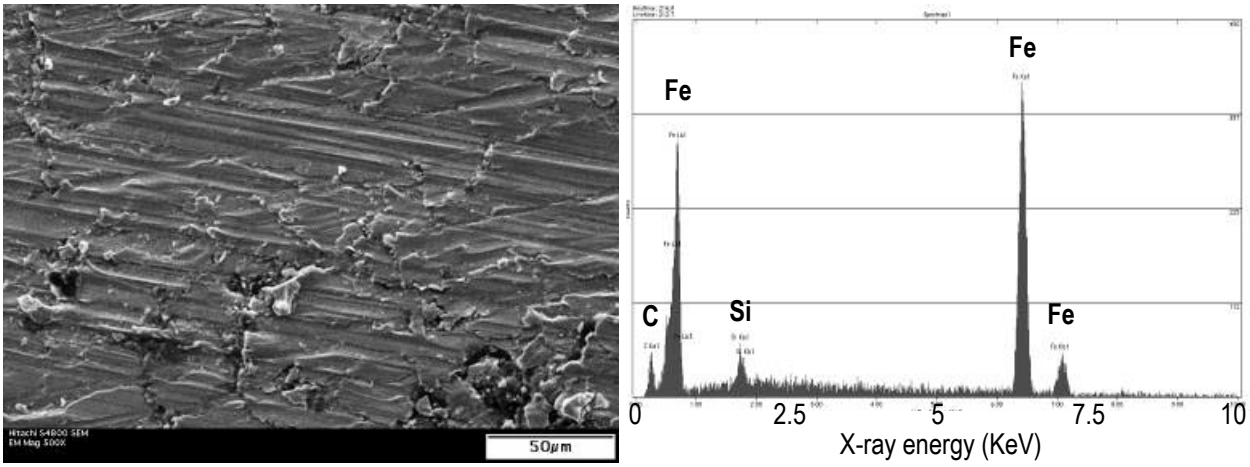


Fig. 3.3.4. Surface morphology and composition of the grey cast iron cylinder liner.

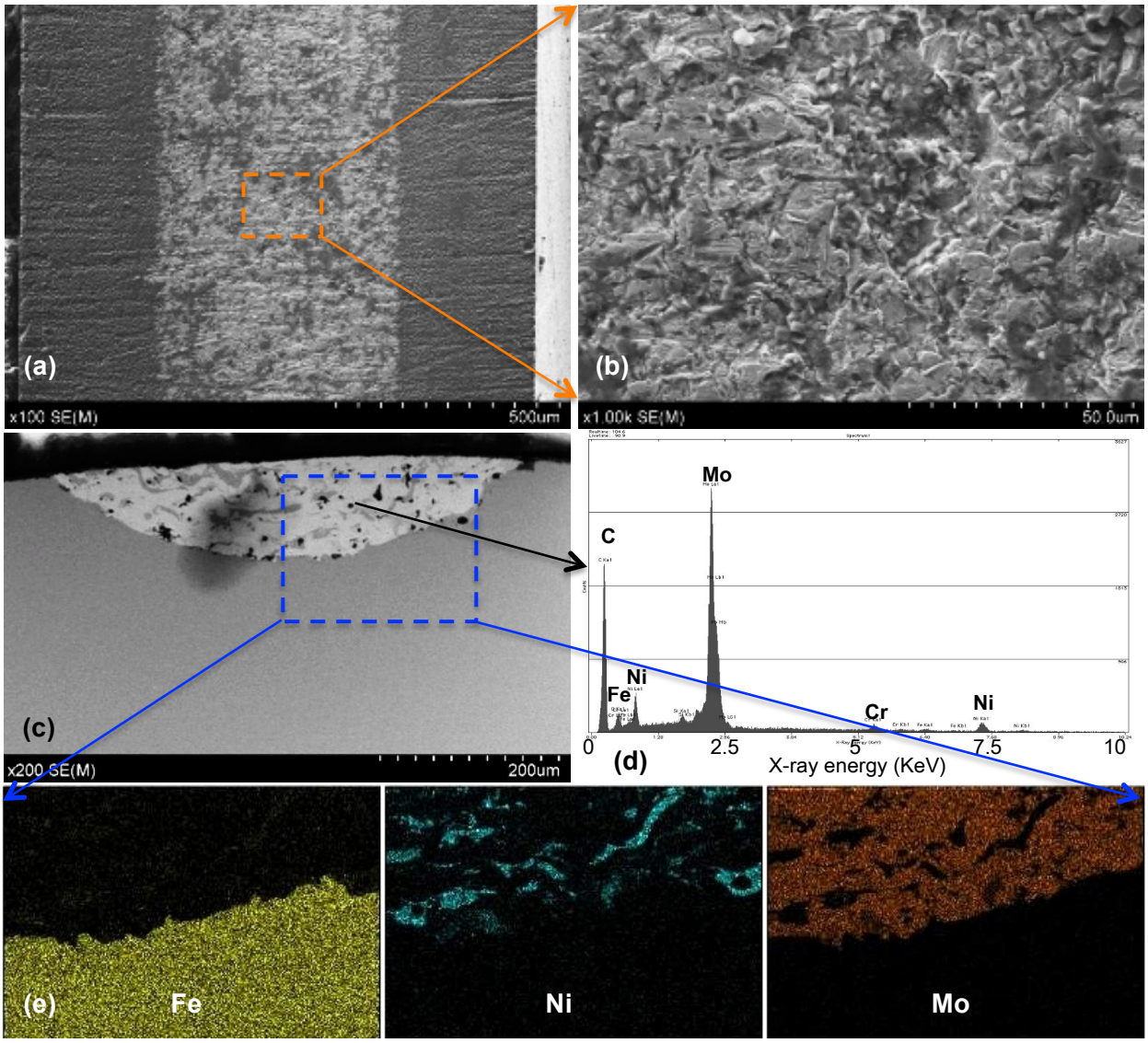


Fig. 3.3.5. Surface morphology and composition of a plasma spray-coated piston top ring. SEM top and cross-section images (a,b,c) showing the width (~550 μm), morphology, and thickness (~110 μm) of the coating; EDS spectrum and element maps (d,e) suggesting the coating primarily composed of a Mo-Ni alloy.

### *3.3.4. Tribological Results and Mechanistic Discussion*

#### *3.3.4.1. Tribo-tests at room temperature*

Figure 3.3.6 compares the friction traces and wear rates in the RT tests for the PAO base oil, PAO+1%ZDDP, and PAO+1%IL. The PAO base oil experienced a scuffing failure with the friction coefficient quickly rising above 0.2 after merely 6 m of sliding (test terminated at 50 m). The wear rates of the ring and liner due to scuffing damage were quite high ($1.0\times10^{-5}$ and $5.9\times10^{-4}$ $mm^3$/N-m, respectively). The scuffed ring and liner surfaces were examined using SEM and EDS (Fig. 3.3.7). Both surfaces show clear evidence of severe adhesive wear and plastic deformation, confirming scuffing damage. The EDS spectrum of the worn ring in Fig. 3.3.7a shows weak molybdenum and nickel signals

but strong iron and oxygen signals, which are distinct from the spectrum of the original unworn ring surface in Fig. 3.3.4d. This suggests that the worn ring surface is largely covered by iron metal and oxides, wear products transferred from the counterface (cast iron liner). The liner wear scar was deep and the worn surface was oxidized (note the high oxygen peak in the EDS spectrum in Fig. 3.3.7b), but little material was transferred from the ring.

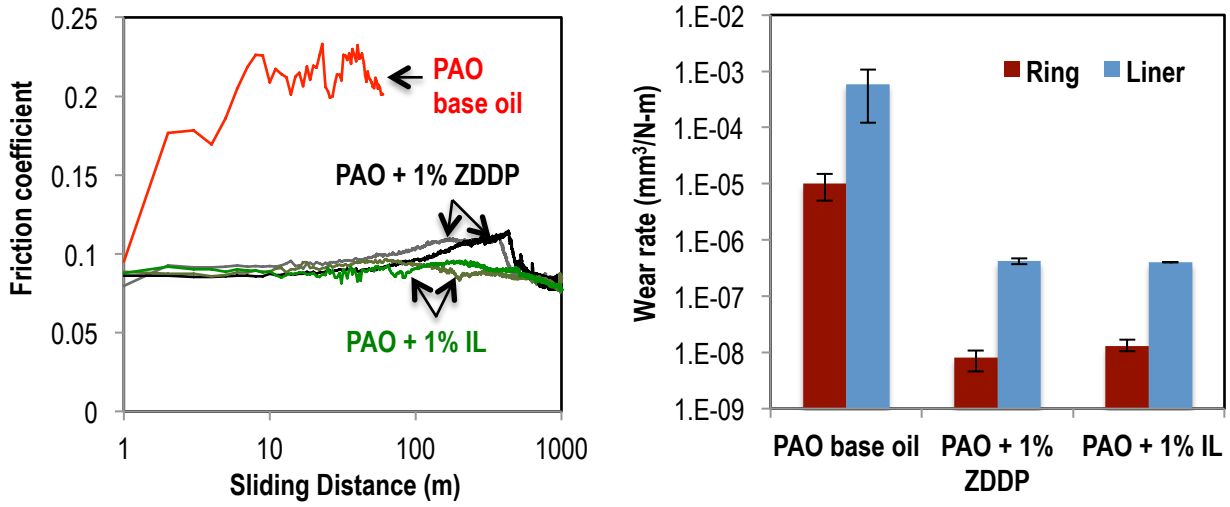


Fig. 3.3.6. Friction and wear results of room temperature tests.

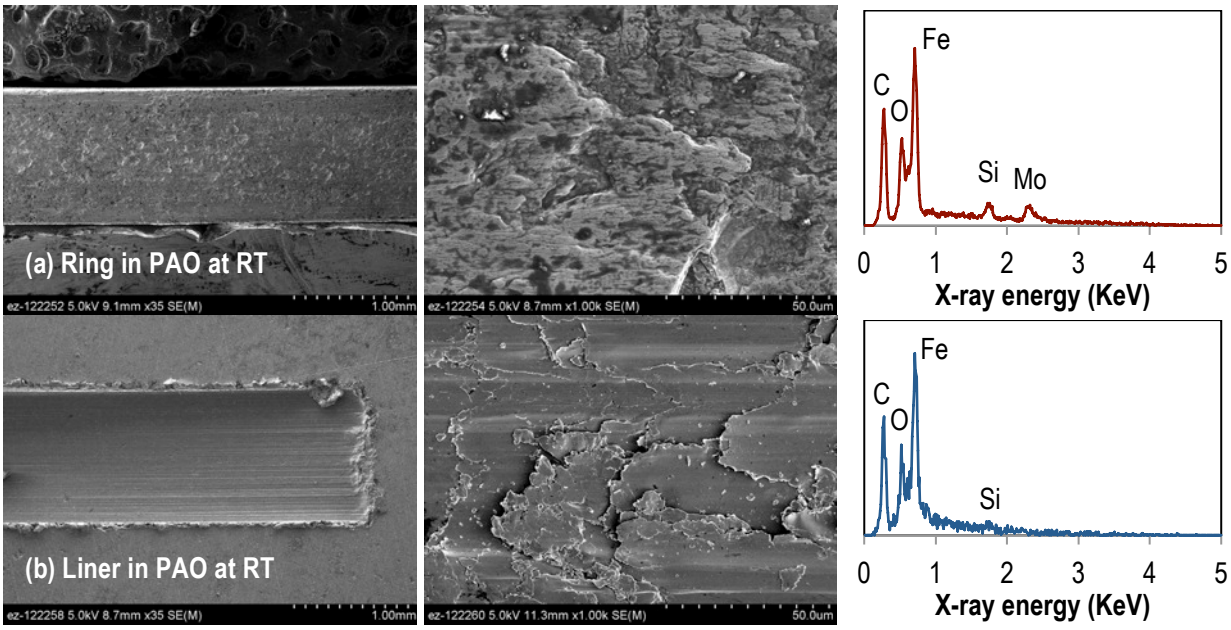


Fig. 3.3.7. SEM images and EDS spectra of scuffed ring (a) and liner (b) in PAO base oil after 50 m sliding at RT.

The addition of ZDDP or IL effectively eliminated scuffing and produced stable friction behavior with a classic boundary lubrication friction coefficient of 0.08-0.11 during the 1000 m sliding, as shown in Fig. 3.3.6. The wear rates of the ring and liner in PAO+1%ZDDP ($0.8\times10^{-8}$ and $4.2\times10^{-7}$ $mm^3$/N-m, respectively) and in PAO+1%IL ($1.3\times10^{-8}$ and $4.0\times10^{-7}$ $mm^3$/N-m, respectively) were similar, three orders of magnitude lower than those in the PAO base oil (see the wear chart in Fig. 3.3.6). Such dramatic wear reduction corresponds to the elimination of scuffing. Figures 3.3.8 and 3.3.9 show the surface morphologies and chemical compositions of the worn rings and liners tested in the two additized oils. These wear scars appear to be relatively smooth and largely covered with "dark patches". For PAO+1%ZDDP, the EDS spectra in Fig. 3.3.8 show significant contents of P, S, and Zn from ZDDP in addition to the elements from the metals, indicating that the dark patches are ZDDP tribo-films, similar to reported [3,43]. Significant iron in the tribo-film on the ring surface (see Fig. 3.3.8a) suggests the liner wear debris transferred onto the ring surface and was involved in the tribo-film formation. For PAO+1%IL, protective tribo-films containing metallic phosphorus compounds were revealed on both the ring and liner worn surfaces (Fig. 3.3.9). Similar to the ZDDP tribo-film, the IL tribo-film on the ring also involves iron, contributed by the liner wear debris.

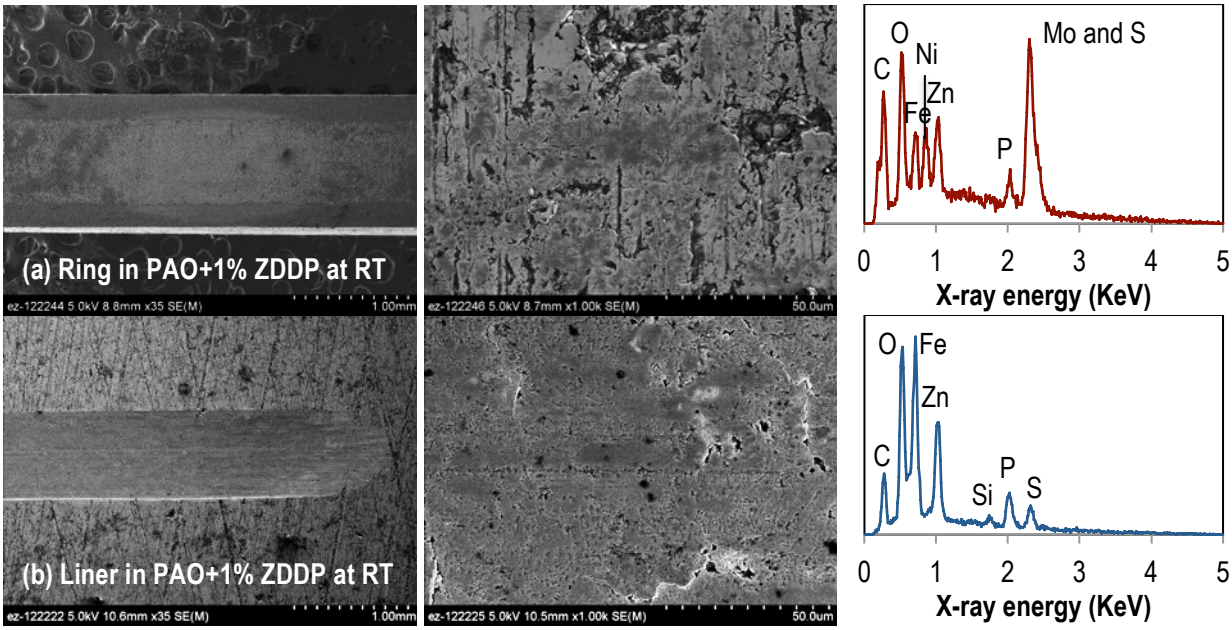


Fig. 3.3.8. SEM images and EDS spectra of worn ring (a) and liner (b) in PAO+1% ZDDP after 1000 m sliding at RT.

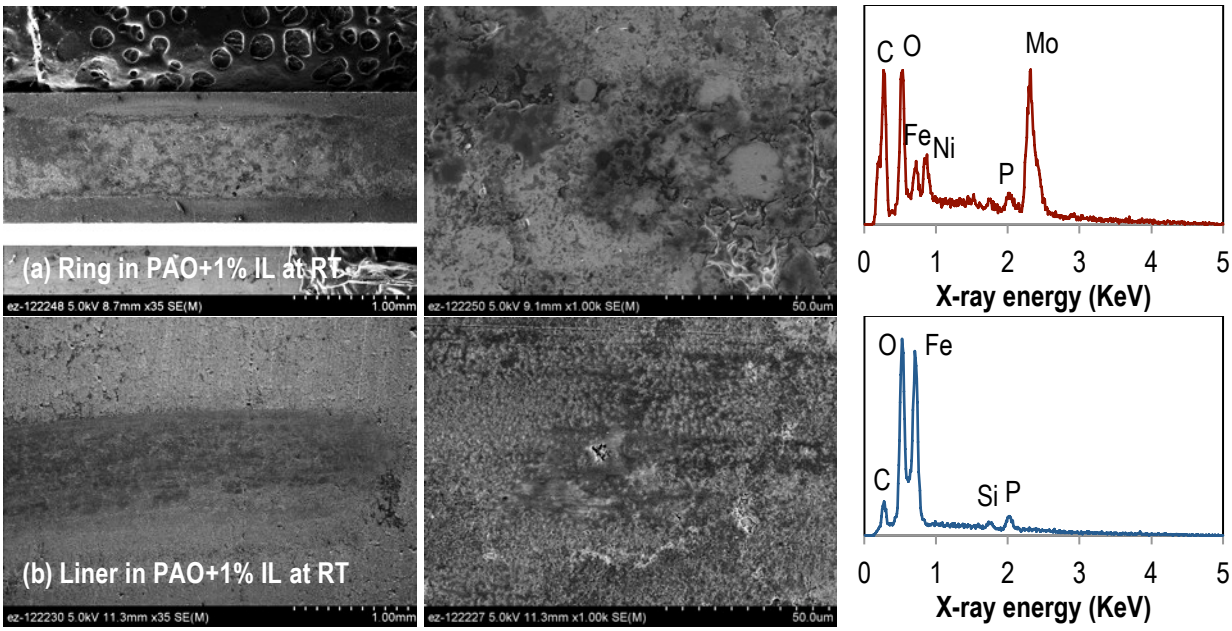


Fig. 3.3.9. SEM images and EDS spectra of worn ring (a) and liner (b) in PAO+1% IL after 1000 m sliding at RT.

*3.3.4.2. Tribo-tests at 100 $^{o}C$*

PAO+1%ZDDP and PAO+1%IL were then benchmarked against each other at 100 $^{o}$C. The HT friction and wear results are summarized in Fig. 3.3.10. Unlike in the RT tests, in which ZDDP effectively eliminated scuffing (Fig. 3.3.6), it failed to do so at HT (Fig. 3.3.10). The friction coefficient had a sudden rise from around 0.1 to above 0.2 after 22 m sliding in the first test and 38 m in the repeat test suggesting the onset of scuffing (when tests were terminated). Consequently, the scuffed rings and liners had relatively high average wear rates of $4.3\times10^{-7}$ and $3.0\times10^{-5}$ mm$^3$/N-m, respectively. The ZDDP failure was probably caused by the much lower oil viscosity at 100 $^{o}$C than at RT (3.9 vs. 35.2 cSt), which induced a lower $\lambda$-ratio and thus more severe asperity contacts where ZDDP could not provide sufficient protection. SEM images and EDS spectra of a scuffed ring and liner pair are shown in Fig. 3.3.11. Both wear scars appear rough; and the liner scar is dominated by scoring (abrasion) and plastic deformation, whereas the ring scar is largely covered by iron compounds transferred from the liner (high iron peak and low molybdenum peak in the EDS spectrum in Fig. 3.3.11a).

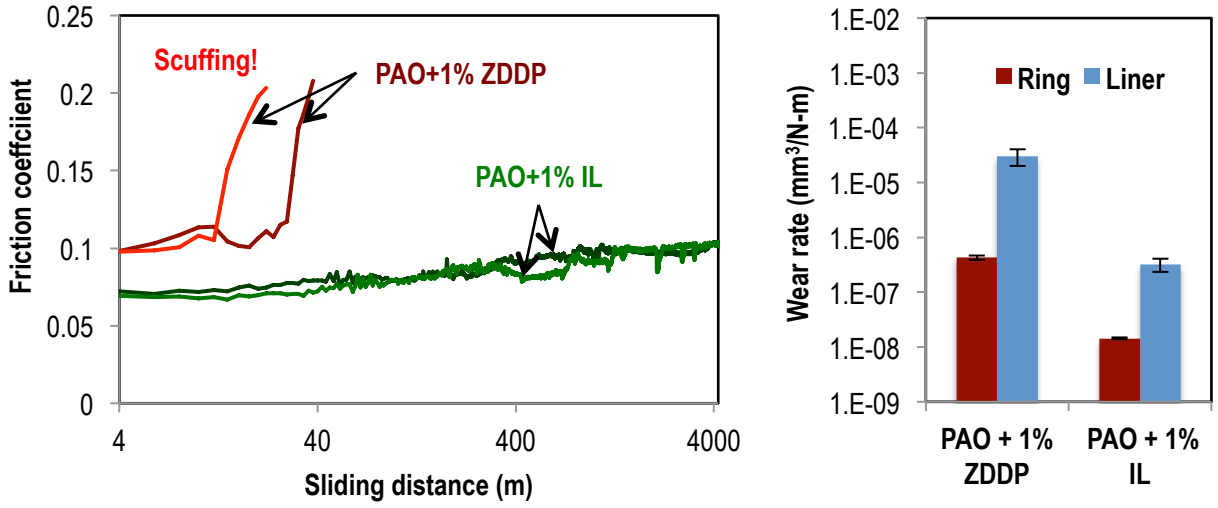


Fig. 3.3.10. Friction and wear results of 100 °C tests.

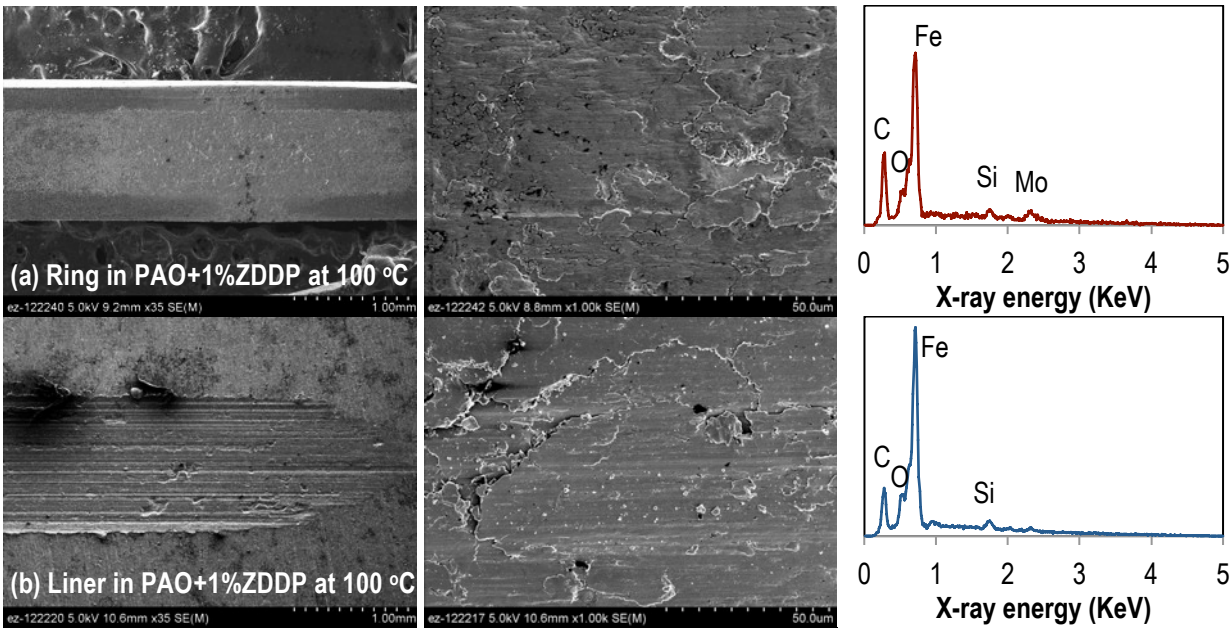


Fig. 3.3.11. SEM images and EDS spectra of scuffed ring (a) and liner (b) in PAO+1% ZDDP after 40 m sliding at 100 °C.

In contrast, the 1.0 wt% of IL successfully prevented scuffing in the HT tests, as shown in Fig. 3.3.10. The friction coefficient started at ~0.07 and gradually increased to 0.10 after 4320 m of sliding. Correspondingly, the ring and liner also experienced low wear in the IL-additized oil. Their wear rates, $1.4\times10^{-8}$ and $3.2\times10^{-7}$ $mm^3$/N-m, respectively, are two orders of magnitude lower than those in the ZDDP-additized oil (Fig. 3.3.10). Similar to those tested at RT (Fig. 3.3.9), the worn ring and liner surfaces tested in PAO+1%IL at HT (Fig. 3.3.12) are relatively smooth with dark patches of tribo-films containing oxides and phosphorus compounds. Again, iron was detected on the ring wear scar (Fig. 3.3.12a), suggesting material transfer.

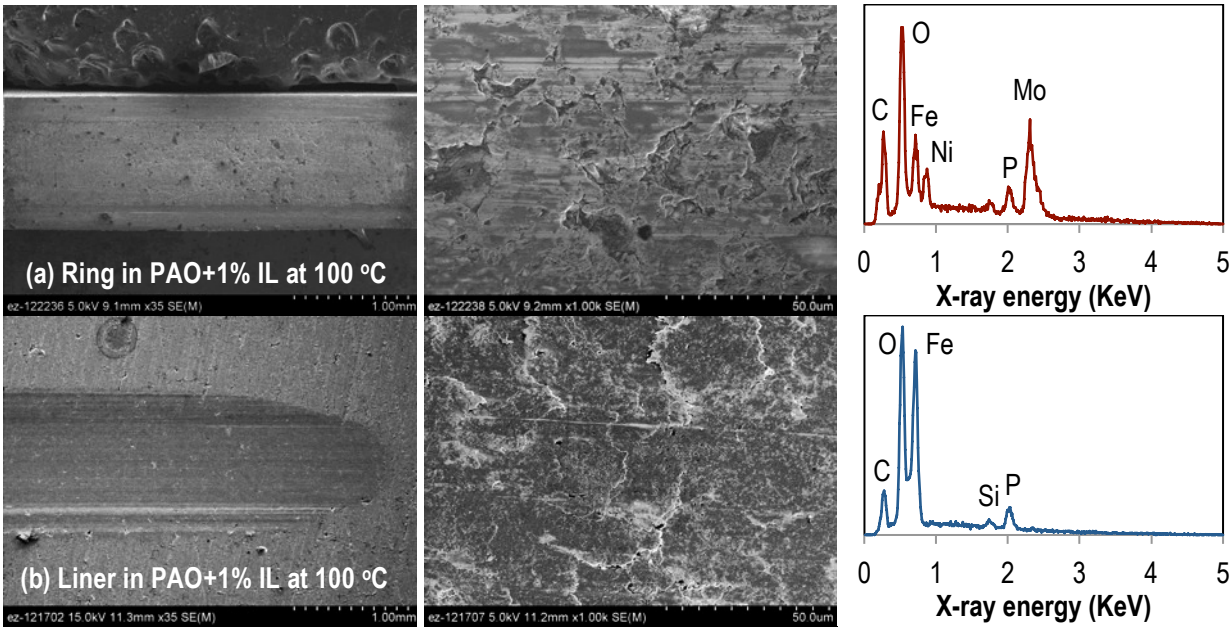


Fig. 3.3.12. SEM images and EDS spectra of worn ring (a) and liner (b) in PAO+1% IL after 4320 m sliding at 100 $^{o}$C.

*3.3.4.3. Thickness, structure, and composition of IL tribo-films formed at 100 $^{o}$C*

The tribo-films formed in PAO+1%IL in the HT test were further examined in cross sections using TEM, electron diffraction, and EDS (samples prepared by FIB), as shown in Fig. 3.3.13. A plastic deformation zone with refined grain structure was observed underneath the tribo-film for both the ring and liner (Figs. 3.3.13a-b). The tribo-films are mainly amorphous with some nanocrystalline material (Figs. 3.3.13c-d), and their thicknesses are 50-150 and 60-220 nm for the ring and liner, respectively (Figs. 3.3.13a-b). Both tribo-films are composed of two layers (Figs. 3.3.13c-f). The bottom layer on the worn ring surface appears dense and homogeneous, and contains Fe, O, and P but no Mo or Ni (Fig. 3.3.13e). This suggests that the film is a product of tribo-chemical reactions between the IL and the wear debris from the iron liner. The top layer on the ring appears to be a porous transfer layer composed of iron and oxygen with only traces of phosphorus (Fig. 3.3.13e). The partially matched iron and oxygen distribution implies that this layer is a mixture of iron metal and iron oxides.

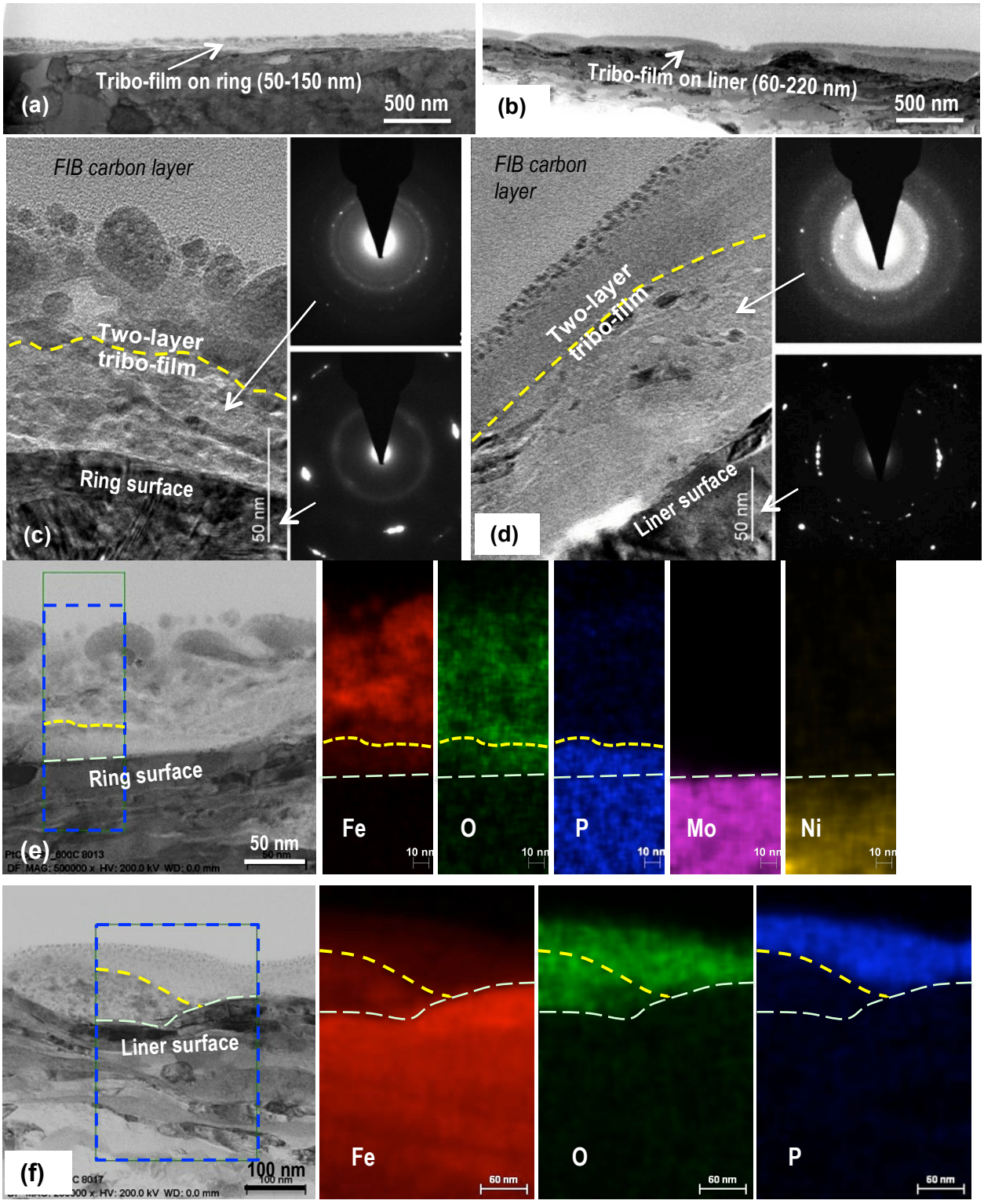


Fig. 3.3.13. Cross sectional TEM images (a-d) and EDS element maps (e,f) revealing two-layer structured tribo-films on the ring (a,c,e) and liner (b,d,f) worn surfaces lubricated by PAO+1%IL after 4320 m sliding at 100 $^{o}$C.

The tribo-film on the worn liner also consists of two layers. The top layer contains Fe, O, and P (Fig. 3.3.13f) and has a continuous coverage as seen across the TEM sample length (Fig. 3.3.13b), whereas the interlayer contains only Fe and O (without P) and is discrete and mostly located in the valleys (Figs. 3.3.13b-f). The top layer contains a high concentration of phosphorus and has a homogeneous nanostructure (Fig. 3.3.13d) and well matched Fe, O, and P distribution (Fig. 3.3.13f), suggesting a high concentration of iron phosphates. The nanoparticles shown in the high-resolution TEM image in Fig. 3.3.13d and the slightly uncorrelated iron and oxygen distribution in the EDS element maps in Fig. 3.3.13f indicate that the interlayer is basically an iron oxide film with a small amount of metallic iron debris. This interlayer was not observed in the previously reported single-layer, phosphorus-containing tribo-film on the iron liner tested in PAO+5%IL at RT in Section 3.2. The lower IL treat rate in this study appear to allow more oxidation of the wear debris and iron surface (other than reacting with the IL), which could also be promoted by the higher testing temperature. It is interesting that the tribo-films on the ring and liner have almost opposite layer structures. The phosphorus layer is the interlayer for the ring but the top film for the liner. The exact formation processes for the two-layer structure tribo-films are not clear and remain to be investigated.

*3.3.4.4. Understanding the IL's superior anti-scuffing/anti-wear performance at 100 °C*

In the RT bench tests, $[P_{66614}][DEHP]$ behaved similarly to ZDDP. However, the HT results indicate that the IL potentially provides more effective anti-scuffing/anti-wear than ZDDP under more severe boundary lubrication conditions (e.g., lower oil viscosity). It is thought that a metallic surface (composed of metallic ions and electrons) naturally attracts IL ions by ionic forces, but does not attract ZDDP neutral molecules, as illustrated in Fig. 3.3.14. Therefore, at a given treat rate (e.g., 1.0 wt% of this study), IL ions tend to attach to metal surfaces, leading to a higher localized concentration than in the bulk oil (Fig. 3.3.14b). These surface-absorbed ions are readily available for tribo-film formation when asperity collisions occur. In contrast, ZDDP molecules are randomly distributed in the oil and so the contact area has a relatively small amount of ZDDP to work with (Fig. 3.3.14a). This advantage of the IL may not be noticeable under mild boundary lubrication conditions, such as the RT tests, but it becomes increasingly critical under more severe circumstances, such as the HT tests, in which adequate protection requires the rapid formation of a tribo-film over a relatively large area (requiring a larger supply of functional molecules at the contact area).

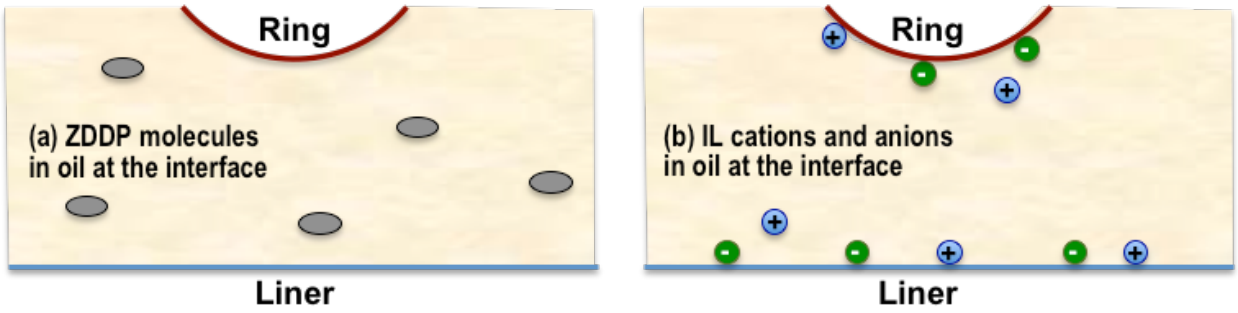


Fig. 3.3.14. Schematic of distribution of ZDDP molecules (a) and IL cations and anions (b) in oil.

### 3.4. Conclusion for development of oil-miscible ionic liquids as ashless lubricant additives

A group of phosphonium-phosphate/phosphinate ILs has been developed, and some of them have shown excellent miscibility with non-polar hydrocarbon oils. These ILs are thermally more stable than conventional lubricants, and are non-corrosive to either ferrous or aluminum alloys. The alkyl chain

length and hydrogen bonding between the cation and the anion seem to influence the oil-solubility of ILs. Viscosities of oils, ILs, and their blends at various temperatures were determined and the measured results of the blends showed good agreement with values calculated by the Refutas equation. Tribological evaluation has demonstrated significant friction and wear reductions from adding a small amount (1-5 wt.%) of the oil-miscible ILs into base oils. Particularly, the anti-scuffing/anti-wear performance and mechanism of $[P_{66614}][DEHP]$ was benchmarked against those of the commercial anti-wear additive ZDDP at the same treat rate of 1.0 wt% in PAO 4 cSt base oil at both room and elevated (100 $^{o}$C) temperatures. In the RT tests, the IL additive performed as effectively as ZDDP in preventing the scuffing damage that was experienced in the base oil alone. At 100 $^{o}$C when the base oil viscosity was much lower, ZDDP failed to prevent scuffing at the early stage of the test resulting in high friction and wear. In contrast, the IL additive maintained a stable boundary lubrication friction coefficient and a low wear rate without scuffing throughout the test. IL ions are believed to have a higher attraction to metallic surfaces than do ZDDP neutral molecules and thus have a higher localized concentration at the contact area to provide better protection. Cross-sectional TEM and EDS examination revealed two-layer structured tribo-films on both ring and liner surfaces lubricated by the IL-additized oil at 100 $^{o}$C. Results of this study suggest that the IL additive possesses superior anti-wear characteristics compared with ZDDP and may potentially enable the use of lower-viscosity engine lubricants, which would increase fuel economy.

## CHAPTER 4. Impact of an Ionic Liquid Additive on Exhaust and Three-Way Catalysts

### 4.1. Thermal decomposition and exhaust analyses

Thermal decomposition analyses of $[P_{66614}][DEHP]$ and ZDDP were conducted in helium and oxygen environments. 1 mg of hexane extracted residue from impingers was analyzed. These are gas phase compounds. Anions in solution analyzed by capillary electrophoresis.

In helium, ZDDP largely decomposed at 200 $^{o}$C with trace amounts when heated to 300 $^{o}$C. Electropherogram of residue pyrolysis showed the presence of non-volatile phosphoric acid anion and unknown anion, as shown in Fig. 4.1.1. In contrast, [P66614][DEHP] had very little decomposition at 200 $^{o}$C. When decomposed at 400 $^{o}$C, electropherogram of residue pyrolysis detected no detectable anions, as shown in Fig. 4.1.2, indicating all volatile phosphorous – ashless.

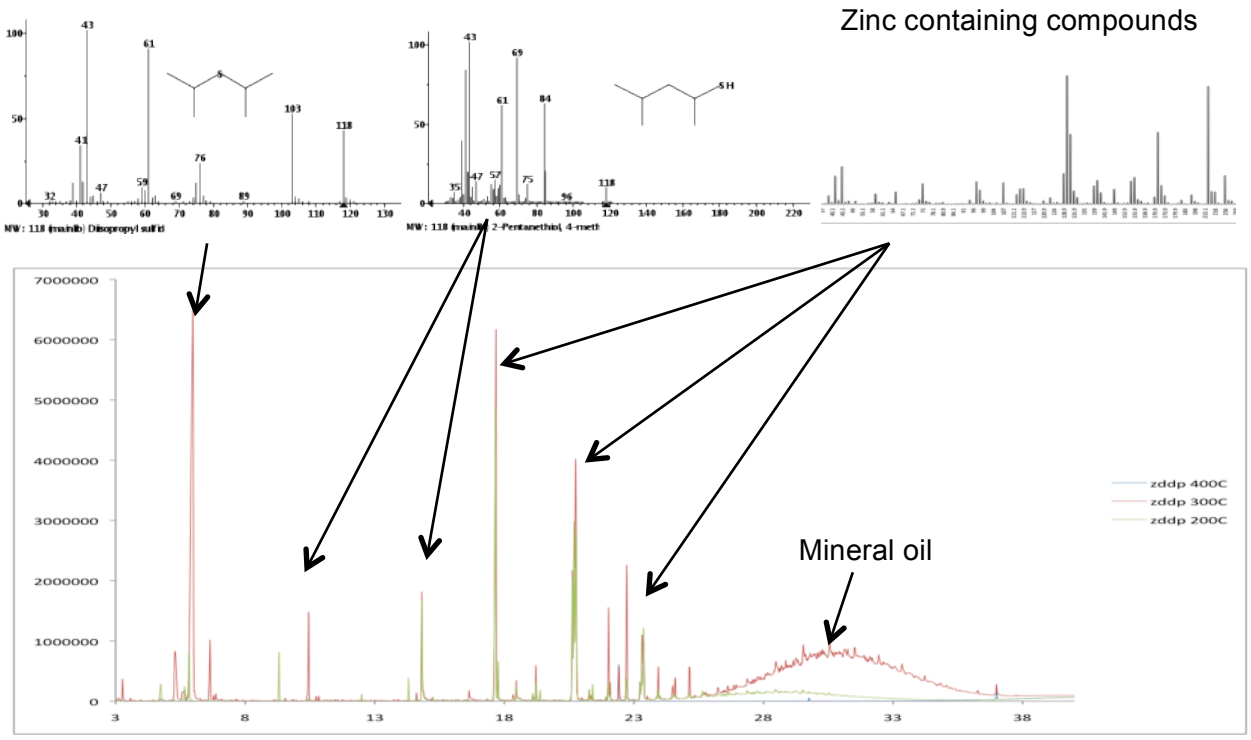


Fig. 4.1.1. Chromatographs of ZDDP pyrolysis (in He).

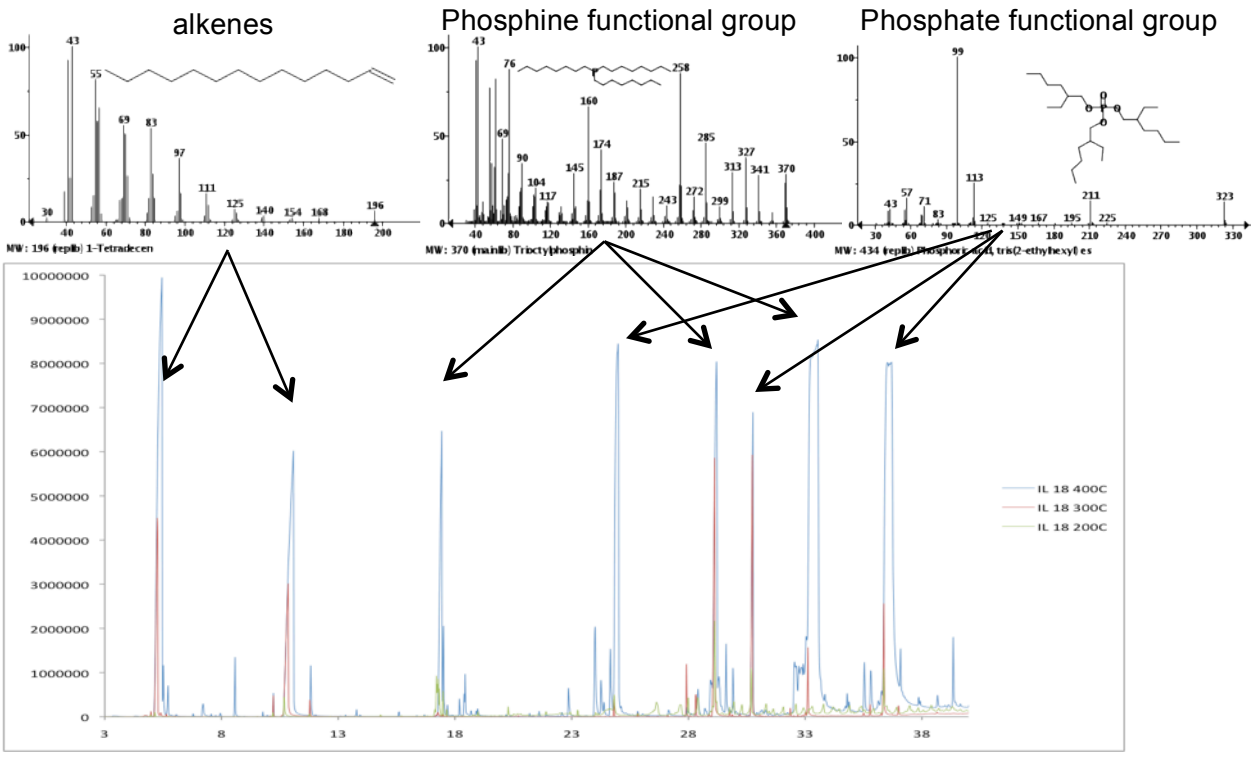


Fig. 4.1.2. Chromatographs of $[P_{66614}][DEHP]$ pyrolysis (in He).

In oxygen thermal decomposition, $[P_{66614}][DEHP]$ was stable below 200 $^{o}$C but completely decomposed at 300 $^{o}$C. Decomposition products were different than those in helium, but again are volatile phosphorous – ashless. Olefin and paraffin compounds no longer exist but large number of carbonyl compounds suggest that the alkyl legs of IL were oxidized. The chromatographs of IL thermal decomposition in oxygen at 300 $^{o}$C are shown in Fig. 4.1.3.

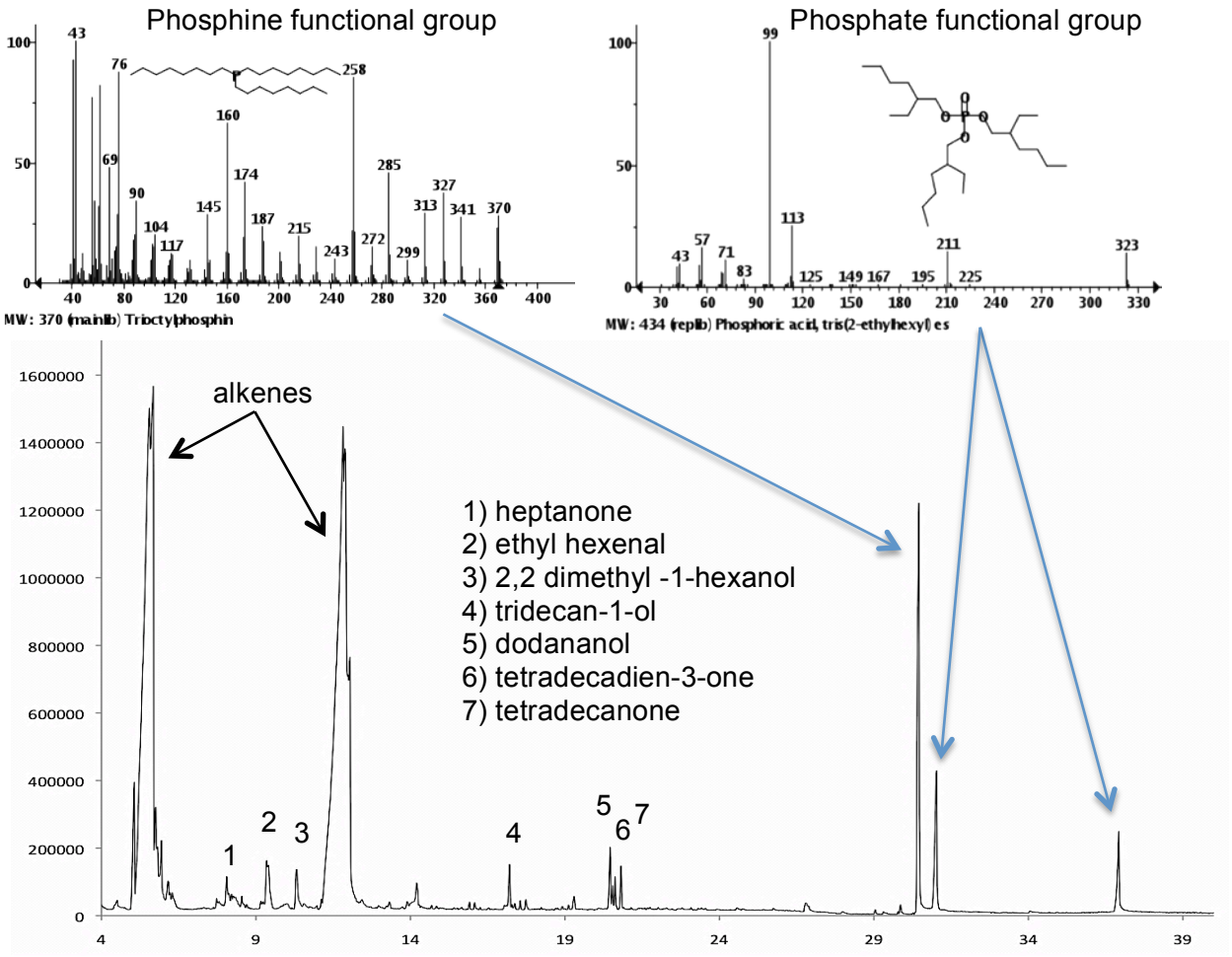


Fig. 4.1.3. Chromatographs of $[P_{66614}][DEHP]$ thermal decomposition products at 300 $^{o}C$ (in $O_2$).

Exhaust analysis for using $[P_{66614}][DEHP]$ as oil additive was conducted at ORNL FEERC. Three fuels, base diesel, base diesel + ZDDP, and base diesel + IL, were evaluated in a single-cylinder research engine. Three engine loads were used, and two replicate tests for a total of 18 tests. A heated (190 °C) stainless steel sample line was used to bring the sample to the filter oven, and a glass filter holder held the filter in the oven. The oven was kept at >120 °C. 81 mm quartz fiber filters (Pall Corp.) were used for particulate collection; the filters were pre-fired at 650 °C in a furnace prior to use. The sample gas then exited the oven and flowed through impingers kept at ice water temperatures for water removal from the exhaust, and then finally to a dry gas meter (American Meter) for volume measurement. Figure 4.1.4a shows a schematic of the sampling system and Fig. 4.1.4b is a photograph of the system hooked up to the engine.

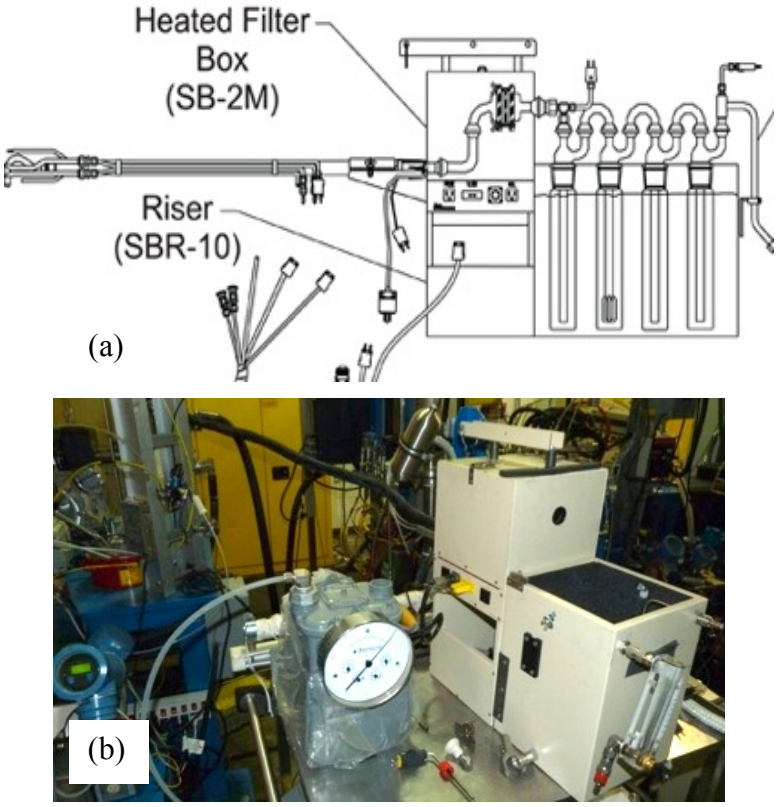


Fig. 4.1.4. (a) Schematic of exhaust sampling system and (b) actual system hooked up to an engine.

Two sets of four 500 ml impingers were labeled 1A-4A and 1B-4B. The sets were used in an alternating rotation throughout the experiment. Prior to each test run, the empty mass for each impinger was recorded. Impingers 1 and 2 were filled with 100 mL of water and each weighed for its initial mass with water. After use of the equipment, exterior moisture was removed and the impingers were weighed for their final mass with water. The content of each impinger was decanted into a 500 mL plastic bottle. The impingers and u-tubes were water rinsed and decanted a minimum of three times until a final volume of 500mL was reached. Following sample collection, impingers were rinsed in the following order: methanol, hexane, methanol, and followed by a triple water rinse. This process was repeated for all 18 test runs.

Impinger samples were concentrated using the TurboVap (Caliper LifeSciences). From the initial 500mL, a volume of 50 mL was measured into test tubes and placed inside the TurboVap. The samples were blown-down to 1 mL. Using a syringe, approximately 800 µL to 1 mL of each blown-down sample was transferred into a glass vial. Depending on the acidity of the sample, 10 to 115 µL of 1 N NaOH was added. Samples were tested for the desired pH of 10 using pH strips. Once at the appropriate pH, 500µL of hexane was added and mixed thoroughly. After allowing the sample to separate, the water phase was removed from the glass vial with a syringe and transferred into a 1mL plastic vial. Between uses, syringes were triple rinsed with water. For each run, laboratory notebooks, filters, plastic sample bottles, glass vials and 1ml plastic vials were all labeled with identical sample names corresponding to each test run. These samples will be analyzed for anions of organic and inorganic acid.

The filters from the high load points and medium load points were heavily loaded and more particulate was generated when the fuel was additized than with the baseline fuel. Figure 4.1.5 shows a visual comparison of the filters for three fuels and loads. Note that the light load filters were sampled for 90 minutes (~1200 L volume), the medium load filters for 40 minutes (~500 L volume) and the heavy

load filters for 20 minutes (~250 L volume). The patterns are caused by the filter support and are obscured as a particulate cake develops on the filter. These filters were analyzed with thermal desorption-gas chromatography-mass spectrometry. Analysis of the residue of hexane extraction of impinger waters showed significant hexane extractable residue at low load only. The high load was clear. Low load had highest concentration anions and phosphoric acid.

Pyrolysis analysis of the loaded PM filters did not detect any decomposition products of the ZDDP or IL. As shown in the chromatographs in Fig. 4.1.6, PAHs, phenolic compounds, alkanes, and alkenes were observed. Carbon backbone of the IL or ZDDP could be contributing to signal, but no P or S compounds observed.

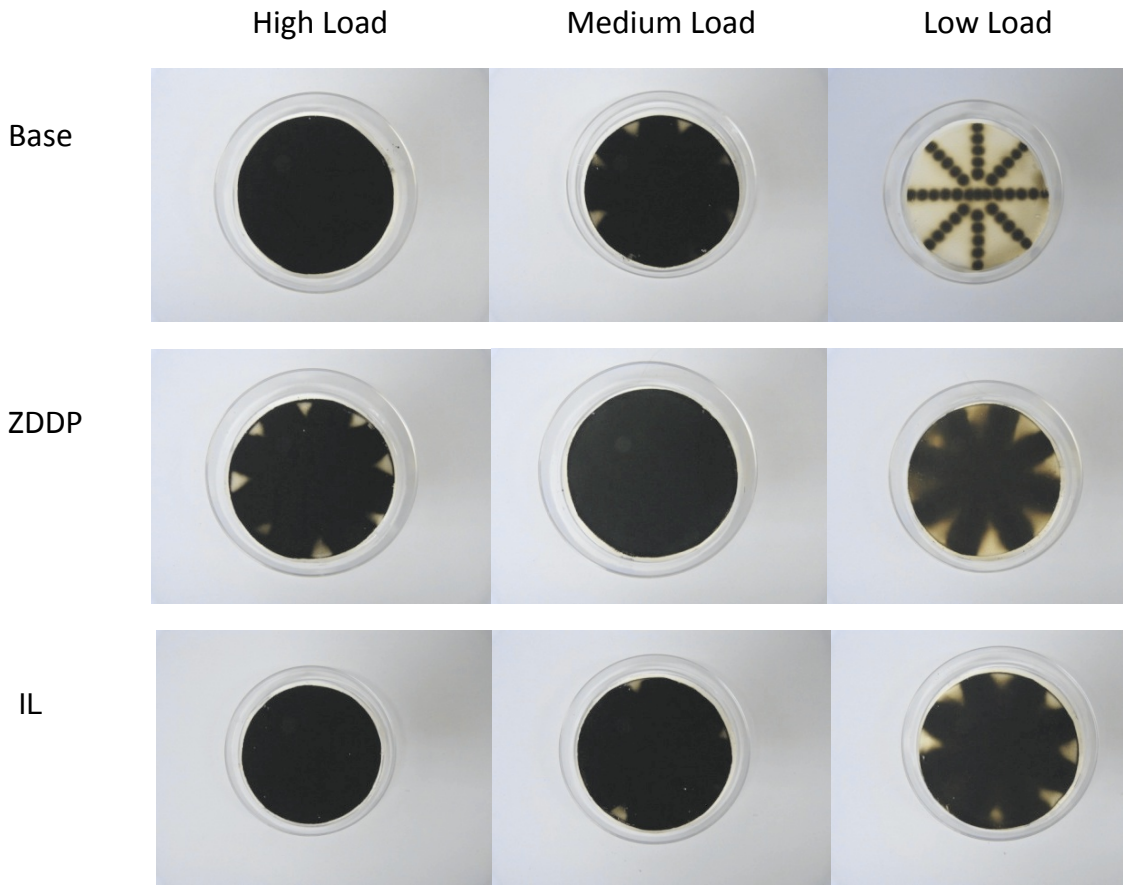


Fig. 4.1.5. PM filters for base diesel, diesel+ZDDP, and diesel+IL at different engine loads.

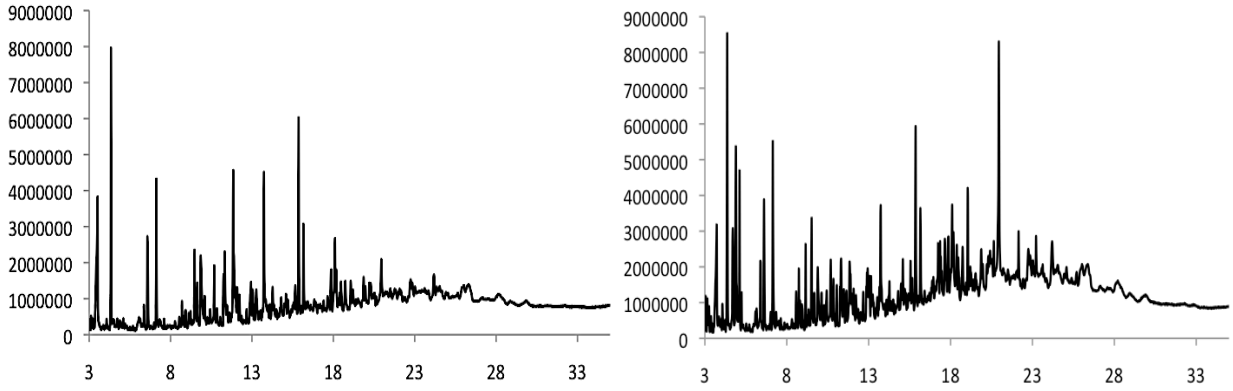


(a) Diesel+ZDDP (b) Diesel+[$P_{66614}$][DEHP]

Fig. 4.1.6. Chromatographs of the low-load PM filter pyrolysis for (a) diesel+ZDDP and (b) diesel+IL.

**4.2. Design and establishment of an accelerated aging system**

ORNL FEERC researchers set up an accelerated aging system to compare the effects of the IL [$P_{66614}$][DEHP] and a commercial secondary ZDDP on three-way catalysts (TWC). The schematic is illustrated in Fig. 4.2.1a and the actual setup is shown in Fig. 4.2.1b. Make-up air was introduced with MFC for controlling lean and rich operations. The UEGO port was before TWC and gas sampling ports were before and after TWC. Thermal couple (TC) connections were before and after TWC with another TC inserted into the mid-catalyst. The AW additive (IL or ZDDP) was blended into the gasoline and the decomposition products of the AW additive along with the combustion exhaust went through the exhaust pipeline to reach the TWC. About 35 g of the IL or ZDDP was used in each test to simulate the maximum lifetime AW additive consumption in a modern automotive engine. The lifetime AW additive consumption was estimated based on the oil consumption data from both vehicle and engine dynamometer tests and assumes 1% additive concentration in the lubricant.

With 950°C max temperature and 900°C target temperature at the mid-catalyst point, it was not possible to operate the TWC under precise stoichiometric operation as would be typical in a vehicle. This is because the genset operates fuel-rich with up to 7-8% CO in the exhaust and at stoichiometric conditions the exhaust temperature will reach well above 1000 °C due to the combustion of all of the reductants. Instead, tests were conducted by altering the genset operation between lean and rich in such a way that the total time on rich matches that on lean. The switch between rich and lean was achieved through changing the flow rate of make-up air. For the engine aging experiments, 7.5 gallons of gasoline was consumed in a time period of more than 20 hours. During the aging process, engine exhaust was analyzed before and after TWC to give some guidance into the impact of fuel additive (e.g., IL and ZDDP) on the performance of TWC. CAI (California Analytical Instruments) 602P digital analyzer was used to monitor the concentrations of $CO_2$, CO, and $O_2$, and CAI 400-HCLD was used to measure $NO_x$.

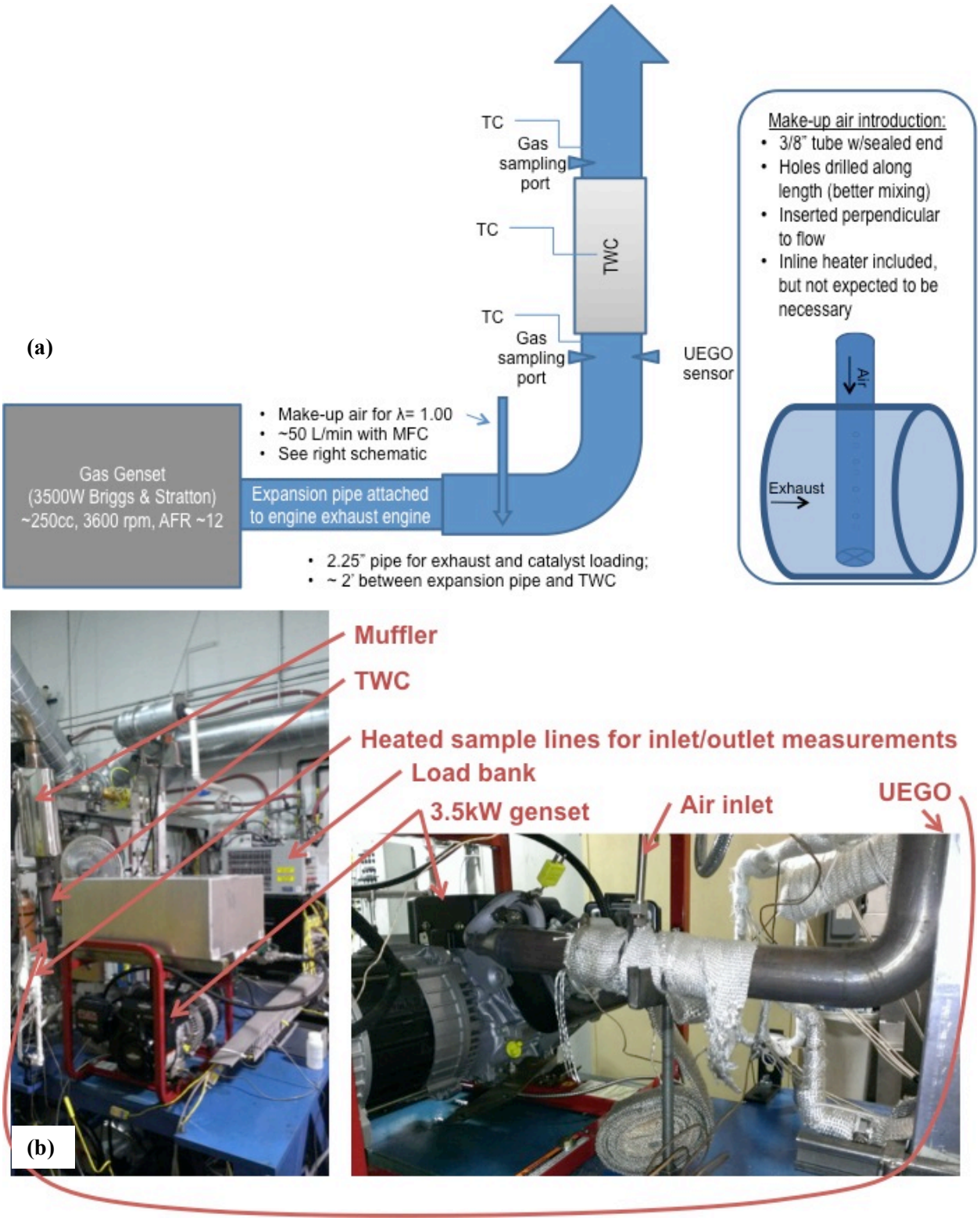


Fig. 4.2.1. Accelerated catalyst aging setup to evaluate the effects of IL and ZDDP on TWC.

Two close-coupled TWCs were provided by GM: one that has been aged to 150K miles, or the equivalent of full useful life (FUL) and the other is slightly more than de-greened (DG), or the equivalent of 4k miles. These catalysts have a two-zone catalyst layer with a different formulation in the front ~1/3 compared to the rear. Large catalyst cores were extracted from the TWCs for the genset (42mm OD and 155 mm in length) and smaller cores were extracted for the bench reactor tests (11x11x50 mm), as illustrated in Fig. 4.2.2.

The bench flow reactor was used to evaluate the two close-coupled TWCs prior to ZDDP- or IL-aging. Reaction conditions were 0.1% $C_3H_6$, 1.8% CO, 0.12% NO, 1.59% $O_2$, 0.6% $H_2$, 5% $H_2O$, 5% $CO_2$, and balance $N_2$. Temperature ramped from 100 to 550 $^oC$ at 2 $^oC$/min. The T90 light-off temperatures of NO, $C_3H_6$, and CO for the DG-TWC were ~200 $^oC$, and those of the FUL-TWC increased to ~230 $^oC$. This indicates deteriorated performance for the FUL-TWC compared with the DG-TWC.

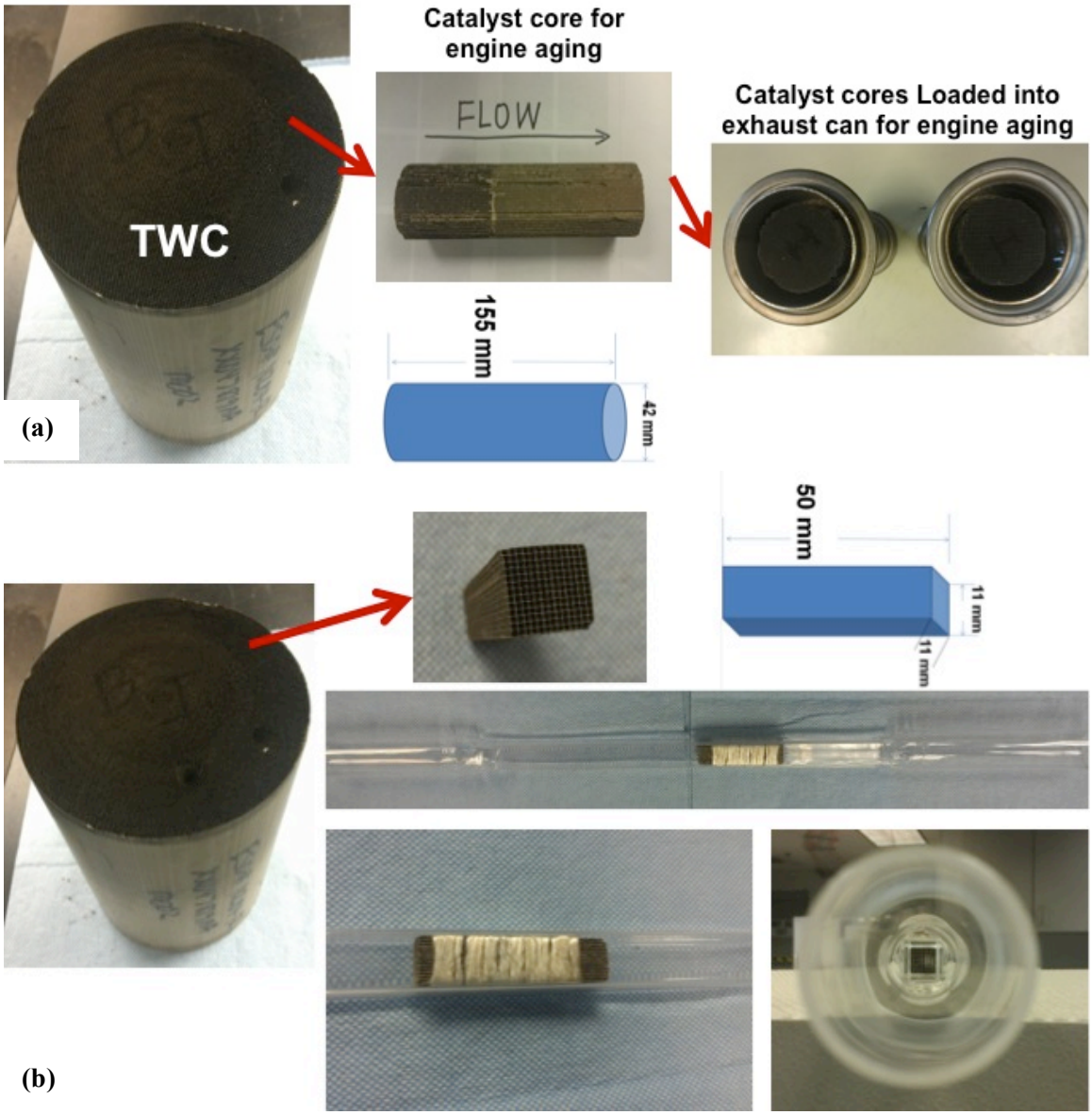


Fig. 4.2.2. Catalyst cores extracted from TWCs for the genset (a) and bench reactor (b).

### 4.3. Impact of [$P_{66614}$][DEHP] and ZDDP on TWC

The temperature profiles of engine aging of the FUL-TWC using gasoline+1%IL are shown in Figure 4.3.1. The three temperatures, catalyst inlet, catalyst outlet, and mid-core, were relatively stable. The temperature for catalyst inlet and outlet were in the range of 300-400 and 600-800 $^{o}$C, respectively. The most import mid-core catalyst temperature was well controlled around the target, 900 $^{o}$C.

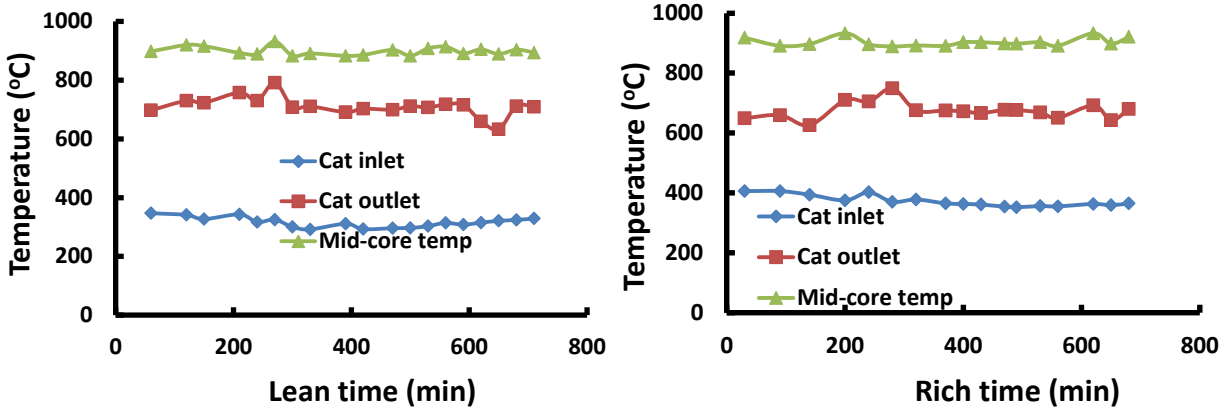


Fig. 4.3.1. Temperature profiles during engine aging of full useful life TWC using gasoline+1%IL.

Fig. 4.3.2 shows the changes of CO and $NO_x$ concentrations during engine IL-aging of the FUL-TWC Pretty. The CO concentration at catalyst outlet under lean is much lower compared with 7-8% CO at engine outlet. The increase trend of CO might be a sign of catalyst deactivation under aging. NOx was not detectable under rich operation.

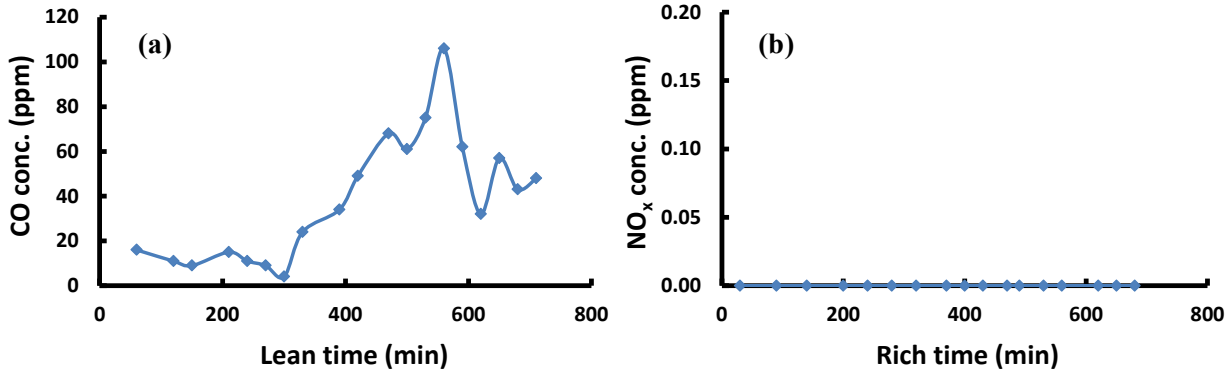


Fig. 4.3.2. Changes of CO and $NO_x$ concentrations during engine aging of FUL-TWC using gasoline+1%IL. (a) CO concentration in lean time and (b) $NO_x$ concentration in rich time.

In order to investigate the impact of IL exposure on the performance of TWC activity, small cores from the FUL-TWCs were evaluated in a bench core reactor before and after IL exposure. A typical metric for the evaluation of TWC is based the measurement of a temperature for a given conversion of either NOx, CO or HCs. This is reported as T50, T80 or T90 for the temperature of 50%, 80% or 90% conversion, respectively. The performances of the TWCs under simulated engine exhaust conditions (i.e.,

$NO_x$, HC, and CO) are shown in Figs. 4.3.3 and 4.3.4. The T90 of NO, $C_3H_6$ and CO for FUL-TWC before IL-aging were 230, 230, and 229, respectively. After exposure to the IL in the genset, the temperature increased to 302, 290, and 291 $^oC$, respectively, thus the T90 increased about 60-70 $^oC$.

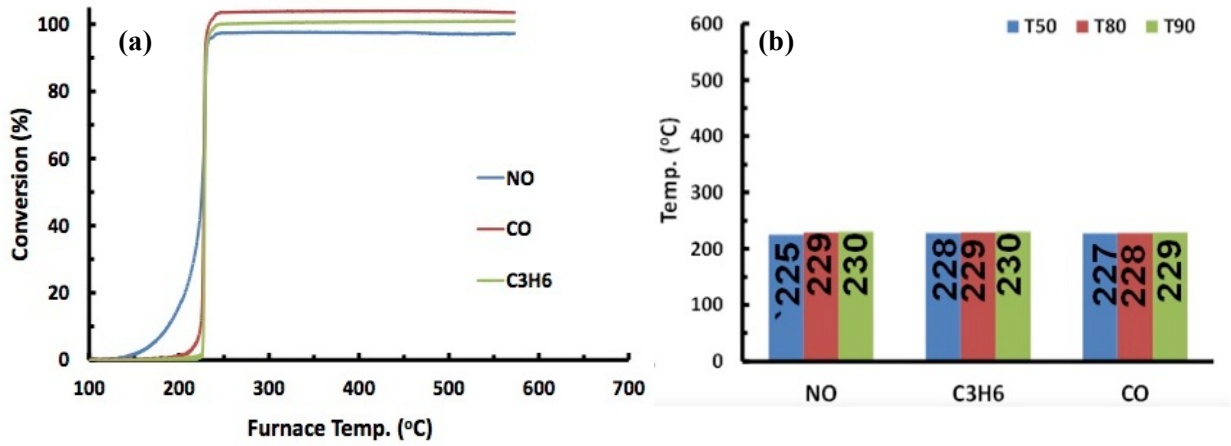


Fig. 4.3.3. NO, CO, and $C_3H_6$ light-off curves (a) and temperatures of T50, T80, and T90 (b) for FUL-TWC. Temperature ramp: $2^oC$/min; under stoichiometric conditions.

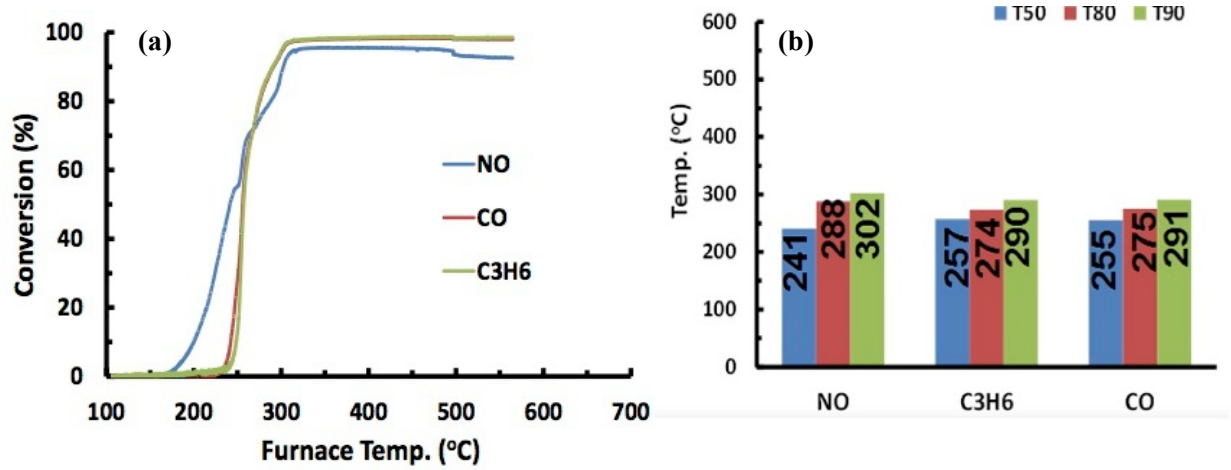


Fig. 4.3.4. NO, CO, and $C_3H_6$ light-off curves (a) and temperatures of T50, T80, and T90 (b) for FUL-TWC aged by gasoline+1%IL. Temperature ramp: $2^oC$/min; under stoichiometric conditions.

For comparison to the industry standard lubricant additive, DG-TWCs were evaluated before and after ZDDP exposure under the same conditions, shown in Figs. 4.3.5 and 4.3.6. The T90 of NO, $C_3H_6$ and CO for the unexposed DG-TWC were 203, 204, and 204 $^oC$, respectively. After ZDDP aging, the T90 increased to 295, 284, and 284 $^oC$, respectively, i.e. ZDDP aging caused an increase of 80-90 $^oC$. Therefore, these observations suggest that IL has moderately less of an impact on the performance of the TWC compared with ZDDP.

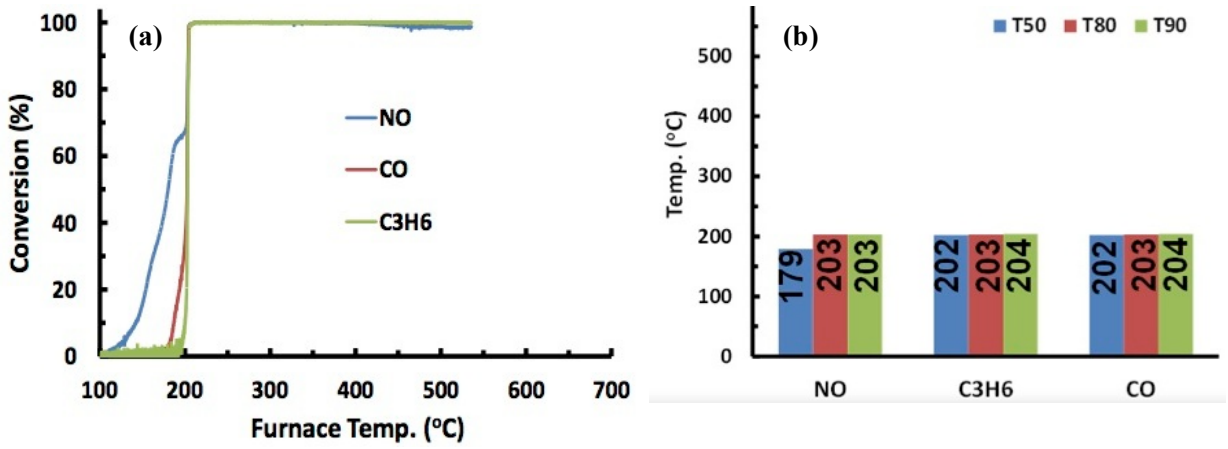


Fig. 4.3.5. NO, CO, and $C_3H_6$ light-off curves (a) and temperatures of T50, T80, and T90 (b) for DG-TWC. Temperature ramp: 2 °C/min; under stoichiometric conditions.

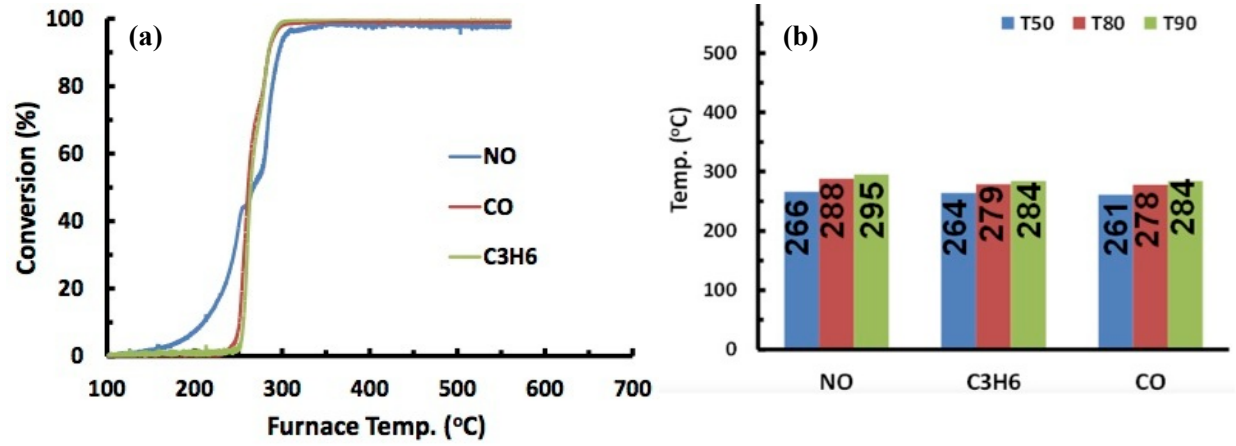


Fig. 4.3.6. NO, CO, and $C_3H_6$ light-off curves (a) and temperatures of T50, T80, and T90 (b) for DG-TWC aged by gasoline+1%ZDDP. Temperature ramp: 2 °C/min; under stoichiometric conditions.

### 4.4. Conclusion for impact of $[P_{66614}][DEHP]$ on three-way catalysts

An accelerated catalyst aging system has been established for comparing the impacts of the IL $[P_{66614}][DEHP]$ and ZDDP on TWC performance in engine emissions control. During engine aging the catalyst temperatures were monitored, and the compositions of engine exhausts before and after TWC were analyzed. In order to well control the catalysts at the target temperature (~900 °C), catalyst aging was periodically switched between rich and lean conditions via altering the flow rate of the make-up air. The performance of the IL- or ZDDP-aged TWCs in engine emissions control was evaluated in a laboratory bench core reactor. Results suggested that the IL may potentially have less adverse impact on TWC compared with ZDDP.

## CHAPTER 5. Lubricant Prototyping and Engine Dynamometer Testing

### 5.1. Formulation of an ultra-low viscosity prototype engine oil using an IL as the AW additive

The CRADA team in collaboration with Lubrizol Company, a world-leading additive company, conducted engine oil formulation and successfully developed the first prototype automotive engine oil using the IL $[P_{66614}][DEHP]$ as the AW additive. A PAO 4 cSt base oil was used as the base fluid and the treat rate of $[P_{66614}][DEHP]$ was 1.0 wt.% to meet the GF-5's phosphorus limitation. Two batches of the prototype engine oil were produced: (1) 300 mL for tribological bench testing and (2) 6 gallons for full-size engine dynamometer testing (see Fig. 5.1.1).

Fig. 5.1.1. Six gallons of the prototype IL-additized fully-formulated engine oil.

The rheology properties of the prototype IL-additized engine oil and two baseline engine oils are compared in Table 5.1.1. The kinematic and high-temperature high-shear (HTHS) viscosities were determined using the ASTM standards D7279 and D5481, respectively. The IL-additized engine oil has ultra low viscosities, which are substantially lower than the newest SAE 0W-16 engine oil [44] and whose HTHS viscosity falls in the proposed SAE 8 grade.

Table 5.1.1. Kinematic and high-temperature high-shear viscosities

| | cSt @ 40 °C | cSt @ 100 °C | HTHS (cP @150 °C) |
|---|---|---|---|
| Mobil 1™ 5W-30 engine oil | 64.3 | 11.4 | 3.11 |
| Mobil Clean™ 5W-30 engine oil | 56.1 | 10.1 | 3.06 |
| *SAE XW-20 engine oil* | | *>6.9, <9.3 [44]* | *>2.6 [44]* |
| *SAE XW-16 engine oil* | | *>6.1, <8.2 [44]* | *>2.3 [44]* |
| *Proposed SAE 12 grade* | | | *>2.0* |
| *Proposed SAE 8 grade* | | | *>1.7* |
| IL-additized engine oil (300 mL batch) | 25.5 | 5.38 | 1.93 |
| IL-additized engine oil (6-gallon batch) | 25.5 | 5.38 | 1.85 |

### 5.2. Tribological bench tests of the prototype IL-additized engine oil

Tribological bench tests were conducted on the IL-additized prototype engine oil at the GM Tech Center. Ball-on-disc rolling-sliding tests were carried out on a Mini Traction Machine (MTM-2) to generate the Stribeck curves as well as evaluate the wear behavior. Both the ball and the disc were made of hardened AISI 52100 bearing steel. The ball had a diameter of 19.5 mm, hardness of 64 $R_c$, and roughness of 0.025 μm ($R_a$). The disc had hardness of 62.5 $R_c$ and roughness of 0.01 mm ($R_a$). The wear track diameter was 42 mm. The amount of oil for each test was 40 mL and the contact interface was submerged. 2-3 repeat tests were conducted for each lubricant at every test condition. Results were benchmarked against those of commercial Mobil 1™ and Mobil Clean™ 5W-30 engine oils.

The Stribeck curve tests were generated at 100 °C under a constant load of 75 N and a sliding-rolling ratio (Equ. 2.2) of 50%. The mean speed started at 3.2 m/s and decreased stepwise to 0.1 m/s with a step size of 0.1 m/s and a step time of 6 sec. The Stribeck curves of the three oils are plotted in Fig. 5.2.1. The prototype IL-additized engine oil showed 20-33% friction reduction in mixed and elastohydrodynamic lubrication (ML/EHL) compared with the two commercial Mobil 5W-30 engine oils. The friction reduction was primarily attributed to the much lower viscosity of the IL-additized engine oil (see Table 5.1.1).

Wear tests were conducted at 100 °C under 75 N using the ball-on-disc test configuration described above. A slow mean speed 0.02 m/s with a sliding-rolling ratio of 95% was used to ensure boundary lubrication (BL). Each test lasted for 15 hours. The wear rates are compared in Fig. 5.2.2, where the prototype IL-additized engine oil showed 38% and 92% less wear than the Mobil 1™ and Mobil Clean™ 5W-30 oils, respectively. This is particularly encouraging when considering the ultra-low kinematic and HTHS viscosities of the IL-additized oil.

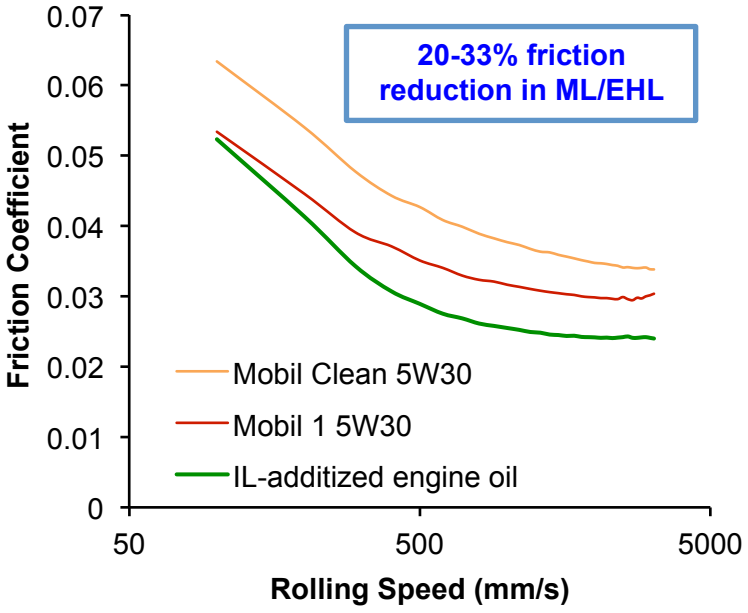


Fig. 5.2.1. Stribeck curves of the prototype IL-additized engine oil benchmarked against commercial Mobil 5W-30 engine oils.

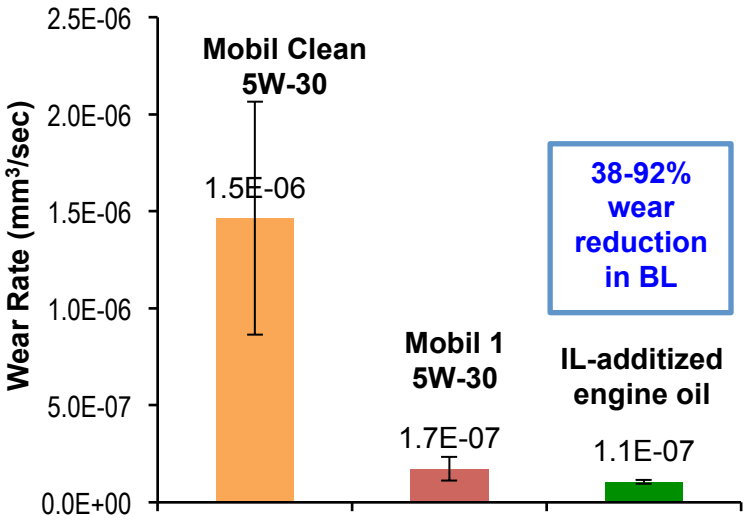


Fig. 5.2.2. Comparison of wear rates of the prototype IL-additized engine oil with commercial Mobil 5W-30 engine oils.

### 5.3. High-temperature high-load engine dynamometer tests

High-temperature high-load (HTHL) engine dynamometer tests were carried out on the prototype IL-additized engine oil at GM Tech Center to evaluate its engine wear protection (given the ultra-low viscosity) and aging behavior at extreme engine operation conditions. The Mobil 1$^{TM}$ 5W-30 engine oil was also tested to establish a baseline. As shown in Fig. 5.3.1, the HTHL test uses a LSX 6.2L Gen4 small block engine with a cast iron block and cast aluminum heads. The engine operates at a compression ratio of 9:1 to generate a power of 450 HP and a torque of 444 ft-lbs. Tests were conducted for 100 hours at 2700 rpm speed, 120 N load, and 145 $^{o}$C oil sump temperature. Oil samples (2 oz) were taken at fresh, 20, 40, 60, 80 and 100 hours. Oil analyses were conducted to track the viscosity change and metal contents.

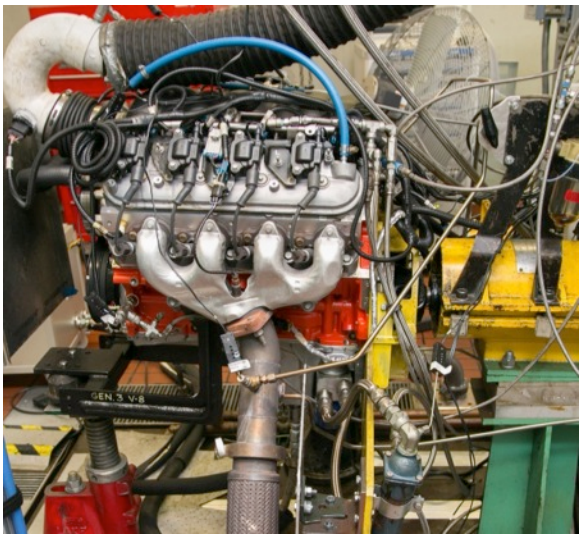

Fig. 5.3.1. High-temperature high-load engine dynamometer test setup at GM Tech Center.

The measured kinematic and HTHS viscosities of the IL-additized oil and Mobil 1™ 5W-30 oil at various test intervals are shown in Table 5.3.1. The kinematic viscosities of the Mobil 1™ 5W-30 oil decreased in the first 60 hours of testing and gradually increased after that. This reflected the two processes affecting the viscosity simultaneously: shear-down of viscosity index improvers (VII) and oil aging. The former dominated at the beginning of the engine testing and as a result, viscosity decreased quickly in the first 20 hrs and then leveled out by 40-60 hrs. During the aging process, some of the hydrogen bonds in the base oil degraded allowing oil molecules to combine with oxygen from surrounding air, and the oil molecules gradually degraded to a point where they "cross-link" or bond together to form "viscosity growth". Such viscosity growth was observed in the second half of the HTHL engine test. In contrast, the prototype IL-additized oil had no VII, and therefore showed a slow, but one-way viscosity change reflecting the aging/oxidation process. The HTHS viscosities of both oils were slightly higher by the end of the engine tests with more increase for the IL-additized oil, again due to the lack of an offset from VII shear-down.

Table 5.3.1. Kinematic and HTHS viscosities of HTHL tested oils.

| | Test time (hr) | 0 | 20 | 40 | 60 | 80 | 100 |
|---|---|---|---|---|---|---|---|
| Mobil 1™ 5W-30 oil | cSt @ 40 °C | 64.2 | 58.4 | 55.2 | 55.1 | 56.8 | 59.5 |
| | cSt @ 100 °C | 11.4 | 10.2 | 9.7 | 9.5 | 9.7 | 10.0 |
| | HTHS (cP) @ 150 °C | 3.11 | | | | | 3.17 |
| Prototype IL-additized oil | cSt @ 40 °C | 25.5 | 27.5 | 28.2 | 28.7 | 29.5 | 30.3 |
| | cSt @ 100 °C | 5.4 | 5.6 | 5.7 | 5.7 | 5.8 | 5.9 |
| | HTHS (cP) @ 150 °C | 1.85 | | | | | 2.03 |

No excessive oil consumption was observed for the low-viscosity IL-additized oil in the HTHL engine tests. The amount of oil consumed during the 100-hr HTHL engine test of the IL-additized oil was 41.2 oz, very similar to the 41.9 oz lost in the test of the Mobil 1™ 5W-30 oil. This suggested no excessive oil leaking or blow-by issues that are generally concerned with low-viscosity engine oils.

The wear-related metallic elements in the oil samples at different test intervals in the HTHL engine test were quantified using inductively coupled plasma atomic emissions spectrometry (ICP-AES) and results are summarized in Fig. 5.3.2. Very encouragingly, the low-viscosity IL-additized oil showed similar amounts of iron (main indicator of engine wear) and less copper (indicator of bronze bearing wear) compared to the Mobil 1™ 5W-30 oil. This suggested that the IL-additized oil provided adequate engine wear protection despite its ultra-low viscosity. This indicates the excellent anti-wear functionality of the IL $[P_{66614}][DEHP]$ as observed in tribological bench tests. The slightly more aluminum and silicon were probably wear products of the cast aluminum bearing housings for the crank shaft and connecting rod, where the lubrication regime may have changed from elastohydrodynamic to mixed lubrication when using the ultra-low viscosity oil. The potentially increased bearing wear caused by oils with HTHS viscosity lower than 2.4 cP has been discussed in [45] and therefore potential viscosity adjustment may be needed for the IL-additized oil.

ICP oil analysis also suggested that the phosphorus content in the prototype IL-additized oil was ~0.12%, higher than the upper limit of 0.08% regulated in the ILSAC GF-5. This will need to be addressed via formulation optimization in follow-on R&D.

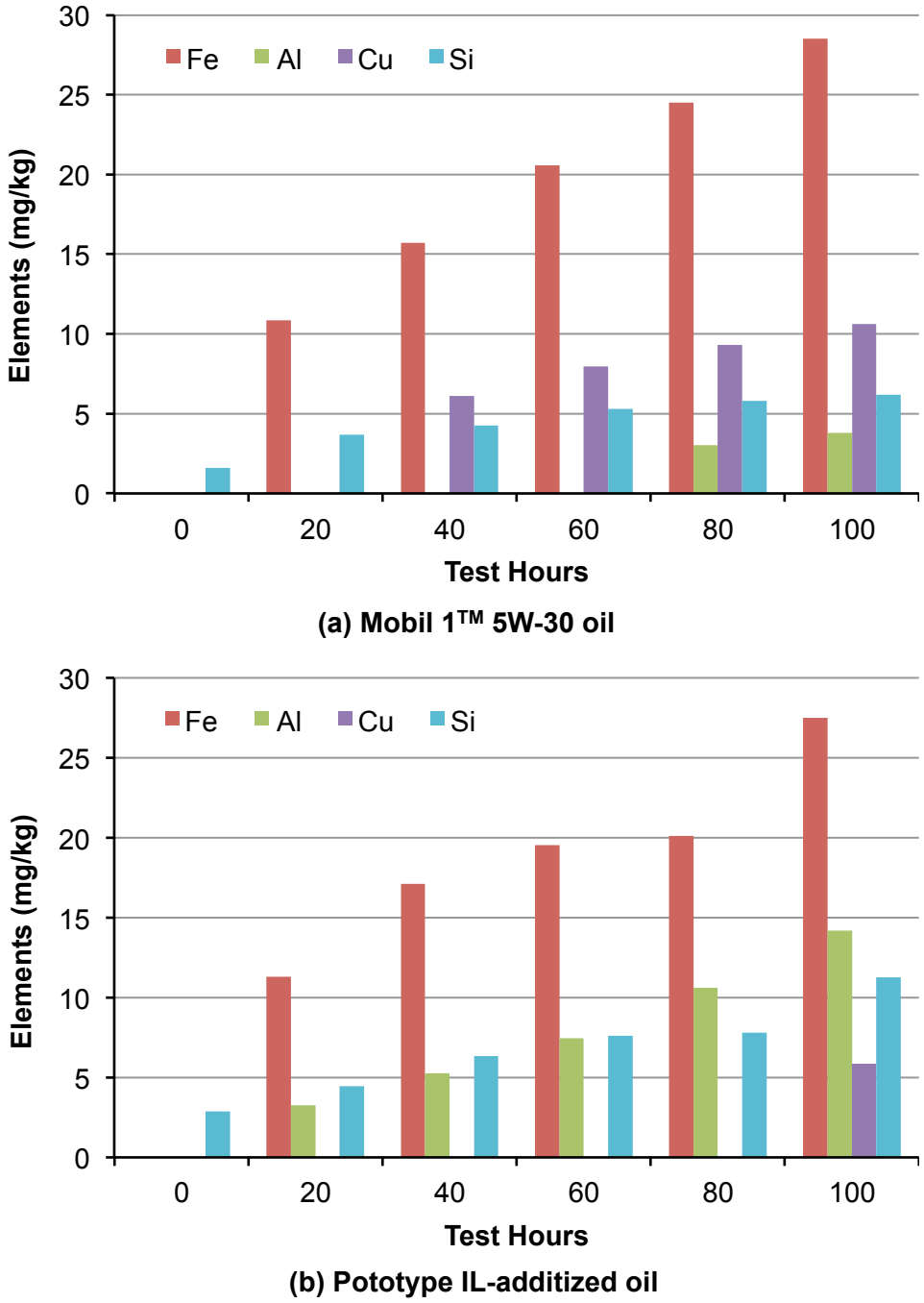


Fig. 5.3.2. Wear-related metallic elements in oil samples of HTHL engine tests.

### 5.4. Sequence VID fuel efficiency engine dynamometer tests

The improvement on fuel economy by the low-viscosity prototype IL-additized engine oil was determined using the GF-5 / Sequence VID fuel efficiency engine dynamometer tests (ASTM D 7589 [46]). The Sequence VID tests were conducted at InterTek Automotive Research and the engine setup is shown in Fig. 5.4.1. This standard fuel efficiency engine dynamometer test compares the performance of a test lubricant to the performance of a baseline lubricant over six different stages of operation. A 2008

Cadillac SRX 3.6L High Feature (HF) V6, 4-cycle engine is used as the test apparatus. The engine incorporates Dual Overhead Camshafts, 4 Valves/Cylinder, Dual Stage Plenum Induction Manifold, 94x85.6 mm Bore & Stroke, with 10.2:1 compression ratio. The Sequence VID test incorporates a flush and run type procedure. The baseline oil is a SAE 20W-30 engine oil without friction modifier or viscosity improver. Each test consists of two 6-stage fuel economy measurements in the conditions shown in Table 5.4.1, one at the beginning of the test and one at the end.

Fig. 5.4.1. Sequence VID engine test setup at InterTek.

Table 5.4.1. Fuel economy measurement (6 stages)

| FE Stage | Speed (r/min) | Torque (N-m) | Oil Temp. (°C) | Coolant Temp. (°C) |
|---|---|---|---|---|
| 1 | 200 | 105 | 115 | 109 |
| 2 | 200 | 105 | 65 | 65 |
| 3 | 1500 | 105 | 115 | 109 |
| 4 | 695 | 20 | 115 | 109 |
| 5 | 695 | 20 | 35 | 35 |
| 6 | 695 | 40 | 115 | 109 |

The prototype IL-additized engine oil was evaluated in between the two baseline runs. The prototype oil was initially aged during 16 hours of engine operation as specified in Table 5.4.2. After the initial aging, a 6-stage fuel economy measurement (Table 5.4.1) was taken. The prototype oil was then aged an additional 84 hours at the engine condition in Table 5.4.2. Following this final aging, the prototype oil once again went through a 6-stage fuel economy measurement. The two fuel economy measurements taken on the baseline oil were used to calculate the baseline fuel economy with 80% weight on the first run and 20% weight on the second run, and then a final value for the fuel efficiency improvement was calculated for the prototype oil. Two repeat Sequence VID tests were carried out for the prototype IL-additized engine oil and another Sequence VID test was conducted on Mobil 1™ 5W-30 engine oil for direct comparison.

Table 5.4.2. Aging conditions

| Aging Stage | Speed (r/min) | Torque (N-m) | Oil Temp. (°C) | Coolant Temp. (°C) |
|---|---|---|---|---|
| 1 & 2 | 2250 | 110 | 120 | 110 |

The Sequence VID test results are shown in Fig. 5.4.2. The fuel economy in running the Mobil 1™ 5W-30 engine oil was 1.92% higher than the baseline, as expected (1.9% minimum required for SAE xW-30 oils). In contrast, the prototype IL-additized engine oil improved the fuel efficiency by 4.18% and 3.68% over the baseline 20W-30 oil in the two repeat tests. That results in an average of 3.93% fuel economy improvement over the baseline oil. This demonstrates a 2.01% higher fuel efficiency for the IL-additized engine oil compared to the Mobil 1™ 5W-30 engine oil. This has met the DOE VTO's goal of 2% fuel efficiency improvement via lubricant advances by 2015.

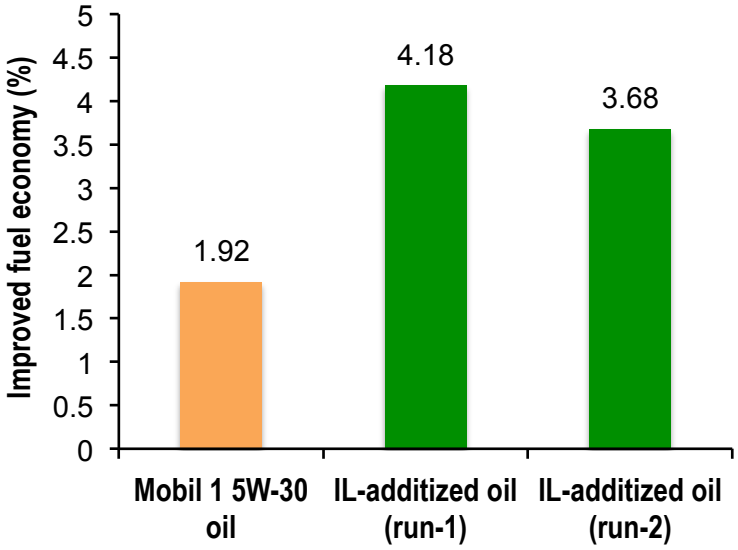


Fig. 5.4.2. Sequence VID fuel efficiency engine dynamometer test results.

### 5.5. Conclusion for lubricant prototyping and engine dynamometer testing

A (the first in the literature) prototype engine oil using the IL $[P_{66614}][DEHP]$ as an anti-wear additive has been developed. Tribological bench tests of the IL-additized oil showed 20-33% lower friction in mixed and elastohydrodynamic lubrication and 38-92% lower wear in boundary lubrication when compared with commercial Mobil 1™ and Mobil Clean™ 5W-30 engine oils. The prototype oil successfully passed the 100-hr HTHL full-size engine dynamometer test. While this IL-additized oil has a very low viscosity (much lower than the newest SAE 0W-16), it demonstrated an engine wear performance similar to Mobil 1™ 5W-30 engine oil. This is evidence that IL could potentially be used as an anti-wear additive in future engine oil formulations. The industrial standard fuel economy engine test (Sequence VID) has demonstrated a 2.01% improved fuel economy improvement for the prototype IL-additized oil compared to Mobil 1 5W-30 oil (or on average a 3.93% improvement over the baseline 20W-30 oil).

## COMMERCIALIZATION POSSIBILITIES AND PLANS FOR FUTURE COLLABORATION

The successful development of oil-miscible ionic liquids with superior anti-wear functionality and promising results of the first prototype IL-additized engine oil suggest a strong potential in commercialization of this technology. With the promising Sequence VID fuel economy results from this work, it is clear that improvements in engine oil formulation can be achieved to increase fuel economy. Going forward one could see new minimum criteria for % fuel economy improvements on the Sequence VID test. This would result in new oil formulations going forward potentially using ionic liquids.

Follow-on research is needed for further development and optimization of IL chemistry and oil formulation to further enhance the engine efficiency and durability and fully meet ILSAC GF-5 specifications. The ORNL-GM team jointly with a new partner Cytec Industries Inc. already submitted a new proposal to the DOE VTO Fuels and Lubricants Technologies Program for conducting a follow-on project to further develop the IL-additized lubricants and extend the application from engine to rear axle lubrication. Cytec is a global leader in phosphine technology and has the capabilities of producing larger-than-lab-scale quantities of ILs to fulfill the needs of engine dynamometer and vehicle tests.

## CONCLUSIONS

This ORNL-GM CRADA has successfully developed a new group of oil-miscible ionic liquids for engine lubrication. Such ILs possess high thermal stability, non-corrosiveness, excellent wettability, and effective anti-scuffing/anti-wear and friction reduction characteristics. Comprehensive characterizations have correlated the lubricating mechanisms of ILs to their physical and chemical interactions with metallic surfaces at the contact interface. The IL $[P_{66614}][DEHP]$, the best performer in fundamental investigation, was selected for oil formulation and engine testing. Working with a leading oil formulation company, a prototype (the first in the literature) IL-additized low-viscosity engine oil has been produced and demonstrated promising lubricating performance in both bench and engine tests. Tribological bench tests of the IL-additized oil showed 20% and 33% lower friction in mixed and elastohydrodynamic lubrication and 38% and 92% lower wear in boundary lubrication when compared with commercial Mobil 1 and Mobil Clean 5W-30 engine oils, respectively. HTHL engine tests showed excellent anti-wear performance for the prototype oil in both fresh and aged conditions. Sequence VID engine dynamometer tests of this IL-additized oil demonstrated an improved fuel economy by 3.93% and 2.01% benchmarked against the 20W-30 baseline and Mobil 1 5W-30 engine oils, respectively. In addition, accelerated catalyst aging tests were conducted on the IL additive and results suggested potentially less poisoning effects on TWCs compared to ZDDP. The team is seeking follow-on joint research for further development and optimization of IL-additized engine oil fully meeting ILSAC GF-5 specifications to enhance the engine efficiency and durability.

**References**


[1]. S.C. Tung, M.L. McMillan, "Automotive tribology overview of current advances and challenges for the future," Tribology International 37 (2004) 517–536.
[2]. L.R. Rudnick, Lubricant Additives – Chemistry and Applications, Marcel Dekker, 2003.
[3]. M.A. Nicholls, Do, T., Norton, P.R., Kasrai, M., Bancroft, G.M., Review of the lubrication of metallic surfaces by zinc dialkyl-dithiophosphates, Tribol. Int. 38, 15–39 (2005).
[4]. Holbrey, J.D., Seddon, K.R., "Ionic Liquids," Clean Products and Processes 1, Springer-Verlag, 1999, pp. 223-236.
[5]. C.F. Ye, W.M. Liu, Y.X. Chen, L.G. Yu, Room Temperature ionic liquids: A novel versatile lubricant, Chemical Communications (2001) 2244–2245.
[6]. X. Liu, F. Zhou, Y. Liang, W. Liu, Tribological performance of phosphonium based ionic liquids for an aluminum-on-steel system and opinions on lubrication mechanism, Wear 261 (2006) 1174–1179.
[7]. J. Qu, J.J. Truhan, S. Dai, H.M. Luo, P.J. Blau, Ionic liquids with ammonium cations as lubricants or additives, Tribol. Lett. 22 (2006) 207–214.
[8]. A.E. Jiménez, M.D. Bermudez, P. Iglesias, F.J. Carrion, G. Martinez-Nicolas, 1-N-alkyl -3-methylimidazolium ionic liquids as neat lubricants and lubricant additives in steel-aluminum contacts, Wear 2006, 260, 766-782
[9]. I. Minami, M. Kita, T. Kubo, H. Nanao, S. Mori, The tribological properties of ionic liquids composed of trifluorotris(pentafluoroethyl) phosphate as a hydrophobic anion, Tribol. Lett. 30 (2008) 215–223.
[10]. T. Itoh, N. Watanabe, K. Inada, A. Ishioka, S. Hayase, M. Kawatsura, I. Minami, S. Mori, Design of alkylsulfate ionic liquids for lubricants, Chem. Lett. 38 (2009) 64–65.
[11]. F. Zhou, Y. Liang, W. Liu, Ionic liquid lubricants: designed chemistry for engineering applications, Chem. Soc. Rev. 38 (2009) 2590–2599.
[12]. I. Minami, Ionic liquids in tribology, Molecules (Basel, Switzerland) 14 (2009) 2286–2305.
[13]. M. Bermúdez, A.-E. Jiménez, J. Sanes, F.-J. Carrión, Ionic Liquids as Advanced Lubricant Fluids, Molecules 14 (2009) 2888-2908.
[14]. J. Qu, P.J. Blau, S. Dai, H. Luo, H.M. Meyer III, Ionic liquids as novel lubricants and additives for diesel engine applications, Tribol. Lett. 35(3) (2009) 181-189.
[15]. J. Qu, P.J. Blau, S. Dai, H.M. Luo, H.M. Meyer III, J.J. Truhan, Tribological characteristics of aluminum alloys sliding against steel lubricated by ammonium and imidazolium ionic liquids, Wear 267 (2009) 1226–1231.
[16]. S.D.A. Lawes, S.V. Hainsworth, P. Blake, K.S. Ryder, A.P. Abbott, Lubrication of steel/steel contacts by choline chloride ionic liquids, Tribol. Lett. 37 (2010) 103–110.
[17]. J. Qu, J.J. Truhan, S. Dai, H.M. Luo, P.J. Blau, Lubricants or lubricant additives composed of ionic liquids containing ammonium cations, U.S. Patent #7,754,664, 2010.
[18]. H. Xiao, D. Guo, S. Liu, G. Pan, X. Lu, Film thickness of ionic liquids under high contact pressures as a function of alkyl chain length, Tribol. Lett. 41 (2011) 471–477.
[19]. K. Mistry, M.F. Fox, M. Priest, Lubrication of an electroplated nickel matrix silicon carbide coated eutectic aluminium-silicon alloy automotive cylinder bore with an ionic liquid as a lubricant additive, J. Eng. Tribol. 2009, 223, 563-569
[20]. A.H. Battez, R. González, J.L. Viesca, D. Blanco, E. Asedegbega, A. Osorio, Tribological behaviour of two imidazolium ionic liquids as lubricant additives for steel/steel contacts. Wear 2009, 266 (11-12), 1224-1228.
[21]. R.G. Lu, H. Nanao, K. Kobayashi, T. Kubo, S. Mori, Effect of lubricant additives on tribochemical decomposition of hydrocarbon oil on nascent steel surfaces, J. Jpn. Petrol. Inst. 2010, 53, 55-60
[22]. A. Schneider, J. Brenner, C. Tomastik, F. Franek, Capacity of selected ionic liquids as alternative EP/AW additive, Lubr. Sci. 2010, 22, 215–223
[23]. A.E. Jimenez, M. D. Bermudez, Imidazolium ionic liquids as additives of the synthetic ester propylene glycol dioleate in aluminium–steel lubrication. Wear 265 (2008) 787-798

[24]. M.H. Yao, Y.M. Liang, Y.Q. Xia, F. Zhou, Bisimidazolium Ionic Liquids as the High-Performance Antiwear Additives in Poly(ethylene glycol) for Steel-Steel Contacts, ACS Appl. Mater. & Inter. 2009, 1, 467-471
[25]. Burke J. Solubility Parameters: Theory and Application. The Book and Paper Group Annual. The American Institute for Conservation. Vol. 3 (1984).
[26]. J. Qu, M.F. Chi, H.M. Meyer III, P.J. Blau, S. Dai, H.M. Luo, Nanostructure and composition of tribo-boundary films formed in ionic liquid lubrication, Tribol. Lett. 43 (2011) 205–211.
[27]. G. Mordukhovich, J. Qu, J.Y. Howe, S.S. Bair, B. Yu, H. Luo, D.J. Smolenski, P.J. Blau, B.G. Bunting, S. Dai, A Low-ViscosityIonic Liquid Demonstrating Superior Lubricating Performance from Mixed to Boundary Lubrication, Wear (2013) 301, 740-746.
[28]. B. Yu, D.G. Bansal, J. Qu, X. Sun, H. Luo, S. Dai, P.J. Blau, B.G. Bunting, G. Mordukhovich, D.J. Smolenski, Oil-Miscible and Non-Corrosive Phosphonium-Based Ionic Liquids as Candidate Lubricant Additives, Wear 289 (2012) 58–64.
[29]. J. Qu, D.G. Bansal, B. Yu, J. Howe, H. Luo, S. Dai, H. Li, P.J. Blau, B.G. Bunting, G. Mordukhovich, D.J. Smolenski, Anti-wear performance and mechanism of an oil-miscible ionic liquid as a lubricant additive, ACS Appl. Mater. & Inter. 4 (2) (2012) 997–1002.
[30]. J. Qu, H. Luo, M. Chi, C. Ma, P.J. Blau, S. Dai, M.B. Viola, "Comparison of an Oil-Miscible Ionic Liquid and ZDDP as a Lubricant Anti-Wear Additive," Tribology International (submitted).
[31]. S. Bair, High Pressure Rheology for Quantitative Elastrohydrodynamics; Elsevier Science, 2007.
[32]. S. Bair, F. Qureshi, Accurate measurements of pressure-viscosity behavior in lubricants, Tribology Transactions 45 (2002) 390–396.
[33]. B.J. Hamrock, D. Dowson, Ball Bearing Lubrication—The Elastohydrodynamics of Elliptical Contacts; John Wiley & Sons: New York, 1981.
[34]. S. Bair, The high pressure rheology of some simple model hydrocarbons, Proc Instn Mech Engrs Part J: J Engineering Tribology 216 (2002) 1–11.
[35]. S. Bair, Pressure-viscosity behavior of lubricants to 1.4 GPa and its relation to EHD traction, Tribology Transactions, 43 (2000) 91–99.
[36]. J. Qu, P.J. Blau, J.Y. Howe, H.M. Meyer III, Oxygen diffusion enables anti-wear boundary film formation on titanium surfaces in zinc-dialkyl-dithiophosphate (ZDDP)-containing lubricants, Scripta Materialia 60 (2009) 886–889.
[37]. Burke J. Solubility Parameters: Theory and Application. The Book and Paper Group Annual. The American Institute for Conservation. Vol. 3 (1984).
[38]. U. Domanska, Solubilities and thermophysical properties of ionic liquids. Pure Appl. Chem. 77 (2005) 543-557.
[39]. M.P. Jensen, R. Chiarizia, V. Urban, Investigation of the aggregation of the neodymium complexes of dialkylphosphoric, -oxothiophosphinic, and -dithiophosphinic acids in toluene. Solvent Extr. Ion Exch. 19 (2001) 865-884.
[40]. Maples R.E. Petroleum Refinery Process Economics (2nd ed.). Pennwell Books (2000).
[41]. R.G. Lu, H. Nanao, K. Kobayashi, T. Kubo, S. Mori, Effect of lubricant additives on tribochemical decomposition of hydrocarbon oil on nascent steel surfaces, Journal of the Japan Petroleum Institute 2010, 53, 55-60
[42]. D.A. Rigney, J.P. Hirth, Plastic deformation and sliding friction of metals, Wear, 53 (1979) 345–370.
[43]. K. Ito, J.-M. Martin, C. Minfray, K. Kato, Low-friction tribofilm formed by the reaction of ZDDP on iron oxide, Tribol. Int. 39 (2006) 1538.
[44]. SAE J300, Engine Oil Viscosity Classification, SAE International, April 2013.
[45]. M.J. Covitch, M. Brown, C. May, T. Selby, I. Goldmints, D. George, Extending SAE J300 to viscosity grades below SAE 20, 2010-01-2286, SAE International Journal of Fuels and Lubricants, 3(2) (2010) 1030-1040.

[46]. ASTM D7589-13, Standard Test Method for Measurement of Effects of Automotive Engine Oils on Fuel Economy of Passenger Cars and Light-Duty Trucks in Sequence VID Spark Ignition Engine, Annual Book of ASTM Standards, 05.04, ASTM International, 2013.